NASA Technical Memorandum 102801

# Experimental Validation Study of an Analytical Model of Discrete Frequency Sound Propagation in Closed-Test-Section Wind Tunnels

Marianne Mosher, Ames Research Center, Moffett Field, California

May 1990

National Aeronautics and
Space Administration

**Ames Research Center**
Moffett Field, California 94035-1000

## SYMBOLS

| | |
|---|---|
| $a$ | diameter of source |
| $A_n, A_n^m, B_n^m$ | coefficients in series expansion of acoustic field of source |
| **A** | vector of coefficients for series expansion of acoustic field of source |
| $c$ | speed of sound in fluid |
| $C_\alpha$ | wall absorption coefficient for normal incidence |
| d | distance from source axis, $\sqrt{x^2+z^2}$ |
| dB | $20 \log(\lvert p \rvert / p_{ref})$ |
| $f$ | source term in Helmholtz equation |
| **f** | matrix of modal shapes for series expansion of acoustic field in duct |
| $f_n^i$ | element of **f** |
| $G_h$ | free-space Green's function for Helmholtz equation |
| $h_n^1$ | Hankel function of 1st kind of order $n$ |
| $h_j$ | $j$th eigenmode of duct |
| $i$ | $\sqrt{-1}$ |
| $j$ | index for duct modes |
| $j_{max}$ | number of modes used |
| $k$ | wave number of acoustic field, $\omega/c$ |
| $k_j$ | modal wave number in duct for jth mode, $\sqrt{k^2-k_{yj}^2-k_{zj}^2}$ |
| $k_{yj}, k_{zj}$ | $j$th eigenvalues of duct modes in $y$- and $z$-directions |
| $l$ | typical duct cross dimension, square root of duct cross section area |
| $n$ | ratio of maximum to minimum pressure in impedance tube, $p_{max}/p_{min}$ |
| $n$ | normal to control surface |

| | |
|---|---|
| $p$ | complex harmonic amplitude |
| $\hat{p}_j^+$ | value of jth mode propagating in $+x$-direction |
| $\hat{p}_j^-$ | value of jth mode propagating in $-x$-direction |
| $p_i$ | incident acoustic pressure |
| $p_{max}$ | pressure in impedance tube at maximum closest to sample |
| $p_{min}$ | pressure in impedance tube at minimum closest to sample |
| $p_r$ | reflected acoustic pressure |
| $p_{ref}$ | harmonic amplitude of reference pressure measured near source |
| $\mathbf{p}$ | vector of measured complex harmonic amplitude of acoustic pressures for curve fit of acoustic source |
| $P$ | acoustic pressure, $P = \Re(pe^{-i\omega t})$ |
| $P_n$, $P_n^m$ | Legendre function |
| $r$ | $\lvert\vec{r} - \vec{r}_s\rvert$ |
| $\vec{r}$ | position, $(x,y,z)$ |
| $\vec{r}_s$ | position of source, $(x_s,y_s,z_s)$ |
| $\Re$ | real part of complex quantity |
| $S$ | control surface |
| $S_d$ | control surface between control volume and semi-infinite region in the $+x$-direction |
| $S_u$ | control surface between control volume and semi-infinite region in the $-x$-direction |
| $S_w$ | control surface on duct wall |
| T | temperature |
| $V$ | control volume |
| $x$ | horizontal coordinate parallel to axis of duct, origin centered at source |
| $y$ | horizontal coordinate parallel to axis of tube, origin centered at source |

| | |
|---|---|
| $y_{min}$ | distance from sample surface to location of minimum acoustic pressure in impedance tube |
| $z$ | vertical coordinate, origin centered at source |
| $z$ | acoustic impedance of a surface |
| $\alpha$ | boundary condition coefficient, $ik\rho_0 c/z$ |
| $\gamma$ | angle of incident plane wave reflecting off a surface |
| $\theta$ | angle from +$y$-axis |
| $\lambda$ | wavelength |
| $\rho_0$ | fluid density |
| $\phi$ | angle in horizontal plane from –z axis |
| $\omega$ | acoustic frequency |

## SUMMARY

A basic experiment was conducted to determine the validity of an analytic model of sound in a duct. The model was developed to study the effects of wall reflections on acoustic measurements in closed-test-section wind tunnels, especially low frequency helicopter noise. Several assumptions were used to produce an acoustic model of known, physically important influences, in a computationally efficient manner. A principal objective of this study is to assess the implications of these assumptions in the analytical model through comparison with experiment.

This study compares measurements and calculations of a simple acoustic source in a rectangular concrete duct lined with foam on the walls and anechoic end terminations. Measuring acoustic pressure for six pairs of wave numbers (twelve wave numbers total) provides variation in frequency and absorption characteristics of the duct walls.

This report documents the experiment. The test and results are described in detail. Comparison of measurements with calculations are shown and discussed. Mixed results were obtained. Some calculations match measurements very well, some very poorly, and many match moderately well. Close to the source, where the interference of wall reflections is minimal, correlation is very good. Away from the source, correlation degrades but tends to improve as the wave number and wall absorption increase. Sensitivity studies show little effect on the predicted results for changes in impedance boundary condition values, source location, measurement location, temperature, and source model for variations spanning the expected measurement error.

## INTRODUCTION

Wind tunnel tests performed with acoustic measurements can provide useful information in the design and development of aircraft. Wind tunnels have been used to study basic aeroacoustic phenomena, test prototypes and design concepts, and test flight vehicles. The standard hard-walled wind tunnel creates an adverse environment for making acoustic measurements due to interference from wall reflections and high background noise levels. Acoustically absorbent linings, permanently or temporary mounted, have been used to reduce the interference due to reflections in many wind tunnels including the 40- by 80-Foot, 80- by 120-Foot, and 7- by 10-Foot Wind Tunnels at NASA Ames Research Center, 8- by 6-ft Transonic Wind Tunnel at NASA Lewis Research Center, the 20- by 20-Foot Low Speed Wind Tunnel at Boeing Helicopter Company, and the Vought 7- by 10-Foot Low Speed Wind Tunnel.

An understanding of the acoustic properties of these tunnels is important for the researcher making acoustic measurements within these facilities. An understanding of these properties also provides critical information for modifying or designing any new closed-test section wind tunnel that could be used to make acoustic measurements. An analytic model and computer program were developed to analyze the reflection problem in wind tunnels (ref. 1). This analysis can be used to determine where uncontaminated measurements can be made for a particular test installation in a wind tunnel or what kind of wall treatment is needed to obtain a given acoustic performance. The purpose of the research reported here is

to evaluate the applicability of the model to studying the effect of the wind tunnel wall reflection on discrete low frequency noise measurements typical of helicopter rotor loading noise.

The present model uses the standard description of sound propagation in air of the convected wave equation, or the Helmholtz equation (ref. 2) in the frequency domain. The convected wave equation and Helmholtz equation have been used successfully for many years to describe low amplitude sound propagation in uniform air. Walls are modeled with the standard impedance boundary condition (ref. 2) which relates the acoustic pressure to the acoustic velocity normal to the boundary at a point. This allows the boundary to absorb some acoustic energy. Since this boundary condition is a local condition specifying properties at an individual point, it does not allow for the interaction of the acoustic waves in the air with any propagating waves which could be induced in the boundary medium. Neither elastic waves propagating in the structure nor acoustic waves propagating in the lining or boundary layer have been taken into account.

In the early part of the 20th century, Sabine (ref. 3) recognized the problem of interference of reflected waves in an acoustic field in a closed space. Through experimentation he developed an analysis relating reverberation to a room's geometry and the absorption characteristics of surfaces. More recently, Tyler and Soffrin (ref. 4) developed an acoustic analysis to study fan noise in a hard circular duct. This model was developed to study jet engine noise suppression with the inclusion of impedance boundary conditions (ref. 5). This model has been tested for its prediction of axial acoustic pressure attenuation and spatial mode shapes (refs. 6-9). Attenuation of a single mode was sometimes well predicted and sometimes not so well predicted. Mode shapes were predicted well for very low order axial modes in circular ducts, but not for radial modes or high order modes. Eversman (ref. 10) used the same physical model, the wave equation with impedance boundary condition, to study the acoustic field of a propeller in a circular wind tunnel. His analysis is similar to the one developed by this author (ref. 1) but is restricted to simpler geometric configurations and is solved by the finite element solution method.

The purpose of this project is to evaluate the accuracy of the physical model reported in reference 1 for describing sound in a duct near a known source. This requires first measuring the acoustic field of the source in the free field with no reflection and in a duct with known acoustic properties, and then comparing the measured effect of the duct on the acoustic field with predictions. Figure 1 outlines the steps used to evaluate the analytical model in this study. The radiation pattern of the single frequency acoustic source was measured in an anechoic chamber. These measurements provide both the baseline measurements of the source for determining the effect of the duct experimentally and the information necessary for an analytic description of the source for the theory. Acoustic measurements were then taken with the same source in the duct. The difference between these measured acoustic fields is the effect of the duct. Predictions were made using measured acoustic properties of the duct surface and the source. Comparison of the predicted effect of the duct with the measured effect of the duct then shows how well the theory predicts discrete frequency sound propagation in the duct.

## EXPERIMENT

### Anechoic Chamber

The interior of the anechoic chamber is 25 ft long by 18 ft wide by 11 ft high. Wedges 25 in. deep cover most of the interior. Individual wedges are 24 in. long and 8 in. wide at the base. Clusters of three wedges are arranged in a checkerboard pattern which alternates the orientation of the wedges. Wedges have a normal absorption coefficient greater than 0.99 at 125 Hz and above. No wedges cover a jet nozzle, collector, nor a section of the floor containing mounting hardware. These regions were covered with foam. A steel grid floor in the chamber allows access to the chamber and reflects some sound. The walls of the chamber have an isolation of 37 dB at 125 Hz and 73 dB at 4800 Hz (private communication from P. T. Soderman, Ames Research Center).

### Duct

Figure 2 shows the duct, a 20-ft long rectangular concrete section with interior dimensions of 4 ft width by 8 ft in height. The walls are 6 in. thick with a reinforcing grid of steel in the middle. One inch of foam covers the interior walls. Mylar sheeting covers the exposed exterior surfaces to help keep the interior at a uniform temperature by reflecting solar radiation. Both ends consist of wood doors covered by foam wedges (the same wedges as in the anechoic chamber) on the interior designed to absorb sound so the finite length duct will mimic an infinite length duct. The foam wedges provided sound absorption greater than 0.99 at frequencies in this study. All instrumentation wiring is routed through a small hole behind a wedge in the corner of one door. A hole in one wall of the duct permits the acoustic source and microphone traverse to be positioned inside the duct.

The experiment is sized to simulate a 1/10th scale version of the NASA Ames 40- by 80-Foot Wind Tunnel, assuming a rectangular test section. The nondimensional parameter for matching frequency and size is $kl$ where $k$ is the wave number and $l$ a typical length. For this study $l$ is the square root of the cross section area. A wind tunnel with similar geometry with a constant $kl$ contains the same number of wavelengths per wind tunnel characteristic dimension. In this study $kl$ ranges from 8.5221 to 26.4577; for each value of $kl$, multiple modes will propagate in the duct. When scaled up to the size of the 40- by 80-Foot Wind Tunnel, this range of $kl$ corresponds to frequencies of 27 to 84 Hz. Absorption of the foam lining in the duct is comparable to absorption in the full-scale wind tunnel with a 6.0-in. liner at the scaled frequencies. At these low frequencies, absorption is typically about 0.1 to 0.2 for acoustic waves propagating perpendicular to the tunnel test section wall.

### Acoustic Source

Figure 3 shows a schematic of the acoustic source used in this experiment. It consists of a speaker in a wooden box attached to a 1-ft-long fiberglass cone tapering down to a 4-ft-long aluminum tube. Sound propagates down the tube to produce a source at the open end of the tube. This configuration was chosen because at resonances of the tube the hard walls of the duct produced minimal effect on the acoustic output of the tube. Measurements were made at six pairs of wave numbers: 1.5065 and 1.5216; 2.2014

and 2.2234; 2.8685 and 2.8972; 3.4801 and 3.5149; 4.0304 and 4.0707; and 4.6308 and 4.6771 $ft^{-1}$. The wave numbers and frequencies in a pair differ by 1% and are spaced at resonances of the tube to provide a good signal-to-noise ratio. By making measurements and calculations in pairs, the sensitivity of the system to small changes in wave number can be found.

Measurements made in the anechoic chamber and the duct close to the source, shown in figure 4, demonstrate the small effect the duct has on the source output and radiation pattern for one representative wave number. In figures 4(a) and 4(b), the microphones point in opposite directions; asymmetry here shows the sensitivity of the acoustic field close to the source, due to the presence of the microphone. When figure 4(b) is flipped about the $x$ axis, measurements line up well with those in figure 4(a). Small variations in microphone distance from the source may account for slightly different levels in the measurements. For the measurements 0.5 in. from the source (figs. 4(a) and 4(b)), moving the microphone 0.125. in further out from the source produces a 1-dB reduction. For the measurements 1.0 in. from the source (fig. 4(c)), moving the microphone 0.25 in. further out from the source produces a 1-dB reduction.

## Instrumentation

Acoustic measurements were made with 0.5-in. condenser microphones. A reference microphone was placed at the end of the source tube parallel to the tube with the sensor 0.125 in. in front of the tube. A survey was taken with another microphone mounted on a traverse which was attached to the source (fig. 2(b)). Two different microphone holders could be attached to the traverse, one positioned the microphone very close to the source, the other positioned the microphone at larger distances from the source. The microphones were connected to the instrumentation system shown in figure 5. Power supplies powered the microphones and provided a gain of +40 dB. Microphone signals were monitored on an oscilloscope and rms voltmeter. Measurements taken with a two-channel analyzer consist of the transfer function from the reference microphone to the survey microphone. Results were stored on disks on a personal computer. The computer controlled the analyzer in the data acquisition and provided the electric signal to drive the speaker in the acoustic source.

## Measurements

Transfer functions from the reference microphone to the survey microphone comprise the measurements of the acoustic field around the source in the anechoic chamber and in the duct. The reference microphone was attached to the source tube, parallel to the tube, with the microphone 0.125 in. in front of the tube exit. This normalization corrects for any amplitude variation in the output of the source to best match the assumptions in the theory being evaluated. Microphones were calibrated with a pistonphone and relative humidity was measured each day before testing. When weather changed, humidity was remeasured. Wet and dry bulb temperatures were taken to determine humidity. Temperature was monitored continuously with three thermocouples, placed at the level of the source, 2.5 ft above the source, and 2.5 ft below the source. The average of the three temperatures was taken to be the duct temperature. Two 12-in.-diameter room fans circulated air within the duct between measurements to reduce temperature gradients. Data were acquired only when the maximum temperature difference was 1.0°F,

and usually the temperature difference was less than 0.5°F. Vertical temperature differences in the anechoic chamber were much smaller than in the duct, so mixing of the air was not needed.

**Anechoic chamber**– Measurements made in the anechoic chamber served three purposes. Measurements very close to the source provide a reference to compare with similar measurements in the duct to check for influence of the duct on the output of the source. Acoustic measurements in a plane 1 in. in front of the source provide a definition of the acoustic field radiating from the source to be compared with measurements in the duct to determine the experimental effect of the duct on the acoustic field. Lastly, measurements made near and far from the source in many directions provide input for an empirically derived analytic expression for the radiated acoustic field used in the computations.

Figure 6(a) shows a plan view of microphone locations close to the source and figure 6(b) shows a plan view of locations far from the source. At circled locations, measurements were also made at 12 locations in 30° increments around the axis of the source tube.

**Duct**– Acoustic measurements were taken in the duct to first check that the source radiation was not affected by the duct and then to determine the acoustic field in the duct to compare with computations. Measurements were taken close to the source along horizontal lines 0.5 in. (locations 2 to 14) and 1.0 in. (locations 15 to 19) in front of the source. To determine the acoustic field for comparison with calculations, measurements were also taken in a plane 1.0 in. in front of the source along radial lines from 0 to 36 in. at the locations shown in figure 7. The radial sweeps were repeated at 30° increments. Actual microphone locations were measured and used in the calculations.

**Impedance**– To obtain the impedance boundary condition, the impedance at normal incidence of the foam lining backed by a solid surface was measured. One standard method of measuring the acoustic impedance of a surface is to measure the amplitude and location of a standing wave produced by a single frequency plane wave and its plane wave reflection off the sample inside a rigid tube. From these measurements and linear acoustic theory the impedance is

$$z = \rho_0 c \left( \frac{1 + re^{i\mu}}{1 - re^{i\mu}} \right) \tag{1}$$

with

$$r = \frac{n-1}{n+1}, \; n = \frac{p_{max}}{p_{min}} \tag{2}$$

and

$$\mu = \left( \frac{4 y_{min}}{\lambda} - 1 \right) \pi \tag{3}$$

With a surface impedance of z, linear acoustic theory states that a plane acoustic wave reflects off the surface to give a reflected acoustic pressure of

$$p_r = \left( \frac{z\cos(\gamma) - \rho_0 c}{z\cos(\gamma) + \rho_0 c} \right) p_i \tag{4}$$

The absorption of acoustic energy, the absorption coefficient, is given by

$$C_\alpha = 1 - \left| \frac{z\cos(\gamma) - \rho_0 c}{z\cos(\gamma) + \rho_0 c} \right|^2 \tag{5}$$

Impedance measurements of foam samples were made in a 1-m-long, 10-cm-diameter standing wave tube shown in figure 8. Figure 9 shows the instrumentation system used to obtain the impedance measurements. The speaker is driven with a sine wave for a fixed wave number from the narrow band analyzer which is controlled by a computer. The analyzer receives the signals from the microphones and then transforms the signals into the frequency domain with a discrete Fourier transform. The amplitude of the signal at the frequency corresponding to the wave number being tested is sent to the computer. Using equations (1) to (3), the measured minimum and maximum amplitude of the acoustic pressure, and the locations of the minimum and maximum acoustic pressures, the computer calculates the impedance and absorption coefficient of the foam sample and prints the results.

At least two (usually three or more) measurements were made of each wave number for the foam sample. For each of the 12 wave numbers used with the 1-in. foam, impedance measurements were made on at least two different days. For each separate measurement, the air temperature in the room was measured. From the temperature measurement, the speed of sound was calculated from $c = 49.01\sqrt{T + 459.67}$ and the frequency for a given wave number was calculated from $\omega = kc$.

Figure 10 shows the results of the impedance measurements. Data scatter is larger for the higher wave numbers, so more data were collected for the higher wave numbers. The scatter in absorption has little effect on the computed acoustic fields, as will be shown later.

## ANALYSIS

### Source model

The acoustic source is modeled as an arbitrary point source with outgoing waves of one frequency. In spherical coordinates the following expansion of Hankel functions in the radial direction, Legendre functions in the elevation angle, and trigonometric functions in the azimuth angle represents any continuous acoustic field radiating from a point source as follows:

$$p(r,\theta,\varphi,k) = \sum_{n=0}^{\infty} \sum_{m=0}^{\infty} h_n^1(kr) \left[ A_n^m \cos(m\varphi) P_n^m \cos(\theta) + B_n^m \sin(m\varphi) P_n^m \cos(\theta) \right] \tag{6}$$

Values of the coefficients, $A_n^m$ and $B_n^m$ determine the amplitude, phase, and radiation pattern from the acoustic source. The source used in this experiment is designed to have cylindrical symmetry with

respect to the azimuthal angle, $\varphi$, so dependence on $\varphi$ is removed. Truncating the expansion produces an excellent approximation for real sources as long as all significant terms are kept.

$$p(r,\theta,\varphi,k) \approx \sum_{n=1}^{N} A_n h_n(kr) P_n(\cos\theta) \tag{7}$$

This acoustic source, radiation from an open tube with a diameter, which is small compared to the wavelength ($ka$ = 0.2511 to 0.7795), is expected to produce a simple radiation pattern that will be well represented with a small number of terms. Measurements (dB referenced to reference microphone close to source) in the anechoic chamber for transverses of $\varphi$ at several locations and one wave number ($ka$ = 0.6717) are shown in figure 11. The measurements are typical for all wave numbers tested; some show slightly more symmetry and some slightly less. For the angular sweeps close to the source ($d$ within 6 in. and $y$ within 1 in.; figs. 11(a)-11(d)) deviations from a constant value are small (range <2 dB). The pattern of deviations remains nearly constant for all wave numbers, but changes at different locations. Close to the source, deviations from a constant probably arise from small variations in microphone position from a constant radius: a deviation of 0.25 in. can change a measurement by about 1 dB. The microphone traverse contained some mechanical free play, especially when rotating the microphone about the $y$ axis, so the microphone position was known only to about 0.25 in. after the microphone had been moved several times. At large distances from the source ($d$ = 36 in.; figs. 11(e) and 11(f)), the range sometimes exceeds 2 dB. The pattern of deviation from a constant changes at the different locations and wave numbers. At 36 in. from the source, a 1-in. deviation in location can produce only about a 0.25-dB change in level, so variations observed must be due to other causes. Measurement error can contribute up to about 1 dB error (but is probably not that high). Reflections off the measurement apparatus, sections of the anechoic chamber covered with flat foam instead of wedges, and the floor grid probably contribute most of the variation at large distances. The pattern of variations with location and wave number measured during the test support the hypothesis that reflections cause the deviations from symmetry at large distances from the source.

The coefficients for modeling the acoustic source are determined by measuring the radiation pattern and fitting the coefficients with a least squares curve fit to the following equations:

$$\begin{aligned} p(r_1,\theta_1,k) &= \sum_{n=1}^{N} A_n h_n(kr_1) P_n(\cos\theta_1) \\ &\vdots \qquad\qquad \vdots \qquad\qquad \vdots \\ p(r_j,\theta_j,k) &= \sum_{n=1}^{N} A_n h_n(kr_j) P_n(\cos\theta_j) \end{aligned} \tag{8}$$

By forming a matrix equation

$$\begin{pmatrix} f_1^1 & \cdots & f_N^1 \\ \vdots & \ddots & \vdots \\ f_1^j & \cdots & f_N^j \end{pmatrix} \begin{pmatrix} A_1 \\ \vdots \\ A_N \end{pmatrix} = \begin{pmatrix} p_1 \\ \vdots \\ pj \end{pmatrix} \tag{9}$$

the unknown coefficients can be estimated by a least squares curve fit

$$\mathbf{f}^T\mathbf{f}\mathbf{A} = \mathbf{f}^T\mathbf{p} \tag{10}$$

Microphone positions and wave number determine the elements of **f**

$$f_n^i = h_n(kr_i)P_n(\cos\varphi_i) \tag{11}$$

and measurements determine the elements of **p**. Equation (10) was solved for the unknown coefficients by factoring the matrix into the product of upper and lower diagonal matrices, the equation was then solved with minimal computation (LU decomposition). Once the coefficients are known, the harmonic amplitude of the acoustic pressure can be estimated everywhere in free space by equation (7).

For each wave number evaluated, coefficients were determined for curve fits that had from one to eight terms and with various groups of measurements from the positions shown in figure 6. The set of 47 locations used for the curve fit consist of all the locations except the measurements made to check symmetry with respect to $\varphi$ and measurements made within 4 in. of the source. Symmetry check points were deleted so that those locations would not be unduly weighted. The acoustic field within two source diameters (4 in.) of the source does not match the point source expansion well due to the finite extent of the source. Deleting the closest points to the source improved the curve fit in regions where the duct wall is located. The model consists of a point singularity while the real source is distributed and finite, so the model is not a good description of the acoustic field of this source near the source. In all cases the error in the curve fit decreased when the number of terms was increased from one (monopole) to two (monopole plus dipole), but did not improve when the number of terms was increased further. Tables 1 to 12 show the measured pressures and the calculated pressures from the curve fit using two terms in the analytic expansion for each wave number investigated. The last two columns list the ratio of the measured amplitude to the curve fit amplitude and that ratio expressed on a decibel scale. For most data, the analytic curve fit is within 1 dB of the measurement. For less than 2% of the data, the difference between the analytic curve fit and measurement exceeds 2 dB. In these few cases the microphone is far from the source, the large difference does not extend to nearby microphones, and the largest differences appear in wave number pairs. Thus, the largest differences between curve fit and measurement are probably due to reflections.

## Duct Model

In order to study how a closed-test-section wind tunnel alters the sound field from an acoustic source, a simplified model containing the relevant physics and amenable to solution using a computer

was developed. References 1 and 11 detail the model's development and solution. This section briefly describes the model and outlines its mathematical development and solution.

The analytic model consists of a known acoustic source in an infinitely long rectangular duct. Acoustic radiation from the source and acoustic propagation in the duct are governed by the convected wave equation. An acoustic impedance boundary condition represents the walls, allowing for absorption of acoustic energy. For this validation study, the flow is zero.

This analytic model, shown in figure 12, contains many assumptions. The first assumption is that linear acoustic waves are propagating through a uniform subsonic flow. Uniform means the fluid has uniform mean temperature, density, pressure, velocity, and speed of sound everywhere in the duct. Linear acoustic theory requires the amplitude of the sound waves to be small so the wave will not form a shock as it propagates. Interaction of the sound field with turbulence or the wall boundary layer is not included. It has been shown (ref. 12) that boundary layers that are thin with respect to the wave length have little effect on sound propagation in low speed duct flows. The convected wave equation and a Fourier decomposition of the acoustic field can be used to model the propagation and reflection of low frequency harmonic noise in a wind tunnel. The second assumption is that the wind tunnel wall may be modeled by an acoustic impedance applied at each point on the wall. Absorption effects from the boundary layer could be included as a small correction in this simple boundary condition. This acoustic impedance boundary condition can therefore model a perfectly rigid wall, which reflects all the acoustic energy, or a lined wall which absorbs some of the sound energy. The point impedance boundary condition does not allow interaction of the acoustic field with any elastic wave propagation in the wall or acoustic propagation in the lining. The third assumption is that the wind tunnel does not change the acoustic impedance of the source. That is, the source radiates the same acoustic field inside the wind tunnel as it would in the same uniform flow without walls. The final assumption is that the wind tunnel is infinitely long and uniform. Changes in cross-sectional area or turns are not included. Turning vanes, turbulence screens, drive systems, and other tunnel components are not included. This allows acoustic outflow upstream and downstream boundary conditions to be developed in a straightforward manner.

The most severe restriction in this model is in not allowing an area change in the duct. The expected results of including an area change are to change, perhaps significantly, the reverberant field away from the source, but not to change the acoustic field in the volume near the source where the direct field dominates.

For the case with no uniform flow and one frequency, the Helmholtz equation

$$\left(\nabla^2 + k^2\right)p = f \tag{12}$$

governs the acoustic pressure with the acoustic pressure equal to

$$P = \Re\left(pe^{-i\omega t}\right) \tag{13}$$

A computational control surface surrounds the acoustic source and divides the duct into three regions as shown in figure 12. The control volume contains all known sources and extends to the walls and some

distance axially from the source. Two semi-infinite regions surround the control volume. Using equation (12), the free space Green's function for the Helmholtz equation, along with Green's second formula, an integro-differential equation relating the complex harmonic amplitude, $p$, its normal derivative, and the free space Green's function is developed:

$$p(\vec{r}) = \iiint G_h(\vec{r};\vec{r}_s) f(\vec{r}_s) dV + \iint \left[ -p(\vec{r}_s) \frac{\partial G_h(\vec{r};\vec{r}_s)}{\partial n} + G_h(\vec{r};\vec{r}_s) \frac{\partial p(\vec{r}_s)}{\partial n} \right] dS \tag{14}$$

with

$$G_h(\vec{r};\vec{r}_s) = \frac{-e^{ikR}}{4\pi R} \tag{15}$$

and

$$R = |\vec{r} - \vec{r}_s| \tag{16}$$

This equation is valid both on the control surface and within the control volume. The volume integral defines the complex harmonic amplitude produced by the source without any walls. The surface integral represents the effect of the walls and the two semi-infinite volumes on either side of the control volume.

The impedance boundary condition at the walls can be expressed as

$$\alpha p = \frac{\partial p}{\partial n} \tag{17}$$

with

$$\alpha = \frac{-ik\rho_0 c}{z} \tag{18}$$

This boundary condition replaces the normal derivative of the complex harmonic amplitude in the part of the surface integral covering the walls. At the boundaries with the semi-infinite regions, the acoustic field is restricted to the form of acoustic waves in a duct propagating away from the source represented as a modal series. For large values of $x$

$$p(x,y,z) = \sum_{j=1}^{\infty} e^{ik_j(x-x_{max})} \hat{p}_j^+ h_j(y,z) \approx \sum_{j=1}^{j_{max}} e^{ik_j(x-x_{max})} \hat{p}_j^+ h_j(y,z) \tag{19}$$

At the right-hand boundary of the control surface

$$p(x_{max},y,z) \approx \sum_{j=1}^{j_{max}} \hat{p}_j^+ h_j(y,z) \tag{20}$$

and

$$\frac{\partial p(x_{max},y,z)}{\partial n} \approx -\sum_{j=1}^{j_{max}} ik_j \hat{p}_j^+ h_j(y,z) \tag{21}$$

For small values of $x$

$$p(x,y,z) = \sum_{j=1}^{\infty} e^{-ik_j(x-x_{min})} \hat{p}_j^- h_j(y,z) \approx \sum_{j=1}^{j_{max}} e^{-ik_j(x-x_{min})} \hat{p}_j^- h_j(y,z) \tag{22}$$

At the left-hand boundary of the control surface

$$p(x_{min},y,z) \approx \sum_{j=1}^{j_{max}} \hat{p}_j^- h_j(y,z) \tag{23}$$

and

$$\frac{\partial p(x_{min},y,z)}{\partial n} \approx -\sum_{j=1}^{j_{max}} ik_j \hat{p}_j^- h_j(y,z) \tag{24}$$

Combining equations (12), (17), (18), (20), (21), (23), and (24) produces an equation which can be discretized and solved numerically.

$$p(\vec{r}) = \iiint G_h(\vec{r};\vec{r}_s) f(\vec{r}_s) dV + \iint \left[ -\frac{\partial G_h(\vec{r};\vec{r}_s)}{\partial n} + \alpha G_h(\vec{r};\vec{r}_s) \right] p(\vec{r}_s) dS_w$$

$$+ \iint -\frac{\partial G_h(\vec{r};\vec{r}_s)}{\partial n} \sum_{j=1}^{j_{max}} \hat{p}_j^+ h_j(y,z) - G_h(\vec{r};\vec{r}_s) \sum_{j=1}^{j_{max}} ik_j \hat{p}_j^+ h_j(y,z) dS_d$$

$$+ \iint -\frac{\partial G_h(\vec{r};\vec{r}_s)}{\partial n} \sum_{j=1}^{j_{max}} \hat{p}_j^- h_j(y,z) - G_h(\vec{r};\vec{r}_s) \sum_{j=1}^{j_{max}} ik_j \hat{p}_j^- h_j(y,z) dS_u \qquad (25)$$

Discretizing equation (25) produces a linear matrix equation for the unknowns of the complex harmonic pressure on the walled portion of the control surface and the modal amplitudes of the complex harmonic pressure on the outflow surfaces of the control volume. After these unknowns are determined with an LU decomposition of the matrix equation, the complex harmonic pressure can be evaluated anywhere in the control volumes with equation (25) and in the semi-infinite volumes with equation (19) or equation (22). This procedure was shown to be accurate in solving the convected wave equation for a known source in a rectangular duct with a point impedance boundary condition on the wall in reference 1.

The acoustic equation and solution method are valid for any frequency. Solutions for individual frequencies can be combined in a transformation to the time domain. Working in the frequency domain allows better modeling of the wall impedance, which naturally depends on frequency. Computations to solve this model are easiest for discrete, low frequency noise. Working in the frequency domain would be inefficient for broadband noise unless the problem were reformulated with a statistical energy method. The number of panels used to represent the walls that can be included in the analysis limits this method to low frequencies. To resolve the acoustic field with adequate fidelity, several panels are needed for one wavelength. The current program uses about nine panels per wavelength.

The panel method provides several important advantages over finite difference and finite element methods. The source is treated separately from the walls, so changing the source model is easy. A rotor and its rotating distributed noise sources cannot be easily embedded in the same simple coordinate system as a wind tunnel, thus, analytical methods are not of much use and generating a grid for both the rotor and the wind tunnel for finite difference methods would be difficult. The panel method used is very robust and contains no convergence, stability, or dissipation problems.

## Differences Between Analytic Model and Experiment

Although the experiment was specifically designed to match the analytical model, some idealized aspects of the source and duct models can not be created in the real world.

The analytic source model consists of a point source radiating outward with cylindrical symmetry (a radiation pattern from low-order poles) which is unaffected by the duct. The real source extends over a finite region. Measurements close to the actual distributed source do not match a relatively simple point

source model. Measurement locations closer than 4 in. (two source diameters) from the center of the source were not used in the analytic source model, thus allowing a much better fit to the source model. These differences should not be important to this test because they affect only the region closest to the source and thus do not affect the reflections. Measurements near the source reveal the symmetry assumption to be good (see fig. 11). The second order curve fit, monopole plus dipole, matched the measurements about as well as the eighth-order curve fit. The difference between the measurement and the curve fit of the analytical model subsequently used in the predictions is mostly less than 0.5 dB, but occasionally goes as high as 2.5 dB for a few locations and wave numbers. The form of the model is good for describing the radiated acoustic field. Measurements in and out of the duct (fig. 4) show the duct has little effect on the radiation from the source. In summary, the analytical source model simulates the source very well for this study.

The duct model assumes linear acoustic waves propagate in a uniform ideal gas in an infinitely long rectangular duct with side walls that reflect the sound like a point impedance. The acoustic waves are very linear since their amplitude is 80 to 90 dB. The air was uniform except for a small vertical temperature gradient. Data collection was restricted to a temperature difference of 1.0°F over the 5-ft distance between the upper and lower thermocouple in the duct. This maximum temperature difference corresponds to a less than 0.2% change in speed of sound and wave number. The duct is a finite length designed with nonreflecting ends. The source was placed asymmetrically in the duct so reflections from the ends would produce asymmetry in the measured data. Thus symmetry in the data indicates the ends of the duct effectively mimicked an infinitely long duct. The duct model does not include reflections off the source tube. In this study, the wave length is large compared to the source tube, so the tube is an inefficient scatterer of sound and thus is expected to have little effect on the sound field in the duct. It would therefore seem that the assumption that the walls act as a point impedance boundary to the sound is the most tenuous assumption used in the duct model design. It describes the surface as moving with a velocity proportional to the acoustic pressure, but does not account for any wave propagation in the surface. This boundary condition has been widely used by other researchers (refs. 2, 5, 8, and 10).

## RESULTS

### Reverberant Field

The test included 12 wave numbers grouped as six wave number pairs. Table 13 lists the basic characteristics of these wave numbers, including the number of modes used in the analytical model to represent the outflow boundary conditions and the number of modes which propagate in the duct as modeled. Figures 13 to 24 show the measurements and calculations for all 12 wave numbers. The horizontal plane containing the sampled locations is 1.0 in. in front of the source and centered on the source. The extent of the measurement domain is shown in figure 7. Contours show dB in the duct minus dB in the anechoic chamber. This parameter shows the effect of the reverberant field on the acoustic field in the duct; it is zero where the reflected field is not interfering, positive (thick contours) where the reflected field adds coherently, and negative (thin contours) where the reflected field combines destructively with the acoustic field radiating from the source. In each figure, the first plot (e.g., fig. 13(a)) shows the difference between measurements in the duct and in the anechoic chamber and the other three plots (e.g., figs. 13(b)-13(d)) show calculations of the reflected field with three different measured specific acoustic

impedances of the foam in order of increasing absorption. The values of the impedance boundary condition used correspond to the minimum (e.g., fig. 13(b)), median (e.g., fig. 13(c)), and maximum (e.g., fig. 13(d)) values of absorption measured in the impedance tube. Table 14 summarizes the normal absorption coefficients and specific acoustic impedances used in the calculations.

All measurements in the duct are nearly, but not exactly, symmetric about a vertical axis. A small amount of asymmetry can be expected from limitations to the accuracy of acoustic pressure measurements (estimated to be <1 dB) and microphone location measurements (estimated to be <0.5 in.). The calculations are very close to symmetric—small asymmetries here are due to asymmetries in the grid used in the computation. Calculations were made at the measured locations. The largest asymmetries consistently occur between 90° and 120° versus between 240° and 270°.

At the center of each figure, the contour is zero, or very close to zero, since it is very close to the source. In the region near the center, values of the contours are small in magnitude. In this region the reflected field produces little influence on the radiated acoustic field. Away from the center, contours take on many widely varying values where the direct and reflected acoustic fields combine. Local minima and maxima far from zero appear where the reflected modal acoustic field dominates. These figures will be discussed in more detail in the next section.

## Sensitivity Study for Test Parameters

Results of the correlation depend on the accuracy to which the parameters are known. This section reviews the influence on the results of small changes to the speed of sound, wall boundary conditions, source model, and locations of the microphones and the acoustic source.

**Speed of sound**– Sensitivity of results to the speed of sound were checked with measurements taken at different temperatures, and measurements and calculations at different wave numbers. To understand sensitivity of the correlation to temperature effects, measurements and calculations were compared in wave number pairs that differed by 1%. Measured values in data pairs are nearly identical (e.g., figs. 13(a) and 14(a) through figs. 23(a) and 24(a)). Computed values in data pairs are nearly identical (e.g., figs. 13(b) and 14(b), 13(c) and 14(c), 13(d) and 14(d) through figs. 23(d) and 24(d)). Any significant differences occur in regions of large acoustic pressure gradients. Maximum temperature gradients existing during the test could cause wave number variations about five times less than the 1% variation in the paired cases. Measurements taken in the duct at different temperatures (fig. 25) show the temperature not affecting the results significantly. This indicates temperature gradients during the test are insignificant for the results. Also, the temperature measurements used to determine the speed of sound and frequency for a wave number were sufficiently accurate for this study.

**Wall boundary conditions**– Sensitivity to wall boundary condition were checked using calculations with different boundary conditions (e.g., figs. 13(b)-13(d) to 24(b)-24(d)). Figures 26 and 27 show measurements and calculations for actual microphone locations in a plane 1.0 in. from the noise source for wave numbers $kl = 8.5221$ (fig. 26) and $kl = 22.7994$ (fig. 27). At lower wave numbers (figs. 13-16, and 26), changes due to scatter in boundary condition measurements are almost imperceptible; and at higher frequencies (figs. 19-24, and 27), changes are present near local minima with steep gradients. Measured values of impedance used in the calculations were sufficiently accurate for this study.

**Microphone and source locations**– Sensitivity to microphone location was tested with calculations at locations in a plane displaced 1.0 in. farther from the source for the first wave number. Figure 28(a) shows contours in the measurement plane $y = 1.0$ in. for $kl = 8.5221$ and $C_\alpha = 0.086$. Figure 28(b) shows contours in the plane $y = 2.0$ in. for the same calculation. The contours are essentially the same. Sensitivity to source location was checked with calculations for the source displaced 1.0 in. in each direction for the lowest frequency calculation with $kl = 8.5221$ and $C_\alpha = 0.086$. Figure 29(a) shows contours with the source moved down 1.0 in. and figure 29(b) shows contours with the source moved 1.0 in. closer to the wall. These two plots are very similar to the standard calculation shown in figure 28(a). Outside the areas of steep gradients, differences in the acoustic field are less than 1 dB. In areas of steep gradients, differences are as high as 20 dB, due to small displacements of the local minima. At larger wave numbers larger differences would probably occur. However uncertainty in the source and the microphone location fails to account for the significant differences between measured and computed acoustic fields in this study.

**Source model**– Sensitivity to small changes in the source model was tested with calculations. Figure 30(a) shows contours for calculations with $kl = 8.5221$ and $C_\alpha = 0.086$ with a source model derived with measurements from more microphone locations, adding locations very close to the source. Figure 30(b) shows contours for calculations with $kl = 8.5221$ and $C_\alpha = 0.086$ with a source model derived with four terms instead of two. These changes in source model within the analysis did not visibly affect the computed reflected field (compare with fig. 28(a)). The analytic source model represents the acoustic source accurately enough for this study.

## Comparison of Calculation to Measurement

All calculations (figs. 13-24) display the correct general characteristics of the acoustic field with no interference effects at the center, small effects surrounding the center, and large effects far from the center location 1 in. from the source. For the first four wave numbers (figs. 13-16) the calculations with different measured impedances for each wave number contain negligible differences at a given wave number. Absorptions measured in the impedance tube vary up to 10% for the first four wave numbers. For the seventh through tenth wave numbers (figs. 19-22), the calculations with different impedances and the same wave number vary a negligible amount except near deep minima with large gradients. Absorptions measured in the impedance tube vary up to 30% for these four wave numbers. For the two highest wave numbers (figs. 23 and 24) the calculated fields vary a significant amount for different impedances at one wave number. These absorptions measured in the impedance tube vary up to 40%. The acoustic fields are the most complicated.

The acoustic field in the duct can be divided into three regions. First, a localized region exists very near the source where the direct acoustic field of the source strongly dominates. Second, a near field region extends farther from the source where the reverberant field combines with the direct acoustic field thereby modifying the acoustic field up to a few dB in a smooth manner. In the near field, the acoustic pressure in the duct is above or below the acoustic pressure without the duct around the source, depending on whether the reflected acoustic field combines coherently or incoherently with the direct acoustic field from the source. The third region is a far field where the reverberant field dominates with a complicated acoustic field containing modal propagation in the duct. Calculations predicted the localized very near field very well in all cases studied. Calculations predicted the near field moderately well

for the lowest wave numbers, increasingly better as the wave number increased from $kl$ = 8.5221 to 23.0274, then not quite as well for the two largest wave numbers, $kl$ =26.1957 and 26.4577. At the lower wave numbers ($kl$ = 8.5221 to 16.2267), the value of the reverberant field was not always well predicted (figs. 13-17), whereas at the higher wave numbers ($kl$ = 16.8982 to 23.0274) the value of the reverberant field was well predicted (figs. 18-24) in the near field. Calculations predicted the far field very poorly for the lower wave numbers and moderately well for the higher wave numbers. At the lower wave numbers calculated acoustic fields have little resemblance to measured far fields. At larger wave numbers the calculations have some resemblance to the measurements.

Figures 26 and 27 illustrate in detail a comparison between the measurements and calculations for the first and ninth wave numbers ($kl$ = 8.5221 and 22.7994). All data, the measurements and the three calculations, are plotted along radial lines. Data for the first wave number (fig. 26) are representative of data for the first four wave numbers ($kl$ = 8.5221 to 12.5775). The data exhibit poor correlation between calculation and measurement except at the center point where the computations are nearly identical to the measurements. The three computations ($C_\alpha$ = 0.086, 0.088, and 0.091) are nearly identical to each other, so distinguishing the three curves in figure 26 is very difficult. Data for the ninth wave number (fig. 27) are representative of data for the seventh through tenth wave numbers ($kl$ = 19.6764 to 23.0274). Correlation between calculations and measurements is good (within 1 dB) from the center out to 9.0 in. (about one-half wave length) and remains good out to farther radii at some angles. The three computations ($C_\alpha$ = 0.161, 0.202, and 0.229) exhibit some differences. These differences remain small except at minima with steep gradients. For intermediate wave numbers, correlation is always good at the center and is good in a larger region about the center as the wave number (and absorption) increase. For the two largest wave numbers, correlations are good from the center out to 3 in. and good to poor at larger radii.

## DISCUSSION

### Comparison of Calculations with Measurements

This validation effort demonstrated that the analysis used in the calculations has some ability to predict the effect of an enclosure on the acoustic field of a known sound source. The analysis worked better for the higher wave numbers which exhibit a higher lining absorption for a given depth of foam. The model does not work well for low frequencies with low absorption, most likely because the point impedance boundary condition is a poor model of the influence of the wall on the acoustic field. The model requires more computer time and memory to calculate as the nondimensional product, $kl$, of the wave number and duct cross dimension increases. Thus this analysis becomes less useful for higher frequencies.

### Poor Correlation for Low Wave Numbers

Close to any real acoustic source relative to the wavelength, some of the velocity perturbation is out of phase with the pressure perturbation comprising the acoustic field. In addition, for sources of higher order than a monopole (more complicated), some of the velocity and pressure perturbations decay faster

than the inverse of the distance from the source. As acoustic energy propagates away from a source, the pressure and velocity perturbations become fully in phase and decay as the inverse of the distance. The region containing significant pressure and velocity perturbations which are either out of phase or decaying faster than the inverse of distance is called the acoustic near field. In the acoustic near field, the wave number times the distance ($kr$) is small. For a monopole source the ratio of the out-of-phase to in-phase velocity perturbation is $1/kr$.

Although the measured pressure of the acoustic source in the anechoic chamber decays as $1/r$ outside about two source diameters, the velocity perturbation derived from the curve fit to the measurements used in the analytical predictions contains out-of-phase components decaying as $1/r^2$. These out-of-phase components present in the analysis are a significant fraction of the perturbation velocity at some wall surfaces for the lowest wave numbers tested. The last column in table 13 lists the ratio of the out-of-phase to in-phase velocity perturbation for the monopole component of the acoustic source at the wall closest to the source. This distance from the source provides a conservative estimate for the out-of-phase to in-phase components along the wall. For the lowest two wave numbers, this ratio is about 0.36 and for the two largest wave numbers this ratio is about 0.12.

In acoustically absorbent linings, viscous fluid damping converts acoustic energy into heat as the acoustic waves interact with the fine structure of the lining. Predictions of acoustic interactions with the foam lining are based on an impedance model which assumes the pressure and velocity perturbations are in phase with a ratio of $\rho_0 c$ for the incident acoustic wave. Measurements of the impedance were done with a plane propagating wave, and thus do not account for an extra out-of-phase velocity perturbation in the incident wave. Thus the boundary condition used in this analysis does not model acoustic interactions at a wall in the near acoustic field. This may explain why correlation of predictions and measurements is so poor for the lowest wave numbers.

More detailed measurements of the acoustic field in the duct could be done to determine how the boundary was behaving. In particular, acoustic pressure and pressure gradient measurements at the walls of the duct would show if the wall impedance in place differed from the impedance measured in the standing wave tube. If the near field velocity caused these impedances to differ from far field measurements, the measured impedance would be different at different parts of the duct, depending on how far that wall was from the source. If the interaction of the acoustic near field with the boundary is the cause of poor correlation at small wave numbers, a different theory would need to be developed to analyze these cases.

## Asymmetry

The observed asymmetry may be due to the effect of humidity on the acoustic properties of the foam. In the wave numbers where the asymmetry appears, the asymmetry occurs in the region of 90° to 120° versus 240° to 270°. Measurements at 240° and 270° were acquired with a higher relative humidity (91%) than the other data (see table 15). According to Harris (ref. 13) and Morfey and Howell (ref. 14), this relative humidity produces a change in the speed of sound of only +0.3% above the speed with zero relative humidity, a change which is insignificant to the predictions in this study, so this mechanism cannot be expected to cause the asymmetry. According to the measurements of Harris (ref. 15), the excess attenuation is very small for the frequencies tested at the temperatures and relative humidity of

the measurement (see table 15). The effect of humidity on absorption of sound in air is very small, so this mechanism is probably not the cause of the asymmetry. To determine the additional effect of sound absorption in air, the absorption taking place between average bounces off the walls was added to the absorption from one bounce. Table 16 shows the additional absorption due to humidity is much smaller than the scatter in measured absorption. The only explanation left for the correlation between high humidity and asymmetry is that the higher humidity changed the acoustic absorption properties of the foam.

## Implications for Using Analysis

This study evaluated the validity of the analysis to predict wall reflection effects for low-frequency simple sources and simple ducts lined with foam that have low absorption of sound waves. The analysis works well at modeling the very near acoustic field local to the source. The analysis works well at modeling the near field for the higher frequencies ($kl > 16.8982$), but loses accuracy at the lower frequencies ($kl < 16.2267$). The analysis is not good at modeling the far field.

The analysis is able to predict the local region about a source where the reverberant field is minimal or causes variations of less than 1 dB. At absorption levels above 0.12 and for wave numbers with $kl > 16.8982$, the analysis did well at predicting the extent of the near field and the effect up to about 5 dB. This means the analysis is good for defining the volume where acoustic data can be taken with no or little interference from the wall reflections in a given wind tunnel setup, and for comparing the near field acoustic characteristics of different wind tunnels. Since the analysis can accurately predict the near field for wave numbers with $kl > 16.8982$ when the absorption level is above 0.12, it could be developed into a wind tunnel wall correction scheme for some situations. The analysis cannot provide accurate far field predictions where wall effects dominate the acoustic field, so it is not suitable for a far field correction scheme.

## Work Needed to Further Validate Analysis

This work examined the validity of the analytical model in an idealized experiment with low to medium frequencies ($kl = 8.5221$ to $26.4577$) and low normal absorptions ($C_\alpha = 0.088$ to $0.264$). More experimentation with moderate (up to 0.8) and high (up to 0.95) absorptions is needed to test the analysis in regions with higher absorptions. Since the predictions improved with increased wall absorption in this study, the analysis can be expected to do well at predicting the local and near acoustic fields for a simple source in a duct with moderate and high absorption.

Computer size and speed limit the practicality of the analysis to low frequencies since the memory size needed to run the program increases as $(kl)^4$ and the time needed to run the program increases as $(kl)^6$. The highest frequencies tested used significant computer resources on a Cray XMP (3 hours of CPU time and 16 megawords of solid state device memory for a single analysis). Currently, calculations on a Cray YMP can probably run cases up to $kl = 30$ to 35. If a similar study were repeated, measurements taken at higher frequencies could determine the accuracy of this model at higher frequencies. Taking data at a slightly lower frequency of $kl = 6.3$ matches 20 Hz in the Ames 40- by 80-Foot Wind Tunnel.

Testing the model in a real wind tunnel is a final step required to evaluate the usefulness of the model. The expected outcome of such a test is that the correlations would remain good for the local field, degrade slightly in the near field, and deteriorate in the far field.

## CONCLUSION AND RECOMMENDATIONS

A study was conducted to test the adequacy of linear acoustics theory with a point impedance boundary condition for modeling effects of walls on the acoustic field in ducts. The model was developed to study the effects of wall reflections on acoustic measurements in closed-test-section wind tunnels, especially low frequency helicopter noise. This study compares measurements and calculations of a simple acoustic source in a rectangular concrete duct that has foam on the walls and anechoic end terminations. Measuring acoustic pressure for six pairs of wave numbers (twelve wave numbers total) provides variation in frequency and absorption characteristics of the duct walls. The conclusions from this study are as follows.

1. The analysis accurately predicts the effect of lined duct walls on a source in a region local to the source for values of wave number times cross section dimension of $kl = 8.5$ to 26.5 and absorption coefficients of $C_\alpha = 0.088$ to 0.265. The local region is the volume closest to the source where reflections alter the acoustic field less than 1 dB. The analysis will probably predict well in the local region for absorptions up to 1.0.

2. The analysis accurately predicts the effect of lined duct walls on a source in the near field for values of wave number times cross section dimension of $kl = 16.9$ to 26.5 and absorptions of $C_\alpha = 0.124$ to 0.265. The near field is the volume surrounding the source where reflections smoothly alter the acoustic field less than 5 dB. The analysis did not work well for lower absorptions of $C_\alpha < 0.12$ or lower wave numbers of $kl < 16.9$. The analysis will probably predict well in the near field for higher absorptions with $kl > 16.9$.

3. This analysis provided poor predictions of the acoustic far field for low frequencies of $kl < 16.9$ and provided general characteristics but not accurate details of the far field for $kl > 16.9$. No application of this theory is likely to be adequate for accurately predicting the details of the acoustic far field in a duct where modal propagation dominates. The far field is the volume away from the source where the acoustic field is changed by the reflections so the field no longer resembles the field radiated by the source without boundaries. With many propagating modes far from the acoustic source, small changes in any mode shape or amplitude can change the details of the acoustic field significantly. This requires a very accurate computation of the duct acoustic modes which are sensitive to duct size, shape, and boundary, and a very accurate computational description of the free field of the acoustic source.

4. Sensitivity studies of small changes of the parameters in the analysis and test set up show that uncertainties in the parameters do not influence the degree of correlation. These parameters include speed of sound in the duct, microphone and source locations, source model, and wall lining absorption.

5. Humidity may effect the acoustic absorption properties of foam.

The recommendations from this study are:

1. The analytical model should be checked for its validity in predicting the near field with moderate and high levels of absorption.

2. Predictions from the analytical model should be validated with data obtained in a real wind tunnel with flow and a finite length test section.

3. To gain a better understanding of why the analysis fails at the low frequency, the acoustic field in the duct should be measured in more detail. Acoustic intensity measurements throughout the duct and impedance measurements at the walls might be very helpful.

4. If an analysis is needed to predict the near acoustic field of a low frequency source ($kl$ < about 17) in a duct a better model needs to be developed. In particular the point impedance boundary condition appears to be inadequate in this regime and a more accurate model needs to be developed.

## REFERENCES


1. Mosher, M: The Influence of Wind-Tunnel Walls on Discrete Frequency Noise. Ph.D. thesis, Stanford University, Stanford, Calif., June 1986.

2. Morse, P. M.; and Ingard, K. U.: Theoretical Acoustics. McGraw-Hill Book Co., New York, 1968.

3. Sabine, W.C.: Collected Papers on Acoustics. Dover Publications Inc., New York, 1964, republication from Harvard University Press, 1922.

4. Tyler, J. M.; and Sofrin, T. G.: Axial Flow Compressor Noise Studies. Preprint 345D SAE Natl. Aero. Meeting, New York, April 1961, pp. 309-322.

5. Rice, E. J.: Attenuation of Sound in Soft Walled Circular Ducts. NASA TM X-52442, May 1968.

6. Feiler, C. E.; and Rice, E. J.: Performance of Inlet Sound Suppressors. NASA SP-189, Oct., 1968, pp. 53-62.

7. Liu, H. K.; and Martenson, A. J.: Optimum Lining Configurations, NASA SP-207, July 1969, pp. 425-434.

8. Plumblee, H. E.: A Theoretical and Experimental Study of Sound Attenuation in an Annular Duct. AIAA Aeroacoustic Conference, Seattle WA, Oct., 1973, AIAA Paper 73-1005.

9. Plumblee, H. E.; Dean, P. D.; Wynne, G. A.; and Burrin, R. H.: Sound Propagation in and Radiation from Acoustically Lined Flow Ducts: A Comparison of Experiment and Theory. NASA CR-2306, Oct. 1973.

10. Eversmann, W.; and Baumeister, K.J: Modeling Wind Tunnel Effects on the Radiation Characteristics of Acoustic Sources. J. Aircraft, vol 23, no. 6, June 1986.

11. Mosher, M.: Effect of a Wind Tunnel on the Acoustic Field from Various Aeroacoustic Sources. AIAA Paper 86-1897, AIAA 10th Aeroacoustics Conference, Seattle, Wash., July 1986.

12. Eversman, E.; and Beckemeyer, R. J.: Transmission of Sound in Ducts with Thin S. ear Layers—Convergence to the Uniform Flow Case. J. Acoust. Soc. America, vol. 52, no. 1, July 1972, pp. 216-220.

13. Harris, C. M: Effects of Humidity on the Velocity of Sound in Air. J. Acoust. Soc. America, vol. 49, no. 3, part 2, 1971.

14. Morfey, C. L.; and Howell, G. P.: Speed of Sound in Air as a Function of Frequency and Humidity. J. Acoust. Soc. America, vol. 68, no. 5, Nov. 1980.

15. Harris, C. M: Absorption of Sound in Air Versus Humidity and Temperature. NASA CR-647, Jan. 1967.

Table 1. Curve fit for $k$ = 1.5065 l/ft.

| Mic | r | $\theta$, deg | $\phi$, deg | Measured pressure Real | Measured pressure Imag | Curve fit Real | Curve fit Imag | Ratio | Difference, dB |
|---|---|---|---|---|---|---|---|---|---|
| 23 | 4.000 | 0.0 | 90. | 0.361 | 0.286 | 0.373 | 0.272 | 1.033 | 0.285 |
| 24 | 5.657 | 45.0 | 90. | 0.243 | 0.492 | 0.241 | 0.499 | 0.990 | –0.090 |
| 25 | 8.944 | 63.4 | 90. | 0.148 | 0.929 | 0.143 | 0.934 | 0.970 | –0.264 |
| 22 | 4.472 | 63.4 | 90. | 0.312 | 0.358 | 0.298 | 0.374 | 0.955 | –0.402 |
| 29 | 4.472 | 153.4 | 90. | 0.228 | 0.534 | 0.231 | 0.528 | 1.013 | 0.112 |
| 140 | 6.324 | 161.6 | 90. | 0.167 | 0.784 | 0.171 | 0.762 | 1.028 | 0.237 |
| 19 | 6.083 | 80.5 | 90. | 0.208 | 0.578 | 0.207 | 0.603 | 0.995 | –0.041 |
| 30 | 36.496 | 170.5 | 90. | 0.028 | –1.718 | 0.033 | –1.741 | 1.179 | 1.430 |
| 31 | 37.108 | 166.0 | 90. | 0.028 | –1.624 | 0.033 | –1.666 | 1.144 | 1.166 |
| 32 | 37.947 | 161.6 | 90. | 0.028 | –1.523 | 0.032 | –1.563 | 1.122 | 1.002 |
| 33 | 39.000 | 157.4 | 90. | 0.028 | –1.371 | 0.031 | –1.433 | 1.111 | 0.914 |
| 34 | 40.249 | 153.4 | 90. | 0.028 | –1.237 | 0.030 | –1.280 | 1.084 | 0.701 |
| 35 | 41.677 | 149.7 | 90. | 0.027 | –1.072 | 0.029 | –1.104 | 1.072 | 0.605 |
| 36 | 43.267 | 146.3 | 90. | 0.027 | –0.919 | 0.028 | –0.908 | 1.047 | 0.403 |
| 37 | 45.000 | 143.1 | 90. | 0.026 | –0.738 | 0.027 | –0.693 | 1.051 | 0.430 |
| 38 | 46.861 | 140.2 | 90. | 0.024 | –0.522 | 0.026 | –0.463 | 1.061 | 0.513 |
| 39 | 48.837 | 137.5 | 90. | 0.023 | –0.307 | 0.025 | –0.219 | 1.100 | 0.824 |
| 40 | 50.912 | 135.0 | 90. | 0.021 | –0.051 | 0.024 | 0.039 | 1.141 | 1.144 |
| 63 | 13.417 | 26.6 | 90. | 0.094 | 1.506 | 0.097 | 1.452 | 1.036 | 0.311 |
| 64 | 15.000 | 36.9 | 90. | 0.083 | 1.694 | 0.086 | 1.659 | 1.029 | 0.250 |
| 65 | 16.970 | 45.0 | 90. | 0.074 | 1.955 | 0.075 | 1.915 | 1.022 | 0.187 |
| 66 | 19.209 | 51.3 | 90. | 0.065 | 2.245 | 0.066 | 2.204 | 1.017 | 0.150 |
| 67 | 21.633 | 56.3 | 90. | 0.057 | 2.556 | 0.058 | 2.515 | 1.013 | 0.113 |
| 68 | 24.187 | 60.3 | 90. | 0.051 | 2.875 | 0.052 | 2.841 | 1.006 | 0.051 |
| 69 | 26.833 | 63.4 | 90. | 0.046 | –3.067 | 0.047 | –3.105 | 1.019 | 0.166 |
| 70 | 29.546 | 66.0 | 90. | 0.041 | –2.720 | 0.042 | –2.760 | 1.021 | 0.178 |
| 71 | 32.311 | 68.2 | 90. | 0.038 | –2.372 | 0.038 | –2.409 | 1.010 | 0.087 |
| 72 | 35.114 | 70.0 | 90. | 0.036 | –2.045 | 0.035 | –2.054 | 0.995 | –0.048 |
| 73 | 37.947 | 71.6 | 90. | 0.033 | –1.756 | 0.033 | –1.696 | 0.976 | –0.208 |
| 41 | 24.739 | 166.0 | 90. | 0.043 | 3.128 | 0.048 | 3.066 | 1.117 | 0.958 |
| 42 | 25.632 | 159.4 | 90. | 0.043 | –3.042 | 0.047 | –3.109 | 1.079 | 0.660 |
| 43 | 26.833 | 153.4 | 90. | 0.041 | –2.872 | 0.045 | –2.963 | 1.086 | 0.718 |
| 44 | 28.302 | 148.0 | 90. | 0.039 | –2.678 | 0.043 | –2.784 | 1.092 | 0.767 |
| 45 | 30.000 | 143.1 | 90. | 0.037 | –2.452 | 0.040 | –2.576 | 1.094 | 0.780 |
| 46 | 31.891 | 138.8 | 90. | 0.036 | –2.233 | 0.038 | –2.344 | 1.061 | 0.513 |
| 47 | 33.941 | 135.0 | 90. | 0.035 | –1.976 | 0.036 | –2.091 | 1.028 | 0.238 |
| 48 | 36.125 | 131.6 | 90. | 0.033 | –1.725 | 0.034 | –1.822 | 1.019 | 0.168 |
| 49 | 38.419 | 128.7 | 90. | 0.031 | –1.440 | 0.032 | –1.538 | 1.011 | 0.099 |
| 50 | 40.804 | 126.0 | 90. | 0.029 | –1.138 | 0.030 | –1.243 | 1.024 | 0.208 |
| 51 | 43.267 | 123.7 | 90. | 0.028 | –0.851 | 0.028 | –0.937 | 1.006 | 0.054 |
| 52 | 6.083 | 80.5 | 90. | 0.208 | 0.593 | 0.207 | 0.603 | 0.993 | –0.064 |
| 53 | 9.056 | 83.7 | 90. | 0.136 | 0.974 | 0.137 | 0.981 | 1.006 | 0.053 |
| 54 | 12.042 | 85.2 | 90. | 0.102 | 1.347 | 0.103 | 1.359 | 1.003 | 0.026 |
| 55 | 15.033 | 86.2 | 90. | 0.082 | 1.704 | 0.082 | 1.736 | 0.999 | –0.007 |
| 56 | 18.028 | 86.8 | 90. | 0.067 | 2.081 | 0.068 | 2.113 | 1.015 | 0.130 |
| 57 | 21.024 | 87.3 | 90. | 0.058 | 2.461 | 0.059 | 2.490 | 1.017 | 0.150 |
| 58 | 24.021 | 87.6 | 90. | 0.049 | 2.837 | 0.051 | 2.867 | 1.049 | 0.417 |
| 59 | 27.019 | 87.9 | 90. | 0.043 | –3.052 | 0.046 | –3.039 | 1.055 | 0.462 |
| 60 | 30.017 | 88.1 | 90. | 0.038 | –2.673 | 0.041 | –2.663 | 1.071 | 0.597 |
| 61 | 33.015 | 88.3 | 90. | 0.035 | –2.287 | 0.037 | –2.286 | 1.051 | 0.435 |
| 62 | 36.014 | 88.4 | 90. | 0.032 | –1.905 | 0.034 | –1.909 | 1.056 | 0.477 |

Table 2. Curve fit for $k$ = 1.5216 l/ft.

| Mic | r | $\theta$, deg | $\phi$, deg | Measured pressure Real | Measured pressure Imag | Curve fit Real | Curve fit Imag | Ratio | Difference, dB |
|---|---|---|---|---|---|---|---|---|---|
| 23 | 4.000 | 0.0 | 90. | 0.360 | 0.286 | 0.372 | 0.275 | 1.034 | 0.287 |
| 24 | 5.657 | 45.0 | 90. | 0.242 | 0.493 | 0.240 | 0.505 | 0.993 | –0.061 |
| 25 | 8.944 | 63.4 | 90. | 0.148 | 0.954 | 0.143 | 0.944 | 0.964 | –0.320 |
| 22 | 4.472 | 63.4 | 90. | 0.312 | 0.363 | 0.297 | 0.379 | 0.953 | –0.421 |
| 29 | 4.472 | 153.4 | 90. | 0.227 | 0.540 | 0.230 | 0.536 | 1.014 | 0.117 |
| 140 | 6.324 | 161.6 | 90. | 0.166 | 0.793 | 0.171 | 0.772 | 1.029 | 0.247 |
| 19 | 6.083 | 80.5 | 90. | 0.208 | 0.586 | 0.206 | 0.610 | 0.991 | –0.080 |
| 30 | 36.496 | 170.5 | 90. | 0.028 | –1.701 | 0.033 | –1.694 | 1.199 | 1.578 |
| 31 | 37.108 | 166.0 | 90. | 0.028 | –1.603 | 0.033 | –1.618 | 1.163 | 1.313 |
| 32 | 37.947 | 161.6 | 90. | 0.028 | –1.496 | 0.032 | –1.514 | 1.143 | 1.161 |
| 33 | 39.000 | 157.4 | 90. | 0.027 | –1.314 | 0.031 | –1.383 | 1.134 | 1.093 |
| 34 | 40.249 | 153.4 | 90. | 0.028 | –1.180 | 0.030 | –1.228 | 1.090 | 0.746 |
| 35 | 41.677 | 149.7 | 90. | 0.027 | –1.000 | 0.029 | –1.050 | 1.073 | 0.609 |
| 36 | 43.267 | 146.3 | 90. | 0.027 | –0.862 | 0.028 | –0.852 | 1.036 | 0.311 |
| 37 | 45.000 | 143.1 | 90. | 0.026 | –0.695 | 0.027 | –0.636 | 1.038 | 0.324 |
| 38 | 46.861 | 140.2 | 90. | 0.025 | –0.486 | 0.026 | –0.404 | 1.041 | 0.346 |
| 39 | 48.837 | 137.5 | 90. | 0.023 | –0.267 | 0.025 | –0.156 | 1.085 | 0.710 |
| 40 | 50.912 | 135.0 | 90. | 0.022 | –0.027 | 0.024 | 0.103 | 1.107 | 0.886 |
| 63 | 13.417 | 26.6 | 90. | 0.097 | 1.518 | 0.097 | 1.468 | 1.003 | 0.028 |
| 64 | 15.000 | 36.9 | 90. | 0.084 | 1.713 | 0.086 | 1.677 | 1.024 | 0.209 |
| 65 | 16.970 | 45.0 | 90. | 0.074 | 1.978 | 0.075 | 1.935 | 1.016 | 0.136 |
| 66 | 19.209 | 51.3 | 90. | 0.065 | 2.270 | 0.066 | 2.227 | 1.012 | 0.108 |
| 67 | 21.633 | 56.3 | 90. | 0.058 | 2.583 | 0.058 | 2.542 | 1.004 | 0.039 |
| 68 | 24.187 | 60.3 | 90. | 0.052 | 2.915 | 0.052 | 2.871 | 0.991 | –0.078 |
| 69 | 26.833 | 63.4 | 90. | 0.046 | –3.029 | 0.046 | –3.072 | 1.019 | 0.160 |
| 70 | 29.546 | 66.0 | 90. | 0.041 | –2.679 | 0.042 | –2.723 | 1.021 | 0.184 |
| 71 | 32.311 | 68.2 | 90. | 0.038 | –2.323 | 0.038 | –2.369 | 1.009 | 0.081 |
| 72 | 35.114 | 70.0 | 90. | 0.036 | –1.991 | 0.035 | –2.011 | 0.991 | –0.081 |
| 73 | 37.947 | 71.6 | 90. | 0.033 | –1.697 | 0.033 | –1.649 | 0.974 | –0.228 |
| 41 | 24.739 | 166.0 | 90. | 0.042 | –3.119 | 0.048 | 3.098 | 1.141 | 1.145 |
| 42 | 25.632 | 159.4 | 90. | 0.044 | –3.008 | 0.047 | –3.076 | 1.061 | 0.516 |
| 43 | 26.833 | 153.4 | 90. | 0.041 | –2.834 | 0.045 | –2.928 | 1.082 | 0.688 |
| 44 | 28.302 | 148.0 | 90. | 0.039 | –2.636 | 0.042 | –2.747 | 1.092 | 0.762 |
| 45 | 30.000 | 143.1 | 90. | 0.037 | –2.398 | 0.040 | –2.537 | 1.097 | 0.801 |
| 46 | 31.891 | 138.8 | 90. | 0.036 | –2.194 | 0.038 | –2.303 | 1.062 | 0.520 |
| 47 | 33.941 | 135.0 | 90. | 0.035 | –1.931 | 0.036 | –2.048 | 1.021 | 0.184 |
| 48 | 36.125 | 131.6 | 90. | 0.033 | –1.686 | 0.034 | –1.776 | 1.013 | 0.114 |
| 49 | 38.419 | 128.7 | 90. | 0.031 | –1.392 | 0.032 | –1.489 | 1.008 | 0.066 |
| 50 | 40.804 | 126.0 | 90. | 0.029 | –1.071 | 0.030 | –1.191 | 1.031 | 0.263 |
| 51 | 43.267 | 123.7 | 90. | 0.028 | –0.793 | 0.028 | –0.882 | 0.995 | –0.040 |
| 52 | 6.083 | 80.5 | 90. | 0.210 | 0.602 | 0.206 | 0.610 | 0.981 | –0.168 |
| 53 | 9.056 | 83.7 | 90. | 0.137 | 0.986 | 0.137 | 0.992 | 1.001 | 0.011 |
| 54 | 12.042 | 85.2 | 90. | 0.103 | 1.366 | 0.102 | 1.374 | 0.996 | –0.033 |
| 55 | 15.033 | 86.2 | 90. | 0.083 | 1.723 | 0.082 | 1.755 | 0.988 | –0.104 |
| 56 | 18.028 | 86.8 | 90. | 0.068 | 2.106 | 0.068 | 2.136 | 1.003 | 0.028 |
| 57 | 21.024 | 87.3 | 90. | 0.059 | 2.492 | 0.058 | 2.516 | 0.995 | –0.046 |
| 58 | 24.021 | 87.6 | 90. | 0.049 | 2.860 | 0.051 | 2.897 | 1.040 | 0.342 |
| 59 | 27.019 | 87.9 | 90. | 0.043 | –3.017 | 0.045 | –3.005 | 1.046 | 0.391 |
| 60 | 30.017 | 88.1 | 90. | 0.038 | –2.647 | 0.041 | –2.625 | 1.075 | 0.628 |
| 61 | 33.015 | 88.3 | 90. | 0.035 | –2.256 | 0.037 | –2.244 | 1.055 | 0.466 |
| 62 | 36.014 | 88.4 | 90. | 0.032 | –1.862 | 0.034 | –1.864 | 1.065 | 0.549 |

Table 3. Curve fit for $k$ = 2.2014 l/ft.

| Mic | r | $\theta$, deg | $\phi$, deg | Measured pressure | | Curve fit | | Ratio | Difference, dB |
|---|---|---|---|---|---|---|---|---|---|
| | | | | Real | Imag | Real | Imag | | |
| 23 | 4.000 | 0.0 | 90. | 0.361 | 0.429 | 0.374 | 0.407 | 1.035 | 0.301 |
| 24 | 5.657 | 45.0 | 90. | 0.242 | 0.729 | 0.239 | 0.735 | 0.989 | –0.093 |
| 25 | 8.944 | 63.4 | 90. | 0.143 | 1.375 | 0.142 | 1.368 | 0.993 | –0.060 |
| 22 | 4.472 | 63.4 | 90. | 0.307 | 0.521 | 0.295 | 0.553 | 0.961 | –0.345 |
| 29 | 4.472 | 153.4 | 90. | 0.223 | 0.789 | 0.222 | 0.778 | 0.996 | –0.035 |
| 140 | 6.324 | 161.6 | 90. | 0.165 | 1.187 | 0.166 | 1.123 | 1.004 | 0.034 |
| 19 | 6.083 | 80.5 | 90. | 0.199 | 0.855 | 0.203 | 0.885 | 1.022 | 0.186 |
| 30 | 36.496 | 170.5 | 90. | 0.032 | 0.569 | 0.032 | 0.369 | 1.001 | 0.006 |
| 31 | 37.108 | 166.0 | 90. | 0.032 | 0.654 | 0.032 | 0.478 | 1.000 | –0.003 |
| 32 | 37.947 | 161.6 | 90. | 0.031 | 0.797 | 0.031 | 0.629 | 1.013 | 0.110 |
| 33 | 39.000 | 157.4 | 90. | 0.028 | 0.992 | 0.030 | 0.818 | 1.065 | 0.547 |
| 34 | 40.249 | 153.4 | 90. | 0.027 | 1.253 | 0.029 | 1.042 | 1.094 | 0.780 |
| 35 | 41.677 | 149.7 | 90. | 0.026 | 1.530 | 0.028 | 1.299 | 1.073 | 0.616 |
| 36 | 43.267 | 146.3 | 90. | 0.028 | 1.792 | 0.027 | 1.585 | 0.990 | –0.086 |
| 37 | 45.000 | 143.1 | 90. | 0.024 | 2.179 | 0.026 | 1.898 | 1.088 | 0.729 |
| 38 | 46.861 | 140.2 | 90. | 0.024 | 2.474 | 0.025 | 2.234 | 1.060 | 0.510 |
| 39 | 48.837 | 137.5 | 90. | 0.023 | 2.761 | 0.024 | 2.591 | 1.078 | 0.648 |
| 40 | 50.912 | 135.0 | 90. | 0.017 | 3.098 | 0.023 | 2.967 | 1.346 | 2.579 |
| 63 | 13.417 | 26.6 | 90. | 0.092 | 2.198 | 0.097 | 2.123 | 1.048 | 0.410 |
| 64 | 15.000 | 36.9 | 90. | 0.082 | 2.489 | 0.085 | 2.426 | 1.038 | 0.325 |
| 65 | 16.970 | 45.0 | 90. | 0.071 | 2.848 | 0.075 | 2.800 | 1.047 | 0.396 |
| 66 | 19.209 | 51.3 | 90. | 0.063 | –2.976 | 0.065 | –3.061 | 1.038 | 0.320 |
| 67 | 21.633 | 56.3 | 90. | 0.059 | –2.453 | 0.058 | –2.607 | 0.975 | –0.218 |
| 68 | 24.187 | 60.3 | 90. | 0.051 | –2.018 | 0.051 | –2.130 | 1.006 | 0.050 |
| 69 | 26.833 | 63.4 | 90. | 0.046 | –1.505 | 0.046 | –1.637 | 1.000 | 0.001 |
| 70 | 29.546 | 66.0 | 90. | 0.042 | –0.999 | 0.042 | –1.133 | 0.981 | –0.167 |
| 71 | 32.311 | 68.2 | 90. | 0.043 | –0.481 | 0.038 | –0.621 | 0.877 | –1.139 |
| 72 | 35.114 | 70.0 | 90. | 0.035 | 0.020 | 0.035 | –0.102 | 1.000 | –0.001 |
| 73 | 37.947 | 71.6 | 90. | 0.032 | 0.366 | 0.032 | 0.422 | 1.014 | 0.117 |
| 41 | 24.739 | 166.0 | 90. | 0.047 | –1.694 | 0.047 | –1.790 | 0.999 | –0.010 |
| 42 | 25.632 | 159.4 | 90. | 0.044 | –1.505 | 0.046 | –1.632 | 1.041 | 0.350 |
| 43 | 26.833 | 153.4 | 90. | 0.036 | –1.331 | 0.044 | –1.419 | 1.216 | 1.699 |
| 44 | 28.302 | 148.0 | 90. | 0.040 | –0.880 | 0.042 | –1.157 | 1.026 | 0.223 |
| 45 | 30.000 | 143.1 | 90. | 0.041 | –0.709 | 0.039 | –0.854 | 0.968 | –0.280 |
| 46 | 31.891 | 138.8 | 90. | 0.032 | –0.286 | 0.037 | –0.515 | 1.147 | 1.195 |
| 47 | 33.941 | 135.0 | 90. | 0.036 | 0.020 | 0.035 | –0.146 | 0.974 | –0.228 |
| 48 | 36.125 | 131.6 | 90. | 0.035 | 0.496 | 0.033 | 0.247 | 0.929 | –0.641 |
| 49 | 38.419 | 128.7 | 90. | 0.032 | 0.655 | 0.031 | 0.661 | 0.964 | –0.319 |
| 50 | 40.804 | 126.0 | 90. | 0.031 | 0.845 | 0.029 | 1.093 | 0.938 | –0.557 |
| 51 | 43.267 | 123.7 | 90. | 0.022 | 1.484 | 0.028 | 1.539 | 1.275 | 2.108 |
| 52 | 6.083 | 80.5 | 90. | 0.203 | 0.884 | 0.203 | 0.885 | 1.004 | 0.035 |
| 53 | 9.056 | 83.7 | 90. | 0.137 | 1.449 | 0.135 | 1.438 | 0.980 | –0.172 |
| 54 | 12.042 | 85.2 | 90. | 0.103 | 1.988 | 0.101 | 1.990 | 0.981 | –0.166 |
| 55 | 15.033 | 86.2 | 90. | 0.079 | 2.578 | 0.081 | 2.541 | 1.015 | 0.130 |
| 56 | 18.028 | 86.8 | 90. | 0.070 | 3.114 | 0.067 | 3.092 | 0.962 | –0.339 |
| 57 | 21.024 | 87.3 | 90. | 0.060 | –2.627 | 0.058 | –2.640 | 0.963 | –0.332 |
| 58 | 24.021 | 87.6 | 90. | 0.050 | –2.108 | 0.050 | –2.089 | 1.004 | 0.033 |
| 59 | 27.019 | 87.9 | 90. | 0.047 | –1.526 | 0.045 | –1.539 | 0.950 | –0.447 |
| 60 | 30.017 | 88.1 | 90. | 0.043 | –1.006 | 0.040 | –0.988 | 0.932 | –0.613 |
| 61 | 33.015 | 88.3 | 90. | 0.038 | –0.359 | 0.037 | –0.438 | 0.951 | –0.440 |
| 62 | 36.014 | 88.4 | 90. | 0.030 | 0.222 | 0.034 | 0.113 | 1.121 | 0.989 |

Table 4. Curve fit for $k$ = 2.2234 l/ft.

| Mic | r | $\theta$, deg | $\phi$, deg | Measured pressure Real | Measured pressure Imag | Curve fit Real | Curve fit Imag | Ratio | Difference, dB |
|---|---|---|---|---|---|---|---|---|---|
| 23 | 4.000 | 0.0 | 90. | 0.363 | 0.441 | 0.374 | 0.420 | 1.030 | 0.261 |
| 24 | 5.657 | 45.0 | 90. | 0.242 | 0.742 | 0.240 | 0.748 | 0.991 | –0.081 |
| 25 | 8.944 | 63.4 | 90. | 0.142 | 1.413 | 0.142 | 1.385 | 1.001 | 0.006 |
| 22 | 4.472 | 63.4 | 90. | 0.307 | 0.529 | 0.295 | 0.563 | 0.961 | –0.346 |
| 29 | 4.472 | 153.4 | 90. | 0.223 | 0.795 | 0.222 | 0.777 | 0.996 | –0.030 |
| 140 | 6.324 | 161.6 | 90. | 0.164 | 1.198 | 0.165 | 1.127 | 1.011 | 0.095 |
| 19 | 6.083 | 80.5 | 90. | 0.193 | 0.865 | 0.203 | 0.896 | 1.053 | 0.452 |
| 30 | 36.496 | 170.5 | 90. | 0.032 | 0.686 | 0.032 | 0.433 | 1.014 | 0.117 |
| 31 | 37.108 | 166.0 | 90. | 0.033 | 0.750 | 0.032 | 0.544 | 0.964 | –0.317 |
| 32 | 37.947 | 161.6 | 90. | 0.032 | 0.892 | 0.031 | 0.696 | 0.965 | –0.311 |
| 33 | 39.000 | 157.4 | 90. | 0.030 | 1.071 | 0.030 | 0.886 | 1.024 | 0.202 |
| 34 | 40.249 | 153.4 | 90. | 0.027 | 1.378 | 0.029 | 1.113 | 1.076 | 0.639 |
| 35 | 41.677 | 149.7 | 90. | 0.027 | 1.625 | 0.028 | 1.373 | 1.060 | 0.506 |
| 36 | 43.267 | 146.3 | 90. | 0.030 | 1.888 | 0.027 | 1.662 | 0.910 | –0.822 |
| 37 | 45.000 | 143.1 | 90. | 0.022 | 2.255 | 0.026 | 1.978 | 1.190 | 1.509 |
| 38 | 46.861 | 140.2 | 90. | 0.026 | 2.666 | 0.025 | 2.317 | 0.989 | –0.095 |
| 39 | 48.837 | 137.5 | 90. | 0.025 | 2.981 | 0.024 | 2.678 | 0.973 | –0.237 |
| 40 | 50.912 | 135.0 | 90. | 0.016 | –3.010 | 0.023 | 3.058 | 1.422 | 3.055 |
| 63 | 13.417 | 26.6 | 90. | 0.095 | 2.194 | 0.097 | 2.150 | 1.023 | 0.197 |
| 64 | 15.000 | 36.9 | 90. | 0.082 | 2.521 | 0.086 | 2.455 | 1.048 | 0.406 |
| 65 | 16.970 | 45.0 | 90. | 0.072 | 2.869 | 0.075 | 2.832 | 1.045 | 0.379 |
| 66 | 19.209 | 51.3 | 90. | 0.063 | –2.920 | 0.065 | –3.026 | 1.044 | 0.376 |
| 67 | 21.633 | 56.3 | 90. | 0.061 | –2.344 | 0.058 | –2.567 | 0.939 | –0.547 |
| 68 | 24.187 | 60.3 | 90. | 0.052 | –1.939 | 0.051 | –2.085 | 0.978 | –0.189 |
| 69 | 26.833 | 63.4 | 90. | 0.047 | –1.433 | 0.046 | –1.588 | 0.979 | –0.189 |
| 70 | 29.546 | 66.0 | 90. | 0.044 | –0.913 | 0.042 | –1.079 | 0.949 | –0.452 |
| 71 | 32.311 | 68.2 | 90. | 0.052 | –0.331 | 0.038 | –0.562 | 0.731 | –2.717 |
| 72 | 35.114 | 70.0 | 90. | 0.035 | 0.157 | 0.035 | –0.038 | 0.998 | –0.021 |
| 73 | 37.947 | 71.6 | 90. | 0.032 | 0.415 | 0.032 | 0.491 | 1.019 | 0.161 |
| 41 | 24.739 | 166.0 | 90. | 0.048 | –1.702 | 0.047 | –1.747 | 0.971 | –0.257 |
| 42 | 25.632 | 159.4 | 90. | 0.041 | –1.475 | 0.045 | –1.588 | 1.108 | 0.887 |
| 43 | 26.833 | 153.4 | 90. | 0.036 | –1.460 | 0.044 | –1.372 | 1.216 | 1.701 |
| 44 | 28.302 | 148.0 | 90. | 0.036 | –0.812 | 0.041 | –1.108 | 1.133 | 1.088 |
| 45 | 30.000 | 143.1 | 90. | 0.042 | –0.617 | 0.039 | –0.801 | 0.931 | –0.617 |
| 46 | 31.891 | 138.8 | 90. | 0.032 | –0.249 | 0.037 | –0.459 | 1.153 | 1.239 |
| 47 | 33.941 | 135.0 | 90. | 0.036 | 0.108 | 0.035 | –0.087 | 0.969 | –0.269 |
| 48 | 36.125 | 131.6 | 90. | 0.035 | 0.667 | 0.033 | 0.311 | 0.927 | –0.656 |
| 49 | 38.419 | 128.7 | 90. | 0.035 | 0.665 | 0.031 | 0.729 | 0.881 | –1.096 |
| 50 | 40.804 | 126.0 | 90. | 0.039 | 0.812 | 0.029 | 1.165 | 0.742 | –2.587 |
| 51 | 43.267 | 123.7 | 90. | 0.018 | 1.459 | 0.027 | 1.616 | 1.558 | 3.851 |
| 52 | 6.083 | 80.5 | 90. | 0.203 | 0.894 | 0.203 | 0.896 | 1.004 | 0.035 |
| 53 | 9.056 | 83.7 | 90. | 0.139 | 1.464 | 0.135 | 1.454 | 0.971 | –0.256 |
| 54 | 12.042 | 85.2 | 90. | 0.103 | 2.006 | 0.101 | 2.011 | 0.977 | –0.199 |
| 55 | 15.033 | 86.2 | 90. | 0.075 | 2.619 | 0.081 | 2.568 | 1.072 | 0.607 |
| 56 | 18.028 | 86.8 | 90. | 0.072 | –3.113 | 0.067 | 3.124 | 0.931 | –0.622 |
| 57 | 21.024 | 87.3 | 90. | 0.061 | –2.577 | 0.058 | –2.603 | 0.937 | –0.563 |
| 58 | 24.021 | 87.6 | 90. | 0.050 | –2.102 | 0.050 | –2.046 | 1.000 | 0.001 |
| 59 | 27.019 | 87.9 | 90. | 0.050 | –1.458 | 0.045 | –1.490 | 0.900 | –0.916 |
| 60 | 30.017 | 88.1 | 90. | 0.048 | –0.957 | 0.040 | –0.934 | 0.842 | –1.490 |
| 61 | 33.015 | 88.3 | 90. | 0.040 | –0.289 | 0.037 | –0.378 | 0.915 | –0.776 |
| 62 | 36.014 | 88.4 | 90. | 0.028 | 0.343 | 0.034 | 0.178 | 1.182 | 1.454 |

Table 5. Curve fit for $k$ = 2.8685 l/ft.

| Mic | r | $\theta$, deg | $\phi$, deg | Measured pressure Real | Measured pressure Imag | Curve fit Real | Curve fit Imag | Ratio | Difference, dB |
|---|---|---|---|---|---|---|---|---|---|
| 23 | 4.000 | 0.0 | 90. | 0.371 | 0.541 | 0.389 | 0.521 | 1.049 | 0.414 |
| 24 | 5.657 | 45.0 | 90. | 0.252 | 0.920 | 0.247 | 0.943 | 0.982 | –0.154 |
| 25 | 8.944 | 63.4 | 90. | 0.147 | 1.721 | 0.146 | 1.765 | 0.993 | –0.059 |
| 22 | 4.472 | 63.4 | 90. | 0.312 | 0.665 | 0.303 | 0.705 | 0.972 | –0.245 |
| 29 | 4.472 | 153.4 | 90. | 0.220 | 1.020 | 0.222 | 0.991 | 1.011 | 0.099 |
| 140 | 6.324 | 161.6 | 90. | 0.162 | 1.519 | 0.166 | 1.444 | 1.025 | 0.214 |
| 19 | 6.083 | 80.5 | 90. | 0.207 | 1.074 | 0.208 | 1.135 | 1.001 | 0.012 |
| 30 | 36.496 | 170.5 | 90. | 0.031 | 2.315 | 0.033 | 2.372 | 1.066 | 0.556 |
| 31 | 37.108 | 166.0 | 90. | 0.029 | 2.604 | 0.032 | 2.514 | 1.091 | 0.753 |
| 32 | 37.947 | 161.6 | 90. | 0.031 | 2.838 | 0.031 | 2.710 | 1.007 | 0.060 |
| 33 | 39.000 | 157.4 | 90. | 0.031 | 3.063 | 0.031 | 2.956 | 0.985 | –0.134 |
| 34 | 40.249 | 153.4 | 90. | 0.030 | –2.910 | 0.030 | –3.035 | 0.988 | –0.101 |
| 35 | 41.677 | 149.7 | 90. | 0.030 | –2.655 | 0.029 | –2.701 | 0.967 | –0.291 |
| 36 | 43.267 | 146.3 | 90. | 0.028 | –2.286 | 0.028 | –2.328 | 0.984 | –0.139 |
| 37 | 45.000 | 143.1 | 90. | 0.028 | –1.875 | 0.027 | –1.921 | 0.952 | –0.427 |
| 38 | 46.861 | 140.2 | 90. | 0.026 | –1.335 | 0.026 | –1.483 | 0.964 | –0.314 |
| 39 | 48.837 | 137.5 | 90. | 0.028 | –0.872 | 0.025 | –1.018 | 0.885 | –1.065 |
| 40 | 50.912 | 135.0 | 90. | 0.025 | –0.388 | 0.024 | –0.529 | 0.939 | –0.550 |
| 63 | 13.417 | 26.6 | 90. | 0.095 | 2.883 | 0.101 | 2.750 | 1.063 | 0.534 |
| 64 | 15.000 | 36.9 | 90. | 0.084 | –3.093 | 0.089 | –3.140 | 1.057 | 0.482 |
| 65 | 16.970 | 45.0 | 90. | 0.071 | –2.586 | 0.077 | –2.653 | 1.088 | 0.732 |
| 66 | 19.209 | 51.3 | 90. | 0.061 | –2.009 | 0.067 | –2.104 | 1.109 | 0.900 |
| 67 | 21.633 | 56.3 | 90. | 0.055 | –1.386 | 0.059 | –1.512 | 1.078 | 0.656 |
| 68 | 24.187 | 60.3 | 90. | 0.051 | –0.811 | 0.053 | –0.890 | 1.036 | 0.309 |
| 69 | 26.833 | 63.4 | 90. | 0.045 | –0.156 | 0.047 | –0.249 | 1.055 | 0.463 |
| 70 | 29.546 | 66.0 | 90. | 0.040 | 0.515 | 0.043 | 0.408 | 1.059 | 0.499 |
| 71 | 32.311 | 68.2 | 90. | 0.037 | 1.171 | 0.039 | 1.076 | 1.057 | 0.480 |
| 72 | 35.114 | 70.0 | 90. | 0.035 | 1.813 | 0.036 | 1.752 | 1.029 | 0.252 |
| 73 | 37.947 | 71.6 | 90. | 0.034 | 2.339 | 0.033 | 2.434 | 0.972 | –0.248 |
| 41 | 24.739 | 166.0 | 90. | 0.043 | –0.241 | 0.047 | –0.442 | 1.094 | 0.779 |
| 42 | 25.632 | 159.4 | 90. | 0.042 | –0.055 | 0.046 | –0.236 | 1.088 | 0.731 |
| 43 | 26.833 | 153.4 | 90. | 0.040 | 0.143 | 0.044 | 0.041 | 1.109 | 0.896 |
| 44 | 28.302 | 148.0 | 90. | 0.037 | 0.550 | 0.042 | 0.382 | 1.138 | 1.123 |
| 45 | 30.000 | 143.1 | 90. | 0.037 | 0.951 | 0.040 | 0.777 | 1.062 | 0.518 |
| 46 | 31.891 | 138.8 | 90. | 0.040 | 1.395 | 0.037 | 1.218 | 0.940 | –0.541 |
| 47 | 33.941 | 135.0 | 90. | 0.036 | 1.710 | 0.035 | 1.698 | 0.987 | –0.116 |
| 48 | 36.125 | 131.6 | 90. | 0.034 | 2.313 | 0.033 | 2.210 | 0.961 | –0.346 |
| 49 | 38.419 | 128.7 | 90. | 0.029 | 2.863 | 0.031 | 2.750 | 1.079 | 0.663 |
| 50 | 40.804 | 126.0 | 90. | 0.031 | –2.897 | 0.029 | –2.971 | 0.958 | –0.375 |
| 51 | 43.267 | 123.7 | 90. | 0.031 | –2.333 | 0.028 | –2.390 | 0.896 | –0.955 |
| 52 | 6.083 | 80.5 | 90. | 0.200 | 1.120 | 0.208 | 1.135 | 1.040 | 0.337 |
| 53 | 9.056 | 83.7 | 90. | 0.132 | 1.849 | 0.137 | 1.855 | 1.041 | 0.346 |
| 54 | 12.042 | 85.2 | 90. | 0.097 | 2.577 | 0.103 | 2.574 | 1.059 | 0.502 |
| 55 | 15.033 | 86.2 | 90. | 0.077 | –2.982 | 0.082 | –2.991 | 1.062 | 0.526 |
| 56 | 18.028 | 86.8 | 90. | 0.065 | –2.236 | 0.068 | –2.273 | 1.053 | 0.449 |
| 57 | 21.024 | 87.3 | 90. | 0.057 | –1.568 | 0.059 | –1.555 | 1.021 | 0.183 |
| 58 | 24.021 | 87.6 | 90. | 0.048 | –0.866 | 0.051 | –0.838 | 1.056 | 0.476 |
| 59 | 27.019 | 87.9 | 90. | 0.040 | –0.146 | 0.045 | –0.120 | 1.128 | 1.050 |
| 60 | 30.017 | 88.1 | 90. | 0.040 | 0.581 | 0.041 | 0.597 | 1.026 | 0.220 |
| 61 | 33.015 | 88.3 | 90. | 0.037 | 1.272 | 0.037 | 1.315 | 1.013 | 0.116 |
| 62 | 36.014 | 88.4 | 90. | 0.030 | 1.979 | 0.034 | 2.032 | 1.145 | 1.180 |

Table 6. Curve fit for $k$ = 2.8972 l/ft.

| Mic | r | $\theta$, deg | $\phi$, deg | Measured pressure Real | Measured pressure Imag | Curve fit Real | Curve fit Imag | Ratio | Difference, dB |
|---|---|---|---|---|---|---|---|---|---|
| 23 | 4.000 | 0.0 | 90. | 0.373 | 0.544 | 0.390 | 0.523 | 1.047 | 0.395 |
| 24 | 5.657 | 45.0 | 90. | 0.255 | 0.933 | 0.248 | 0.952 | 0.972 | –0.244 |
| 25 | 8.944 | 63.4 | 90. | 0.146 | 1.749 | 0.146 | 1.784 | 1.000 | 0.000 |
| 22 | 4.472 | 63.4 | 90. | 0.312 | 0.661 | 0.305 | 0.712 | 0.978 | –0.195 |
| 29 | 4.472 | 153.4 | 90. | 0.222 | 1.036 | 0.225 | 1.014 | 1.016 | 0.136 |
| 140 | 6.324 | 161.6 | 90. | 0.165 | 1.535 | 0.169 | 1.469 | 1.022 | 0.191 |
| 19 | 6.083 | 80.5 | 90. | 0.209 | 1.093 | 0.209 | 1.149 | 0.999 | –0.010 |
| 30 | 36.496 | 170.5 | 90. | 0.031 | 2.322 | 0.033 | 2.464 | 1.065 | 0.551 |
| 31 | 37.108 | 166.0 | 90. | 0.030 | 2.637 | 0.033 | 2.608 | 1.101 | 0.834 |
| 32 | 37.947 | 161.6 | 90. | 0.032 | 2.933 | 0.032 | 2.806 | 1.009 | 0.076 |
| 33 | 39.000 | 157.4 | 90. | 0.032 | –3.123 | 0.031 | 3.054 | 0.964 | –0.314 |
| 34 | 40.249 | 153.4 | 90. | 0.031 | –2.756 | 0.030 | –2.934 | 0.972 | –0.249 |
| 35 | 41.677 | 149.7 | 90. | 0.031 | –2.516 | 0.029 | –2.597 | 0.924 | –0.687 |
| 36 | 43.267 | 146.3 | 90. | 0.031 | –2.190 | 0.028 | –2.220 | 0.890 | –1.016 |
| 37 | 45.000 | 143.1 | 90. | 0.032 | –1.765 | 0.027 | –1.809 | 0.843 | –1.484 |
| 38 | 46.861 | 140.2 | 90. | 0.028 | –1.209 | 0.026 | –1.367 | 0.913 | –0.786 |
| 39 | 48.837 | 137.5 | 90. | 0.030 | –0.709 | 0.025 | –0.897 | 0.835 | –1.571 |
| 40 | 50.912 | 135.0 | 90. | 0.027 | –0.253 | 0.024 | –0.403 | 0.872 | –1.190 |
| 63 | 13.417 | 26.6 | 90. | 0.091 | 2.941 | 0.101 | 2.778 | 1.108 | 0.893 |
| 64 | 15.000 | 36.9 | 90. | 0.084 | –3.043 | 0.089 | –3.107 | 1.063 | 0.527 |
| 65 | 16.970 | 45.0 | 90. | 0.070 | –2.537 | 0.077 | –2.616 | 1.108 | 0.891 |
| 66 | 19.209 | 51.3 | 90. | 0.059 | –1.936 | 0.068 | –2.060 | 1.151 | 1.219 |
| 67 | 21.633 | 56.3 | 90. | 0.054 | –1.301 | 0.059 | –1.462 | 1.094 | 0.783 |
| 68 | 24.187 | 60.3 | 90. | 0.052 | –0.710 | 0.053 | –0.834 | 1.018 | 0.156 |
| 69 | 26.833 | 63.4 | 90. | 0.046 | –0.056 | 0.047 | –0.186 | 1.024 | 0.205 |
| 70 | 29.546 | 66.0 | 90. | 0.042 | 0.602 | 0.043 | 0.478 | 1.021 | 0.176 |
| 71 | 32.311 | 68.2 | 90. | 0.040 | 1.221 | 0.039 | 1.152 | 0.983 | –0.145 |
| 72 | 35.114 | 70.0 | 90. | 0.035 | 1.871 | 0.036 | 1.835 | 1.014 | 0.120 |
| 73 | 37.947 | 71.6 | 90. | 0.035 | 2.399 | 0.033 | 2.525 | 0.949 | –0.456 |
| 41 | 24.739 | 166.0 | 90. | 0.039 | –0.242 | 0.048 | –0.377 | 1.240 | 1.865 |
| 42 | 25.632 | 159.4 | 90. | 0.038 | –0.020 | 0.047 | –0.169 | 1.223 | 1.750 |
| 43 | 26.833 | 153.4 | 90. | 0.038 | 0.149 | 0.045 | 0.111 | 1.175 | 1.399 |
| 44 | 28.302 | 148.0 | 90. | 0.035 | 0.568 | 0.042 | 0.455 | 1.225 | 1.764 |
| 45 | 30.000 | 143.1 | 90. | 0.036 | 1.011 | 0.040 | 0.853 | 1.116 | 0.955 |
| 46 | 31.891 | 138.8 | 90. | 0.039 | 1.482 | 0.038 | 1.299 | 0.979 | –0.186 |
| 47 | 33.941 | 135.0 | 90. | 0.037 | 1.685 | 0.036 | 1.783 | 0.970 | –0.261 |
| 48 | 36.125 | 131.6 | 90. | 0.032 | 2.348 | 0.033 | 2.301 | 1.043 | 0.364 |
| 49 | 38.419 | 128.7 | 90. | 0.032 | 3.029 | 0.031 | 2.846 | 0.992 | –0.068 |
| 50 | 40.804 | 126.0 | 90. | 0.034 | –2.713 | 0.030 | –2.870 | 0.886 | –1.049 |
| 51 | 43.267 | 123.7 | 90. | 0.033 | –2.149 | 0.028 | –2.283 | 0.847 | –1.441 |
| 52 | 6.083 | 80.5 | 90. | 0.197 | 1.133 | 0.209 | 1.149 | 1.059 | 0.494 |
| 53 | 9.056 | 83.7 | 90. | 0.133 | 1.885 | 0.138 | 1.877 | 1.038 | 0.320 |
| 54 | 12.042 | 85.2 | 90. | 0.098 | 2.612 | 0.103 | 2.603 | 1.056 | 0.475 |
| 55 | 15.033 | 86.2 | 90. | 0.078 | –2.930 | 0.082 | –2.954 | 1.058 | 0.493 |
| 56 | 18.028 | 86.8 | 90. | 0.066 | –2.190 | 0.069 | –2.229 | 1.041 | 0.352 |
| 57 | 21.024 | 87.3 | 90. | 0.060 | –1.536 | 0.059 | –1.504 | 0.984 | –0.144 |
| 58 | 24.021 | 87.6 | 90. | 0.052 | –0.865 | 0.051 | –0.779 | 0.992 | –0.072 |
| 59 | 27.019 | 87.9 | 90. | 0.039 | –0.184 | 0.046 | –0.054 | 1.172 | 1.380 |
| 60 | 30.017 | 88.1 | 90. | 0.041 | 0.604 | 0.041 | 0.670 | 1.013 | 0.109 |
| 61 | 33.015 | 88.3 | 90. | 0.038 | 1.297 | 0.037 | 1.395 | 0.993 | –0.063 |
| 62 | 36.014 | 88.4 | 90. | 0.027 | 1.956 | 0.034 | 2.120 | 1.262 | 2.019 |

Table 7. Curve fit for $k$ = 3.4801 1/ft.

| Mic | r | $\theta$, deg | $\phi$, deg | Measured pressure Real | Measured pressure Imag | Curve fit Real | Curve fit Imag | Ratio | Difference, dB |
|---|---|---|---|---|---|---|---|---|---|
| 23 | 4.000 | 0.0 | 90. | 0.374 | 0.674 | 0.393 | 0.657 | 1.050 | 0.425 |
| 24 | 5.657 | 45.0 | 90. | 0.252 | 1.138 | 0.250 | 1.159 | 0.989 | –0.093 |
| 25 | 8.944 | 63.4 | 90. | 0.152 | 2.106 | 0.146 | 2.147 | 0.965 | –0.308 |
| 22 | 4.472 | 63.4 | 90. | 0.316 | 0.814 | 0.304 | 0.863 | 0.962 | –0.337 |
| 29 | 4.472 | 153.4 | 90. | 0.218 | 1.190 | 0.215 | 1.165 | 0.986 | –0.123 |
| 140 | 6.324 | 161.6 | 90. | 0.152 | 1.790 | 0.160 | 1.721 | 1.050 | 0.425 |
| 19 | 6.083 | 80.5 | 90. | 0.208 | 1.307 | 0.207 | 1.376 | 0.995 | –0.041 |
| 30 | 36.496 | 170.5 | 90. | 0.025 | –1.747 | 0.031 | –2.082 | 1.256 | 1.982 |
| 31 | 37.108 | 166.0 | 90. | 0.027 | –1.528 | 0.031 | –1.909 | 1.164 | 1.320 |
| 32 | 37.947 | 161.6 | 90. | 0.026 | –1.334 | 0.030 | –1.672 | 1.164 | 1.318 |
| 33 | 39.000 | 157.4 | 90. | 0.026 | –1.064 | 0.029 | –1.373 | 1.121 | 0.994 |
| 34 | 40.249 | 153.4 | 90. | 0.026 | –0.761 | 0.029 | –1.019 | 1.080 | 0.672 |
| 35 | 41.677 | 149.7 | 90. | 0.026 | –0.368 | 0.028 | –0.613 | 1.046 | 0.391 |
| 36 | 43.267 | 146.3 | 90. | 0.026 | 0.091 | 0.027 | –0.160 | 1.026 | 0.224 |
| 37 | 45.000 | 143.1 | 90. | 0.026 | 0.578 | 0.026 | 0.334 | 0.990 | –0.091 |
| 38 | 46.861 | 140.2 | 90. | 0.026 | 1.109 | 0.025 | 0.865 | 0.963 | –0.326 |
| 39 | 48.837 | 137.5 | 90. | 0.026 | 1.633 | 0.024 | 1.430 | 0.923 | –0.697 |
| 40 | 50.912 | 135.0 | 90. | 0.024 | 2.161 | 0.023 | 2.024 | 0.941 | –0.525 |
| 63 | 13.417 | 26.6 | 90. | 0.096 | –2.814 | 0.103 | –2.930 | 1.072 | 0.606 |
| 64 | 15.000 | 36.9 | 90. | 0.085 | –2.382 | 0.090 | –2.456 | 1.059 | 0.494 |
| 65 | 16.970 | 45.0 | 90. | 0.076 | –1.770 | 0.078 | –1.868 | 1.037 | 0.318 |
| 66 | 19.209 | 51.3 | 90. | 0.065 | –1.090 | 0.068 | –1.204 | 1.048 | 0.409 |
| 67 | 21.633 | 56.3 | 90. | 0.058 | –0.367 | 0.060 | –0.488 | 1.028 | 0.240 |
| 68 | 24.187 | 60.3 | 90. | 0.052 | 0.335 | 0.053 | 0.264 | 1.018 | 0.158 |
| 69 | 26.833 | 63.4 | 90. | 0.046 | 1.142 | 0.048 | 1.041 | 1.039 | 0.331 |
| 70 | 29.546 | 66.0 | 90. | 0.041 | 1.923 | 0.043 | 1.837 | 1.034 | 0.291 |
| 71 | 32.311 | 68.2 | 90. | 0.038 | 2.706 | 0.039 | 2.646 | 1.035 | 0.297 |
| 72 | 35.114 | 70.0 | 90. | 0.032 | –2.773 | 0.036 | –2.818 | 1.107 | 0.881 |
| 73 | 37.947 | 71.6 | 90. | 0.030 | –2.111 | 0.033 | –1.991 | 1.113 | 0.928 |
| 41 | 24.739 | 166.0 | 90. | 0.047 | 1.001 | 0.046 | 0.786 | 0.966 | –0.304 |
| 42 | 25.632 | 159.4 | 90. | 0.046 | 1.232 | 0.044 | 1.036 | 0.955 | –0.398 |
| 43 | 26.833 | 153.4 | 90. | 0.044 | 1.584 | 0.042 | 1.373 | 0.974 | –0.233 |
| 44 | 28.302 | 148.0 | 90. | 0.041 | 2.050 | 0.040 | 1.787 | 0.994 | –0.050 |
| 45 | 30.000 | 143.1 | 90. | 0.038 | 2.485 | 0.038 | 2.266 | 0.993 | –0.061 |
| 46 | 31.891 | 138.8 | 90. | 0.035 | 3.040 | 0.036 | 2.802 | 1.019 | 0.166 |
| 47 | 33.941 | 135.0 | 90. | 0.033 | –2.656 | 0.034 | –2.899 | 1.020 | 0.173 |
| 48 | 36.125 | 131.6 | 90. | 0.033 | –2.069 | 0.032 | –2.277 | 0.969 | –0.274 |
| 49 | 38.419 | 128.7 | 90. | 0.030 | –1.394 | 0.030 | –1.622 | 0.996 | –0.035 |
| 50 | 40.804 | 126.0 | 90. | 0.029 | –0.775 | 0.029 | –0.939 | 0.995 | –0.041 |
| 51 | 43.267 | 123.7 | 90. | 0.026 | –0.040 | 0.027 | –0.234 | 1.058 | 0.487 |
| 52 | 6.083 | 80.5 | 90. | 0.202 | 1.336 | 0.207 | 1.376 | 1.025 | 0.212 |
| 53 | 9.056 | 83.7 | 90. | 0.131 | 2.220 | 0.137 | 2.247 | 1.044 | 0.376 |
| 54 | 12.042 | 85.2 | 90. | 0.096 | 3.104 | 0.102 | 3.118 | 1.058 | 0.486 |
| 55 | 15.033 | 86.2 | 90. | 0.076 | –2.307 | 0.081 | –2.294 | 1.066 | 0.556 |
| 56 | 18.028 | 86.8 | 90. | 0.063 | –1.415 | 0.068 | –1.423 | 1.075 | 0.627 |
| 57 | 21.024 | 87.3 | 90. | 0.053 | –0.545 | 0.058 | –0.553 | 1.099 | 0.822 |
| 58 | 24.021 | 87.6 | 90. | 0.046 | 0.363 | 0.051 | 0.318 | 1.094 | 0.780 |
| 59 | 27.019 | 87.9 | 90. | 0.042 | 1.246 | 0.045 | 1.188 | 1.070 | 0.589 |
| 60 | 30.017 | 88.1 | 90. | 0.038 | 2.088 | 0.041 | 2.059 | 1.070 | 0.587 |
| 61 | 33.015 | 88.3 | 90. | 0.034 | 3.026 | 0.037 | 2.929 | 1.088 | 0.730 |
| 62 | 36.014 | 88.4 | 90. | 0.031 | –2.397 | 0.034 | –2.484 | 1.102 | 0.842 |

Table 8. Curve fit for $k$ = 3.5149 l/ft.

| Mic | r | $\theta$, deg | $\phi$, deg | Measured pressure Real | Measured pressure Imag | Curve fit Real | Curve fit Imag | Ratio | Difference, dB |
|---|---|---|---|---|---|---|---|---|---|
| 23 | 4.000 | 0.0 | 90. | 0.374 | 0.681 | 0.393 | 0.658 | 1.049 | 0.418 |
| 24 | 5.657 | 45.0 | 90. | 0.252 | 1.143 | 0.249 | 1.168 | 0.988 | –0.101 |
| 25 | 8.944 | 63.4 | 90. | 0.150 | 2.138 | 0.146 | 2.168 | 0.972 | –0.245 |
| 22 | 4.472 | 63.4 | 90. | 0.314 | 0.821 | 0.303 | 0.871 | 0.965 | –0.309 |
| 29 | 4.472 | 153.4 | 90. | 0.219 | 1.216 | 0.215 | 1.194 | 0.982 | –0.156 |
| 140 | 6.324 | 161.6 | 90. | 0.156 | 1.814 | 0.161 | 1.753 | 1.030 | 0.258 |
| 19 | 6.083 | 80.5 | 90. | 0.205 | 1.322 | 0.206 | 1.392 | 1.004 | 0.031 |
| 30 | 36.496 | 170.5 | 90. | 0.025 | –1.592 | 0.032 | –1.968 | 1.278 | 2.129 |
| 31 | 37.108 | 166.0 | 90. | 0.026 | –1.345 | 0.031 | –1.793 | 1.195 | 1.548 |
| 32 | 37.947 | 161.6 | 90. | 0.025 | –1.164 | 0.030 | –1.553 | 1.216 | 1.700 |
| 33 | 39.000 | 157.4 | 90. | 0.025 | –0.899 | 0.030 | –1.252 | 1.183 | 1.459 |
| 34 | 40.249 | 153.4 | 90. | 0.025 | –0.606 | 0.029 | –0.894 | 1.142 | 1.150 |
| 35 | 41.677 | 149.7 | 90. | 0.025 | –0.200 | 0.028 | –0.484 | 1.100 | 0.826 |
| 36 | 43.267 | 146.3 | 90. | 0.025 | 0.262 | 0.027 | –0.028 | 1.064 | 0.535 |
| 37 | 45.000 | 143.1 | 90. | 0.025 | 0.755 | 0.026 | 0.471 | 1.018 | 0.159 |
| 38 | 46.861 | 140.2 | 90. | 0.025 | 1.288 | 0.025 | 1.008 | 1.006 | 0.050 |
| 39 | 48.837 | 137.5 | 90. | 0.025 | 1.824 | 0.024 | 1.578 | 0.952 | –0.431 |
| 40 | 50.912 | 135.0 | 90. | 0.024 | 2.345 | 0.023 | 2.178 | 0.946 | –0.480 |
| 63 | 13.417 | 26.6 | 90. | 0.096 | –2.792 | 0.102 | –2.899 | 1.067 | 0.563 |
| 64 | 15.000 | 36.9 | 90. | 0.085 | –2.358 | 0.090 | –2.420 | 1.060 | 0.505 |
| 65 | 16.970 | 45.0 | 90. | 0.075 | –1.727 | 0.078 | –1.826 | 1.039 | 0.331 |
| 66 | 19.209 | 51.3 | 90. | 0.064 | –1.031 | 0.068 | –1.154 | 1.063 | 0.529 |
| 67 | 21.633 | 56.3 | 90. | 0.058 | –0.284 | 0.060 | –0.430 | 1.034 | 0.293 |
| 68 | 24.187 | 60.3 | 90. | 0.052 | 0.423 | 0.053 | 0.330 | 1.016 | 0.137 |
| 69 | 26.833 | 63.4 | 90. | 0.046 | 1.247 | 0.047 | 1.115 | 1.030 | 0.253 |
| 70 | 29.546 | 66.0 | 90. | 0.042 | 2.026 | 0.043 | 1.919 | 1.011 | 0.093 |
| 71 | 32.311 | 68.2 | 90. | 0.039 | 2.810 | 0.039 | 2.737 | 0.998 | –0.016 |
| 72 | 35.114 | 70.0 | 90. | 0.033 | –2.655 | 0.036 | –2.719 | 1.089 | 0.742 |
| 73 | 37.947 | 71.6 | 90. | 0.031 | –2.005 | 0.033 | –1.883 | 1.072 | 0.606 |
| 41 | 24.739 | 166.0 | 90. | 0.046 | 1.106 | 0.046 | 0.867 | 0.993 | –0.059 |
| 42 | 25.632 | 159.4 | 90. | 0.047 | 1.342 | 0.044 | 1.119 | 0.952 | –0.427 |
| 43 | 26.833 | 153.4 | 90. | 0.043 | 1.711 | 0.043 | 1.459 | 0.992 | –0.070 |
| 44 | 28.302 | 148.0 | 90. | 0.039 | 2.178 | 0.041 | 1.877 | 1.026 | 0.222 |
| 45 | 30.000 | 143.1 | 90. | 0.039 | 2.617 | 0.038 | 2.361 | 0.987 | –0.109 |
| 46 | 31.891 | 138.8 | 90. | 0.035 | –3.109 | 0.036 | 2.902 | 1.042 | 0.360 |
| 47 | 33.941 | 135.0 | 90. | 0.033 | –2.519 | 0.034 | –2.794 | 1.042 | 0.357 |
| 48 | 36.125 | 131.6 | 90. | 0.034 | –1.912 | 0.032 | –2.165 | 0.951 | –0.432 |
| 49 | 38.419 | 128.7 | 90. | 0.030 | –1.235 | 0.030 | –1.504 | 0.997 | –0.026 |
| 50 | 40.804 | 126.0 | 90. | 0.030 | –0.590 | 0.029 | –0.815 | 0.942 | –0.516 |
| 51 | 43.267 | 123.7 | 90. | 0.026 | 0.109 | 0.027 | –0.103 | 1.052 | 0.444 |
| 52 | 6.083 | 80.5 | 90. | 0.201 | 1.354 | 0.206 | 1.392 | 1.025 | 0.210 |
| 53 | 9.056 | 83.7 | 90. | 0.131 | 2.247 | 0.136 | 2.272 | 1.039 | 0.332 |
| 54 | 12.042 | 85.2 | 90. | 0.097 | –3.134 | 0.102 | –3.131 | 1.046 | 0.392 |
| 55 | 15.033 | 86.2 | 90. | 0.077 | –2.253 | 0.081 | –2.251 | 1.056 | 0.474 |
| 56 | 18.028 | 86.8 | 90. | 0.064 | –1.358 | 0.068 | –1.371 | 1.053 | 0.450 |
| 57 | 21.024 | 87.3 | 90. | 0.053 | –0.509 | 0.058 | –0.492 | 1.085 | 0.706 |
| 58 | 24.021 | 87.6 | 90. | 0.047 | 0.412 | 0.051 | 0.388 | 1.070 | 0.591 |
| 59 | 27.019 | 87.9 | 90. | 0.042 | 1.318 | 0.045 | 1.267 | 1.060 | 0.502 |
| 60 | 30.017 | 88.1 | 90. | 0.038 | 2.152 | 0.041 | 2.146 | 1.060 | 0.505 |
| 61 | 33.015 | 88.3 | 90. | 0.033 | 3.131 | 0.037 | 3.025 | 1.107 | 0.883 |
| 62 | 36.014 | 88.4 | 90. | 0.030 | –2.298 | 0.034 | –2.379 | 1.118 | 0.972 |

Table 9. Curve fit for $k$ = 4.0304 l/ft.

| Mic | r | $\theta$, deg | $\phi$, deg | Measured pressure Real | Measured pressure Imag | Curve fit Real | Curve fit Imag | Ratio | Difference, dB |
|---|---|---|---|---|---|---|---|---|---|
| 23 | 4.000 | 0.0 | 90. | 0.375 | 0.786 | 0.395 | 0.777 | 1.052 | 0.442 |
| 24 | 5.657 | 45.0 | 90. | 0.253 | 1.328 | 0.251 | 1.352 | 0.994 | –0.054 |
| 25 | 8.944 | 63.4 | 90. | 0.153 | 2.451 | 0.147 | 2.489 | 0.964 | –0.319 |
| 22 | 4.472 | 63.4 | 90. | 0.318 | 0.950 | 0.304 | 1.003 | 0.956 | –0.393 |
| 29 | 4.472 | 153.4 | 90. | 0.219 | 1.376 | 0.211 | 1.311 | 0.964 | –0.320 |
| 140 | 6.324 | 161.6 | 90. | 0.151 | 2.059 | 0.157 | 1.958 | 1.040 | 0.339 |
| 19 | 6.083 | 80.5 | 90. | 0.209 | 1.524 | 0.207 | 1.589 | 0.990 | –0.084 |
| 30 | 36.496 | 170.5 | 90. | 0.038 | –0.101 | 0.031 | –0.453 | 0.798 | –1.961 |
| 31 | 37.108 | 166.0 | 90. | 0.034 | 0.101 | 0.030 | –0.252 | 0.891 | –1.005 |
| 32 | 37.947 | 161.6 | 90. | 0.032 | 0.339 | 0.029 | 0.023 | 0.907 | –0.851 |
| 33 | 39.000 | 157.4 | 90. | 0.030 | 0.675 | 0.029 | 0.369 | 0.942 | –0.522 |
| 34 | 40.249 | 153.4 | 90. | 0.029 | 1.063 | 0.028 | 0.780 | 0.976 | –0.207 |
| 35 | 41.677 | 149.7 | 90. | 0.027 | 1.526 | 0.027 | 1.251 | 0.994 | –0.051 |
| 36 | 43.267 | 146.3 | 90. | 0.025 | 2.036 | 0.026 | 1.775 | 1.024 | 0.204 |
| 37 | 45.000 | 143.1 | 90. | 0.024 | 2.616 | 0.025 | 2.348 | 1.055 | 0.462 |
| 38 | 46.861 | 140.2 | 90. | 0.023 | 3.127 | 0.024 | 2.964 | 1.035 | 0.302 |
| 39 | 48.837 | 137.5 | 90. | 0.022 | –2.529 | 0.023 | –2.664 | 1.049 | 0.412 |
| 40 | 50.912 | 135.0 | 90. | 0.017 | –1.953 | 0.022 | –1.976 | 1.319 | 2.404 |
| 63 | 13.417 | 26.6 | 90. | 0.097 | –2.206 | 0.104 | –2.384 | 1.076 | 0.633 |
| 64 | 15.000 | 36.9 | 90. | 0.087 | –1.715 | 0.092 | –1.837 | 1.055 | 0.464 |
| 65 | 16.970 | 45.0 | 90. | 0.076 | –1.044 | 0.079 | –1.159 | 1.043 | 0.367 |
| 66 | 19.209 | 51.3 | 90. | 0.068 | –0.262 | 0.069 | –0.392 | 1.019 | 0.160 |
| 67 | 21.633 | 56.3 | 90. | 0.060 | 0.538 | 0.061 | 0.435 | 1.011 | 0.092 |
| 68 | 24.187 | 60.3 | 90. | 0.052 | 1.353 | 0.054 | 1.305 | 1.021 | 0.184 |
| 69 | 26.833 | 63.4 | 90. | 0.046 | 2.304 | 0.048 | 2.203 | 1.042 | 0.354 |
| 70 | 29.546 | 66.0 | 90. | 0.040 | –3.055 | 0.043 | 3.124 | 1.089 | 0.740 |
| 71 | 32.311 | 68.2 | 90. | 0.037 | –2.125 | 0.039 | –2.224 | 1.074 | 0.624 |
| 72 | 35.114 | 70.0 | 90. | 0.034 | –1.159 | 0.036 | –1.275 | 1.074 | 0.617 |
| 73 | 37.947 | 71.6 | 90. | 0.032 | –0.350 | 0.033 | –0.318 | 1.051 | 0.432 |
| 41 | 24.739 | 166.0 | 90. | 0.038 | 2.216 | 0.045 | 1.875 | 1.174 | 1.390 |
| 42 | 25.632 | 159.4 | 90. | 0.041 | 2.405 | 0.043 | 2.165 | 1.061 | 0.513 |
| 43 | 26.833 | 153.4 | 90. | 0.036 | 2.833 | 0.041 | 2.556 | 1.157 | 1.267 |
| 44 | 28.302 | 148.0 | 90. | 0.038 | –2.966 | 0.039 | 3.036 | 1.037 | 0.315 |
| 45 | 30.000 | 143.1 | 90. | 0.037 | –2.484 | 0.037 | –2.691 | 0.998 | –0.016 |
| 46 | 31.891 | 138.8 | 90. | 0.036 | –1.838 | 0.035 | –2.069 | 0.979 | –0.187 |
| 47 | 33.941 | 135.0 | 90. | 0.037 | –1.152 | 0.033 | –1.394 | 0.905 | –0.869 |
| 48 | 36.125 | 131.6 | 90. | 0.034 | –0.516 | 0.031 | –0.673 | 0.922 | –0.703 |
| 49 | 38.419 | 128.7 | 90. | 0.033 | 0.299 | 0.030 | 0.087 | 0.897 | –0.946 |
| 50 | 40.804 | 126.0 | 90. | 0.031 | 1.007 | 0.028 | 0.878 | 0.919 | –0.730 |
| 51 | 43.267 | 123.7 | 90. | 0.030 | 1.767 | 0.027 | 1.695 | 0.872 | –1.195 |
| 52 | 6.083 | 80.5 | 90. | 0.204 | 1.538 | 0.207 | 1.589 | 1.010 | 0.088 |
| 53 | 9.056 | 83.7 | 90. | 0.132 | 2.558 | 0.136 | 2.597 | 1.036 | 0.306 |
| 54 | 12.042 | 85.2 | 90. | 0.095 | –2.702 | 0.102 | –2.678 | 1.068 | 0.575 |
| 55 | 15.033 | 86.2 | 90. | 0.077 | –1.702 | 0.081 | –1.670 | 1.057 | 0.484 |
| 56 | 18.028 | 86.8 | 90. | 0.064 | –0.681 | 0.068 | –0.662 | 1.061 | 0.511 |
| 57 | 21.024 | 87.3 | 90. | 0.054 | 0.324 | 0.058 | 0.346 | 1.076 | 0.636 |
| 58 | 24.021 | 87.6 | 90. | 0.047 | 1.381 | 0.051 | 1.354 | 1.081 | 0.674 |
| 59 | 27.019 | 87.9 | 90. | 0.040 | 2.392 | 0.045 | 2.362 | 1.138 | 1.123 |
| 60 | 30.017 | 88.1 | 90. | 0.035 | –2.914 | 0.041 | –2.913 | 1.158 | 1.273 |
| 61 | 33.015 | 88.3 | 90. | 0.033 | –1.780 | 0.037 | –1.905 | 1.110 | 0.904 |
| 62 | 36.014 | 88.4 | 90. | 0.033 | –0.787 | 0.034 | –0.897 | 1.019 | 0.161 |

Table 10. Curve fit for $k$ = 4.0707 l/ft.

| Mic | r | $\theta$, deg | $\phi$, deg | Measured pressure Real | Measured pressure Imag | Curve fit Real | Curve fit Imag | Ratio | Difference, dB |
|---|---|---|---|---|---|---|---|---|---|
| 23 | 4.000 | 0.0 | 90. | 0.375 | 0.788 | 0.395 | 0.782 | 1.052 | 0.440 |
| 24 | 5.657 | 45.0 | 90. | 0.253 | 1.336 | 0.252 | 1.364 | 0.994 | –0.051 |
| 25 | 8.944 | 63.4 | 90. | 0.152 | 2.473 | 0.147 | 2.513 | 0.969 | –0.272 |
| 22 | 4.472 | 63.4 | 90. | 0.318 | 0.961 | 0.305 | 1.012 | 0.958 | –0.372 |
| 29 | 4.472 | 153.4 | 90. | 0.220 | 1.392 | 0.213 | 1.323 | 0.969 | –0.276 |
| 140 | 6.324 | 161.6 | 90. | 0.152 | 2.076 | 0.158 | 1.975 | 1.038 | 0.324 |
| 19 | 6.083 | 80.5 | 90. | 0.209 | 1.538 | 0.207 | 1.604 | 0.993 | –0.063 |
| 30 | 36.496 | 170.5 | 90. | 0.041 | 0.109 | 0.031 | –0.336 | 0.757 | –2.419 |
| 31 | 37.108 | 166.0 | 90. | 0.035 | 0.243 | 0.030 | –0.133 | 0.876 | –1.151 |
| 32 | 37.947 | 161.6 | 90. | 0.033 | 0.477 | 0.030 | 0.145 | 0.885 | –1.058 |
| 33 | 39.000 | 157.4 | 90. | 0.031 | 0.812 | 0.029 | 0.495 | 0.919 | –0.732 |
| 34 | 40.249 | 153.4 | 90. | 0.029 | 1.203 | 0.028 | 0.910 | 0.957 | –0.384 |
| 35 | 41.677 | 149.7 | 90. | 0.028 | 1.678 | 0.027 | 1.385 | 0.976 | –0.211 |
| 36 | 43.267 | 146.3 | 90. | 0.026 | 2.181 | 0.026 | 1.915 | 1.006 | 0.056 |
| 37 | 45.000 | 143.1 | 90. | 0.024 | 2.765 | 0.025 | 2.494 | 1.047 | 0.397 |
| 38 | 46.861 | 140.2 | 90. | 0.024 | –2.979 | 0.024 | 3.116 | 1.019 | 0.161 |
| 39 | 48.837 | 137.5 | 90. | 0.023 | –2.345 | 0.023 | –2.506 | 1.019 | 0.167 |
| 40 | 50.912 | 135.0 | 90. | 0.018 | –1.886 | 0.022 | –1.811 | 1.231 | 1.802 |
| 63 | 13.417 | 26.6 | 90. | 0.097 | –2.154 | 0.105 | –2.345 | 1.079 | 0.664 |
| 64 | 15.000 | 36.9 | 90. | 0.086 | –1.664 | 0.092 | –1.793 | 1.063 | 0.529 |
| 65 | 16.970 | 45.0 | 90. | 0.076 | –1.006 | 0.080 | –1.108 | 1.044 | 0.373 |
| 66 | 19.209 | 51.3 | 90. | 0.067 | –0.215 | 0.069 | –0.334 | 1.030 | 0.255 |
| 67 | 21.633 | 56.3 | 90. | 0.060 | 0.604 | 0.061 | 0.502 | 1.015 | 0.131 |
| 68 | 24.187 | 60.3 | 90. | 0.052 | 1.427 | 0.054 | 1.380 | 1.026 | 0.220 |
| 69 | 26.833 | 63.4 | 90. | 0.046 | 2.396 | 0.048 | 2.288 | 1.052 | 0.440 |
| 70 | 29.546 | 66.0 | 90. | 0.040 | –2.972 | 0.043 | –3.066 | 1.092 | 0.763 |
| 71 | 32.311 | 68.2 | 90. | 0.037 | –2.024 | 0.039 | –2.121 | 1.075 | 0.627 |
| 72 | 35.114 | 70.0 | 90. | 0.034 | –1.041 | 0.036 | –1.163 | 1.073 | 0.609 |
| 73 | 37.947 | 71.6 | 90. | 0.031 | –0.255 | 0.033 | –0.196 | 1.070 | 0.591 |
| 41 | 24.739 | 166.0 | 90. | 0.034 | 2.282 | 0.045 | 1.953 | 1.325 | 2.445 |
| 42 | 25.632 | 159.4 | 90. | 0.041 | 2.523 | 0.043 | 2.246 | 1.056 | 0.473 |
| 43 | 26.833 | 153.4 | 90. | 0.034 | 2.909 | 0.042 | 2.641 | 1.241 | 1.876 |
| 44 | 28.302 | 148.0 | 90. | 0.036 | –2.867 | 0.040 | 3.126 | 1.098 | 0.814 |
| 45 | 30.000 | 143.1 | 90. | 0.037 | –2.396 | 0.038 | –2.595 | 1.024 | 0.202 |
| 46 | 31.891 | 138.8 | 90. | 0.037 | –1.714 | 0.035 | –1.968 | 0.965 | –0.308 |
| 47 | 33.941 | 135.0 | 90. | 0.039 | –1.057 | 0.033 | –1.285 | 0.870 | –1.214 |
| 48 | 36.125 | 131.6 | 90. | 0.035 | –0.360 | 0.032 | –0.557 | 0.903 | –0.886 |
| 49 | 38.419 | 128.7 | 90. | 0.033 | 0.416 | 0.030 | 0.210 | 0.[illegible]03 | –0.882 |
| 50 | 40.804 | 126.0 | 90. | 0.032 | 1.145 | 0.028 | 1.009 | 0.886 | –1.052 |
| 51 | 43.267 | 123.7 | 90. | 0.031 | 1.957 | 0.027 | 1.835 | 0.869 | –1.222 |
| 52 | 6.083 | 80.5 | 90. | 0.206 | 1.549 | 0.207 | 1.604 | 1.005 | 0.047 |
| 53 | 9.056 | 83.7 | 90. | 0.132 | 2.573 | 0.137 | 2.621 | 1.038 | 0.321 |
| 54 | 12.042 | 85.2 | 90. | 0.095 | –2.679 | 0.102 | –2.643 | 1.079 | 0.663 |
| 55 | 15.033 | 86.2 | 90. | 0.077 | –1.651 | 0.082 | –1.625 | 1.053 | 0.452 |
| 56 | 18.028 | 86.8 | 90. | 0.064 | –0.615 | 0.068 | –0.606 | 1.060 | 0.504 |
| 57 | 21.024 | 87.3 | 90. | 0.054 | 0.388 | 0.058 | 0.412 | 1.070 | 0.587 |
| 58 | 24.021 | 87.6 | 90. | 0.049 | 1.470 | 0.051 | 1.430 | 1.046 | 0.393 |
| 59 | 27.019 | 87.9 | 90. | 0.040 | 2.426 | 0.045 | 2.448 | 1.122 | 0.999 |
| 60 | 30.017 | 88.1 | 90. | 0.034 | –2.888 | 0.041 | –2.818 | 1.181 | 1.448 |
| 61 | 33.015 | 88.3 | 90. | 0.031 | –1.687 | 0.037 | –1.800 | 1.181 | 1.442 |
| 62 | 36.014 | 88.4 | 90. | 0.032 | –0.650 | 0.034 | –0.782 | 1.073 | 0.614 |

Table 11. Curve fit for $k$ = 4.6308 l/ft.

| Mic | r | $\theta$, deg | $\phi$, deg | Measured pressure Real | Measured pressure Imag | Curve fit Real | Curve fit Imag | Ratio | Difference, dB |
|---|---|---|---|---|---|---|---|---|---|
| 23 | 4.000 | 0.0 | 90. | 0.377 | 0.895 | 0.389 | 0.873 | 1.034 | 0.289 |
| 24 | 5.657 | 45.0 | 90. | 0.250 | 1.522 | 0.248 | 1.543 | 0.992 | –0.072 |
| 25 | 8.944 | 63.4 | 90. | 0.152 | 2.827 | 0.146 | 2.855 | 0.956 | –0.393 |
| 22 | 4.472 | 63.4 | 90. | 0.313 | 1.086 | 0.301 | 1.143 | 0.962 | –0.339 |
| 29 | 4.472 | 153.4 | 90. | 0.223 | 1.592 | 0.217 | 1.514 | 0.970 | –0.262 |
| 140 | 6.324 | 161.6 | 90. | 0.153 | 2.341 | 0.161 | 2.248 | 1.052 | 0.437 |
| 19 | 6.083 | 80.5 | 90. | 0.207 | 1.770 | 0.205 | 1.821 | 0.988 | –0.104 |
| 30 | 36.496 | 170.5 | 90. | 0.034 | 1.427 | 0.031 | 1.336 | 0.926 | –0.668 |
| 31 | 37.108 | 166.0 | 90. | 0.027 | 1.747 | 0.031 | 1.567 | 1.139 | 1.130 |
| 32 | 37.947 | 161.6 | 90. | 0.026 | 2.062 | 0.030 | 1.884 | 1.169 | 1.353 |
| 33 | 39.000 | 157.4 | 90. | 0.026 | 2.507 | 0.029 | 2.282 | 1.133 | 1.083 |
| 34 | 40.249 | 153.4 | 90. | 0.026 | 2.968 | 0.028 | 2.755 | 1.077 | 0.641 |
| 35 | 41.677 | 149.7 | 90. | 0.026 | –2.738 | 0.027 | –2.987 | 1.062 | 0.523 |
| 36 | 43.267 | 146.3 | 90. | 0.025 | –2.076 | 0.026 | –2.384 | 1.066 | 0.552 |
| 37 | 45.000 | 143.1 | 90. | 0.026 | –1.404 | 0.025 | –1.725 | 0.990 | –0.085 |
| 38 | 46.861 | 140.2 | 90. | 0.027 | –0.744 | 0.024 | –1.017 | 0.920 | –0.727 |
| 39 | 48.837 | 137.5 | 90. | 0.025 | –0.081 | 0.023 | –0.265 | 0.933 | –0.600 |
| 40 | 50.912 | 135.0 | 90. | 0.022 | 0.755 | 0.023 | 0.527 | 1.032 | 0.277 |
| 63 | 13.417 | 26.6 | 90. | 0.094 | –1.617 | 0.103 | –1.807 | 1.097 | 0.803 |
| 64 | 15.000 | 36.9 | 90. | 0.084 | –1.063 | 0.091 | –1.178 | 1.074 | 0.617 |
| 65 | 16.970 | 45.0 | 90. | 0.074 | –0.226 | 0.079 | –0.399 | 1.062 | 0.527 |
| 66 | 19.209 | 51.3 | 90. | 0.067 | 0.695 | 0.068 | 0.483 | 1.024 | 0.207 |
| 67 | 21.633 | 56.3 | 90. | 0.060 | 1.615 | 0.060 | 1.434 | 1.006 | 0.054 |
| 68 | 24.187 | 60.3 | 90. | 0.053 | 2.548 | 0.053 | 2.433 | 0.994 | –0.055 |
| 69 | 26.833 | 63.4 | 90. | 0.047 | –2.679 | 0.047 | –2.817 | 1.017 | 0.146 |
| 70 | 29.546 | 66.0 | 90. | 0.041 | –1.582 | 0.043 | –1.760 | 1.049 | 0.415 |
| 71 | 32.311 | 68.2 | 90. | 0.037 | –0.496 | 0.039 | –0.684 | 1.050 | 0.421 |
| 72 | 35.114 | 70.0 | 90. | 0.034 | 0.529 | 0.036 | 0.405 | 1.036 | 0.304 |
| 73 | 37.947 | 71.6 | 90. | 0.032 | 1.410 | 0.033 | 1.505 | 1.015 | 0.131 |
| 41 | 24.739 | 166.0 | 90. | 0.044 | –2.785 | 0.045 | 3.077 | 1.022 | 0.191 |
| 42 | 25.632 | 159.4 | 90. | 0.045 | –2.494 | 0.044 | –2.873 | 0.977 | –0.201 |
| 43 | 26.833 | 153.4 | 90. | 0.042 | –2.099 | 0.042 | –2.423 | 0.999 | –0.005 |
| 44 | 28.302 | 148.0 | 90. | 0.039 | –1.552 | 0.040 | –1.871 | 1.018 | 0.151 |
| 45 | 30.000 | 143.1 | 90. | 0.037 | –0.939 | 0.038 | –1.231 | 1.014 | 0.118 |
| 46 | 31.891 | 138.8 | 90. | 0.037 | –0.231 | 0.036 | –0.516 | 0.956 | –0.392 |
| 47 | 33.941 | 135.0 | 90. | 0.035 | 0.519 | 0.034 | 0.260 | 0.960 | –0.359 |
| 48 | 36.125 | 131.6 | 90. | 0.032 | 1.337 | 0.032 | 1.090 | 0.981 | –0.171 |
| 49 | 38.419 | 128.7 | 90. | 0.029 | 2.237 | 0.030 | 1.963 | 1.021 | 0.182 |
| 50 | 40.804 | 126.0 | 90. | 0.028 | –3.138 | 0.028 | 2.872 | 0.995 | –0.045 |
| 51 | 43.267 | 123.7 | 90. | 0.025 | –2.256 | 0.027 | –2.472 | 1.052 | 0.439 |
| 52 | 6.083 | 80.5 | 90. | 0.203 | 1.821 | 0.205 | 1.821 | 1.007 | 0.060 |
| 53 | 9.056 | 83.7 | 90. | 0.137 | 2.999 | 0.135 | 2.980 | 0.985 | –0.131 |
| 54 | 12.042 | 85.2 | 90. | 0.102 | –2.154 | 0.101 | –2.144 | 0.993 | –0.060 |
| 55 | 15.033 | 86.2 | 90. | 0.082 | –1.017 | 0.081 | –0.986 | 0.991 | –0.083 |
| 56 | 18.028 | 86.8 | 90. | 0.066 | 0.139 | 0.067 | 0.173 | 1.012 | 0.100 |
| 57 | 21.024 | 87.3 | 90. | 0.053 | 1.294 | 0.058 | 1.331 | 1.078 | 0.649 |
| 58 | 24.021 | 87.6 | 90. | 0.047 | 2.514 | 0.050 | 2.489 | 1.075 | 0.624 |
| 59 | 27.019 | 87.9 | 90. | 0.043 | –2.615 | 0.045 | –2.636 | 1.047 | 0.396 |
| 60 | 30.017 | 88.1 | 90. | 0.037 | –1.450 | 0.040 | –1.478 | 1.077 | 0.647 |
| 61 | 33.015 | 88.3 | 90. | 0.036 | –0.241 | 0.037 | –0.320 | 1.011 | 0.093 |
| 62 | 36.014 | 88.4 | 90. | 0.034 | 0.833 | 0.034 | 0.838 | 0.984 | –0.142 |

Table 12. Curve fit for $k$ = 4.6771 l/ft.

| Mic | r | $\theta$, deg | $\phi$, deg | Measured pressure Real | Measured pressure Imag | Curve fit Real | Curve fit Imag | Ratio | Difference, dB |
|---|---|---|---|---|---|---|---|---|---|
| 23 | 4.000 | 0.0 | 90. | 0.374 | 0.901 | 0.387 | 0.876 | 1.034 | 0.293 |
| 24 | 5.657 | 45.0 | 90. | 0.249 | 1.535 | 0.248 | 1.554 | 0.996 | –0.035 |
| 25 | 8.944 | 63.4 | 90. | 0.151 | 2.866 | 0.146 | 2.880 | 0.964 | –0.319 |
| 22 | 4.472 | 63.4 | 90. | 0.312 | 1.094 | 0.301 | 1.149 | 0.964 | –0.323 |
| 29 | 4.472 | 153.4 | 90. | 0.226 | 1.607 | 0.220 | 1.518 | 0.975 | –0.217 |
| 140 | 6.324 | 161.6 | 90. | 0.153 | 2.349 | 0.163 | 2.258 | 1.062 | 0.525 |
| 19 | 6.083 | 80.5 | 90. | 0.206 | 1.790 | 0.205 | 1.834 | 0.997 | –0.029 |
| 30 | 36.496 | 170.5 | 90. | 0.037 | 1.558 | 0.031 | 1.461 | 0.857 | –1.345 |
| 31 | 37.108 | 166.0 | 90. | 0.029 | 1.852 | 0.031 | 1.694 | 1.075 | 0.629 |
| 32 | 37.947 | 161.6 | 90. | 0.027 | 2.149 | 0.030 | 2.014 | 1.138 | 1.119 |
| 33 | 39.000 | 157.4 | 90. | 0.026 | 2.592 | 0.029 | 2.417 | 1.140 | 1.138 |
| 34 | 40.249 | 153.4 | 90. | 0.026 | 3.080 | 0.029 | 2.895 | 1.097 | 0.806 |
| 35 | 41.677 | 149.7 | 90. | 0.025 | –2.626 | 0.028 | –2.842 | 1.082 | 0.688 |
| 36 | 43.267 | 146.3 | 90. | 0.024 | –1.973 | 0.027 | –2.232 | 1.116 | 0.956 |
| 37 | 45.000 | 143.1 | 90. | 0.024 | –1.266 | 0.026 | –1.566 | 1.082 | 0.681 |
| 38 | 46.861 | 140.2 | 90. | 0.026 | –0.549 | 0.025 | –0.851 | 0.964 | –0.320 |
| 39 | 48.837 | 137.5 | 90. | 0.026 | 0.131 | 0.024 | –0.091 | 0.925 | –0.681 |
| 40 | 50.912 | 135.0 | 90. | 0.022 | 0.947 | 0.023 | 0.709 | 1.050 | 0.420 |
| 63 | 13.417 | 26.6 | 90. | 0.093 | –1.579 | 0.103 | –1.765 | 1.102 | 0.840 |
| 64 | 15.000 | 36.9 | 90. | 0.085 | –1.010 | 0.090 | –1.129 | 1.058 | 0.487 |
| 65 | 16.970 | 45.0 | 90. | 0.074 | –0.160 | 0.078 | –0.342 | 1.060 | 0.507 |
| 66 | 19.209 | 51.3 | 90. | 0.066 | 0.787 | 0.068 | 0.548 | 1.032 | 0.276 |
| 67 | 21.633 | 56.3 | 90. | 0.060 | 1.714 | 0.060 | 1.508 | 1.002 | 0.021 |
| 68 | 24.187 | 60.3 | 90. | 0.054 | 2.646 | 0.053 | 2.517 | 0.979 | –0.181 |
| 69 | 26.833 | 63.4 | 90. | 0.047 | –2.587 | 0.047 | –2.723 | 1.004 | 0.036 |
| 70 | 29.546 | 66.0 | 90. | 0.041 | –1.460 | 0.043 | –1.655 | 1.050 | 0.424 |
| 71 | 32.311 | 68.2 | 90. | 0.036 | –0.367 | 0.039 | –0.569 | 1.080 | 0.669 |
| 72 | 35.114 | 70.0 | 90. | 0.033 | 0.709 | 0.036 | 0.531 | 1.094 | 0.783 |
| 73 | 37.947 | 71.6 | 90. | 0.032 | 1.634 | 0.033 | 1.642 | 1.039 | 0.334 |
| 41 | 24.739 | 166.0 | 90. | 0.043 | –2.679 | 0.046 | –3.127 | 1.074 | 0.618 |
| 42 | 25.632 | 159.4 | 90. | 0.044 | –2.384 | 0.044 | –2.789 | 1.000 | 0.000 |
| 43 | 26.833 | 153.4 | 90. | 0.042 | –1.984 | 0.042 | –2.335 | 1.019 | 0.161 |
| 44 | 28.302 | 148.0 | 90. | 0.038 | –1.425 | 0.040 | -1.777 | 1.067 | 0.561 |
| 45 | 30.000 | 143.1 | 90. | 0.036 | –0.806 | 0.038 | –1.130 | 1.065 | 0.549 |
| 46 | 31.891 | 138.8 | 90. | 0.037 | –0.087 | 0.036 | –0.408 | 0.974 | –0.226 |
| 47 | 33.941 | 135.0 | 90. | 0.034 | 0.644 | 0.034 | 0.377 | 0.983 | –0.145 |
| 48 | 36.125 | 131.6 | 90. | 0.032 | 1.476 | 0.032 | 1.215 | 1.005 | 0.040 |
| 49 | 38.419 | 128.7 | 90. | 0.028 | 2.404 | 0.030 | 2.097 | 1.082 | 0.682 |
| 50 | 40.804 | 126.0 | 90. | 0.029 | –2.926 | 0.028 | 3.016 | 0.995 | –0.042 |
| 51 | 43.267 | 123.7 | 90. | 0.026 | –2.100 | 0.027 | –2.318 | 1.038 | 0.326 |
| 52 | 6.083 | 80.5 | 90. | 0.203 | 1.835 | 0.205 | 1.834 | 1.011 | 0.094 |
| 53 | 9.056 | 83.7 | 90. | 0.137 | 3.035 | 0.136 | 3.005 | 0.990 | –0.090 |
| 54 | 12.042 | 85.2 | 90. | 0.102 | –2.126 | 0.102 | –2.108 | 0.996 | –0.036 |
| 55 | 15.033 | 86.2 | 90. | 0.080 | –0.956 | 0.081 | –0.938 | 1.012 | 0.107 |
| 56 | 18.028 | 86.8 | 90. | 0.066 | 0.238 | 0.067 | 0.232 | 1.029 | 0.248 |
| 57 | 21.024 | 87.3 | 90. | 0.054 | 1.380 | 0.058 | 1.402 | 1.065 | 0.548 |
| 58 | 24.021 | 87.6 | 90. | 0.047 | 2.605 | 0.051 | 2.572 | 1.081 | 0.673 |
| 59 | 27.019 | 87.9 | 90. | 0.044 | –2.501 | 0.045 | –2.542 | 1.013 | 0.109 |
| 60 | 30.017 | 88.1 | 90. | 0.038 | –1.345 | 0.040 | –1.372 | 1.051 | 0.431 |
| 61 | 33.015 | 88.3 | 90. | 0.036 | –0.102 | 0.037 | –0.203 | 1.021 | 0.177 |
| 62 | 36.014 | 88.4 | 90. | 0.036 | 0.993 | 0.034 | 0.967 | 0.932 | –0.615 |

Table 13. Wave numbers and frequencies tested.

| *ka* | *kl* | *k*, 1/ft | *k*, 1/m | Frequency at 70°F, Hz | No. propagating modes | No. modes modeled | $1/(kr_w)$ |
|---|---|---|---|---|---|---|---|
| 0.2511 | 8.5221 | 1.5065 | 4.9428 | 270.38 | 7 | 50 | 0.3671 |
| 0.2536 | 8.6075 | 1.5216 | 4.9922 | 273.08 | 7 | 50 | 0.3634 |
| 0.3669 | 12.4530 | 2.2014 | 7.2227 | 395.09 | 13 | 98 | 0.2512 |
| 0.3706 | 12.5775 | 2.2234 | 7.2949 | 399.04 | 15 | 98 | 0.2487 |
| 0.4781 | 16.2267 | 2.8685 | 9.4114 | 514.82 | 23 | 162 | 0.1928 |
| 0.4829 | 16.8982 | 2.8972 | 9.5055 | 519.97 | 23 | 171 | 0.1909 |
| 0.5800 | 19.6764 | 3.4801 | 11.4177 | 624.57 | 32 | 242 | 0.1589 |
| 0.5858 | 19.8832 | 3.5149 | 11.5319 | 630.81 | 34 | 253 | 0.1573 |
| 0.6717 | 22.7994 | 4.0304 | 13.2233 | 723.34 | 42 | 338 | 0.1372 |
| 0.6785 | 23.0274 | 4.0707 | 13.3555 | 730.57 | 42 | 338 | 0.1358 |
| 0.7718 | 26.1957 | 4.6308 | 15.1932 | 831.09 | 54 | 450 | 0.1194 |
| 0.7795 | 26.4577 | 4.6771 | 15.3451 | 839.40 | 56 | 450 | 0.1182 |

Table 14. Measured normal absorption coefficients and specific acoustic impedances used in predictions, and corresponding figure numbers.

| k, 1/ft | $C_{\alpha 1}$ | $z_1/\rho_0 c$ | Figure no. | $C_{\alpha 2}$ | $z_2/\rho_0 c$ | Figure no. | $C_{\alpha 3}$ | $z_3/\rho_0 c$ | Figure no. |
|---|---|---|---|---|---|---|---|---|---|
| 1.5065 | 0.086 | (1.241, –7.270) | 13b | 0.088 | (1.427, –7.663) | 13c | 0.091 | (1.465, –7.649) | 13d |
| 1.5216 | 0.083 | (1.343, –7.692) | 14b | 0.089 | (1.184, –6.975) | 14c | 0.091 | (1.253, –7.088) | 14d |
| 2.2014 | 0.097 | (0.666, –4.961) | 15b | 0.101 | (0.695, –4.954) | 15c | 0.118 | (0.936, –5.300) | 15d |
| 2.2234 | 0.103 | (0.676, –4.840) | 16b | 0.118 | (0.803, –4.898) | 16c | | | |
| 2.8685 | 0.120 | (0.551, –3.998) | 17b | 0.122 | (0.590, –4.091) | 17c | 0.128 | (0.550, –3.852) | 17d |
| 2.8972 | 0.124 | (0.569, –3.993) | 18b | 0.128 | (0.613, –4.067) | 18c | 0.137 | (0.526, –3.617) | 18d |
| 3.4801 | 0.153 | (0.506, –3.311) | 19b | 0.154 | (0.490, –3.245) | 19c | 0.156 | (0.579, –3.520) | 19d |
| 3.5149 | 0.156 | (0.541, –3.393) | 20b | 0.156 | (0.475, –3.168) | 20c | 0.161 | (0.606, –3.533) | 20d |
| 4.0304 | 0.161 | (0.414, –2.875) | 21b | 0.202 | (0.559, –2.936) | 21c | 0.229 | (0.579, –2.785) | 21d |
| 4.0707 | 0.197 | (0.450, –2.649) | 22b | 0.198 | (0.458, –2.670) | 22c | 0.260 | (1.012, –3.391) | 22d |
| 4.6308 | 0.154 | (0.291, –2.422) | 23b | 0.191 | (0.394, –2.509) | 23c | 0.234 | (0.410, –2.238) | 23d |
| 4.6771 | 0.162 | (0.321, –2.490) | 24b | 0.187 | (0.393, –2.543) | 24c | 0.264 | (0.395, –2.490) | 24d |

Table 15. Excess attenuation due to absorption in the atmosphere.

| φ, deg | T, deg F | Relative humidity | Attenuation per 1000 ft, dB | | |
|---|---|---|---|---|---|
| | | | 250 Hz | 500 Hz | 1000 Hz |
| 0 | 67 | 73 | 0.20 | 0.47 | 1.13 |
| 30 | 71 | 73 | 0.20 | 0.47 | 1.13 |
| 60 | 70 | 52 | 0.22 | 0.53 | 1.27 |
| 90 | 71 | 57 | 0.21 | 0.51 | 1.27 |
| 120 | 74 | 57 | 0.21 | 0.51 | 1.23 |
| 150 | 76 | 57 | 0.21 | 0.51 | 1.23 |
| 180 | 70 | 51 | 0.22 | 0.53 | 1.28 |
| 210 | 70 | 51 | 0.22 | 0.53 | 1.28 |
| 240 | 65 | 91 | 0.18 | 0.43 | 1.04 |
| 270 | 65 | 91 | 0.18 | 0.43 | 1.04 |
| 300 | 65 | 58 | 0.21 | 0.51 | 1.22 |
| 330 | 66 | 47 | 0.23 | 0.55 | 1.32 |
| 0 | 47 | 79 | 0.20 | 0.47 | 1.15 |

Table 16. Maximum effect of temperature and relative humidity on measured absorption due to absorption in the air.

| k, 1/ft | $C_{\alpha 1}$ | $C_{\alpha 1+}$ | $C_{\alpha 2}$ | $C_{\alpha 2+}$ | $C_{\alpha 3}$ | $C_{\alpha 3+}$ |
|---|---|---|---|---|---|---|
| 1.5065 | 0.086 | 0.086 | 0.088 | 0.088 | 0.091 | 0.091 |
| 1.5216 | 0.083 | 0.083 | 0.089 | 0.089 | 0.091 | 0.091 |
| 2.2014 | 0.097 | 0.098 | 0.101 | 0.102 | 0.118 | 0.119 |
| 2.2234 | 0.103 | 0.104 | 0.118 | 0.119 | | |
| 2.8685 | 0.120 | 0.121 | 0.122 | 0.123 | 0.128 | 0.129 |
| 2.8972 | 0.124 | 0.125 | 0.128 | 0.129 | 0.137 | 0.138 |
| 3.4801 | 0.153 | 0.154 | 0.154 | 0.155 | 0.156 | 0.157 |
| 3.5149 | 0.156 | 0.157 | 0.156 | 0.157 | 0.161 | 0.162 |
| 4.0304 | 0.161 | 0.163 | 0.202 | 0.204 | 0.229 | 0.231 |
| 4.0707 | 0.197 | 0.199 | 0.198 | 0.200 | 0.260 | 0.261 |
| 4.6308 | 0.154 | 0.156 | 0.191 | 0.193 | 0.234 | 0.236 |
| 4.6771 | 0.162 | 0.164 | 0.187 | 0.189 | 0.264 | 0.265 |

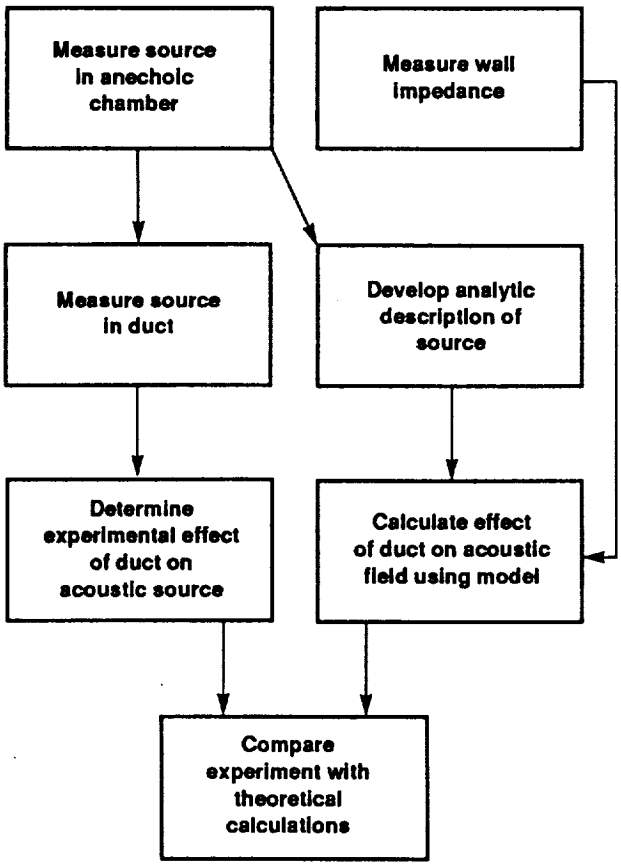


Figure 1. Steps to evaluate analytical model in this study.

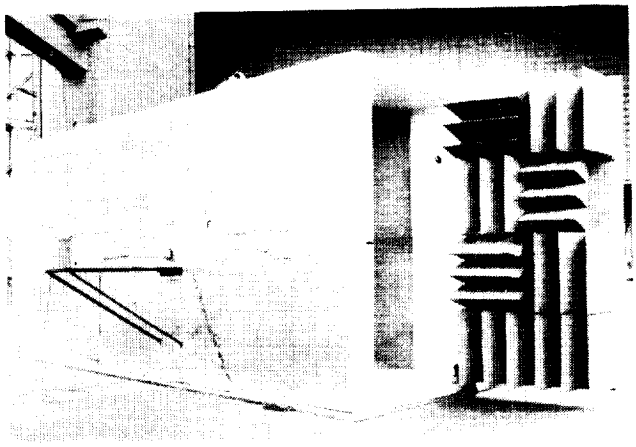

(a)

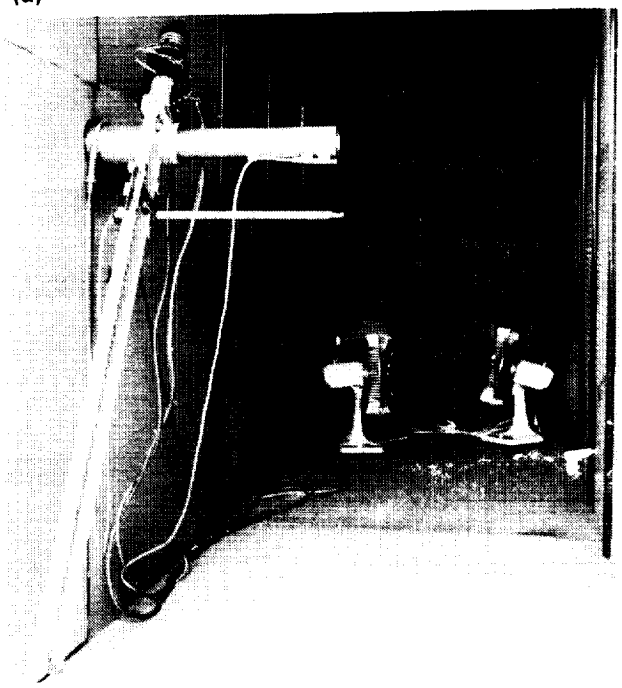

(b)

Figure 2. Duct. (a) Outside photograph; (b) inside photograph.

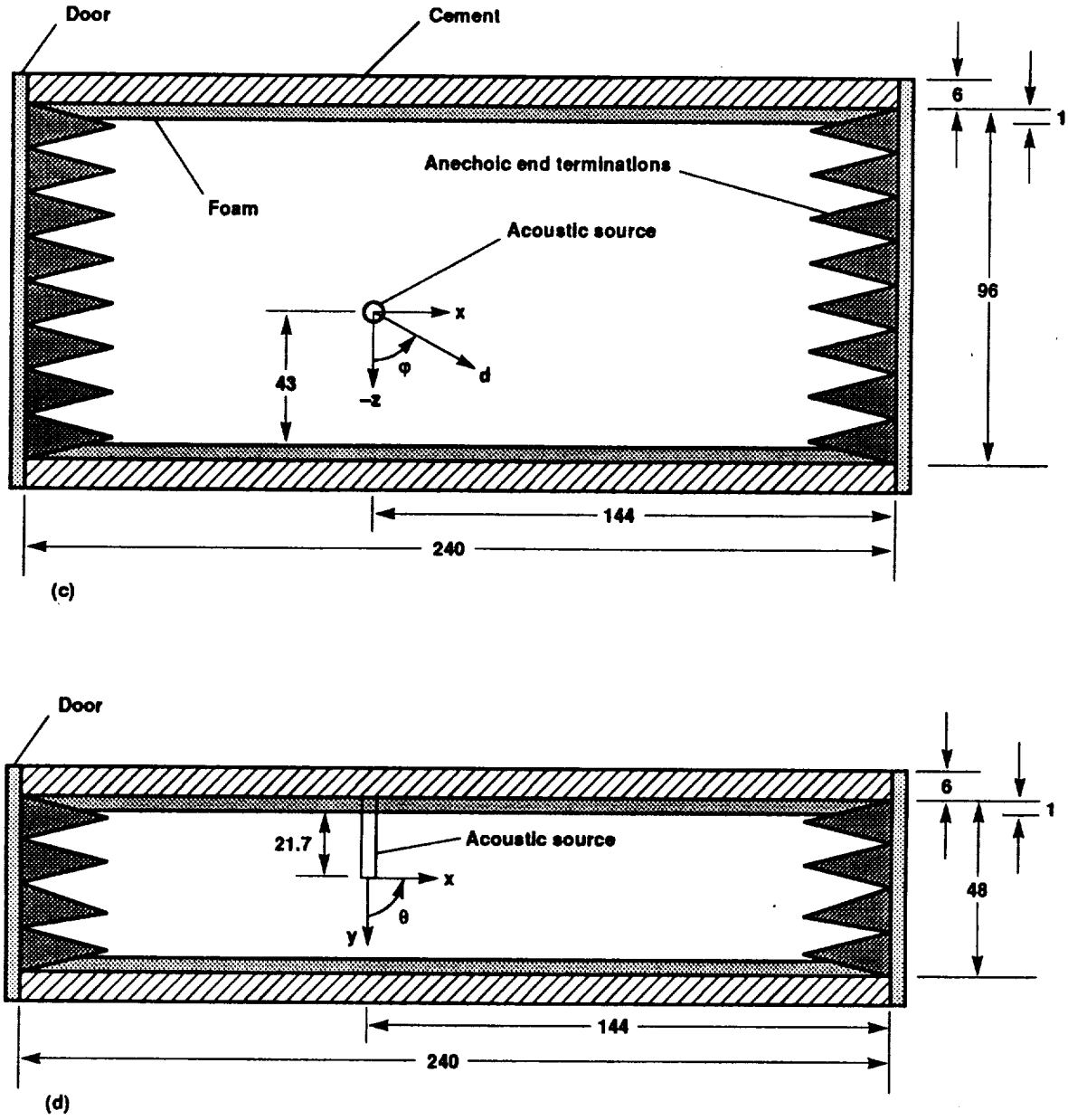


Figure 2. Concluded. (c) Side view; (d) plan view.

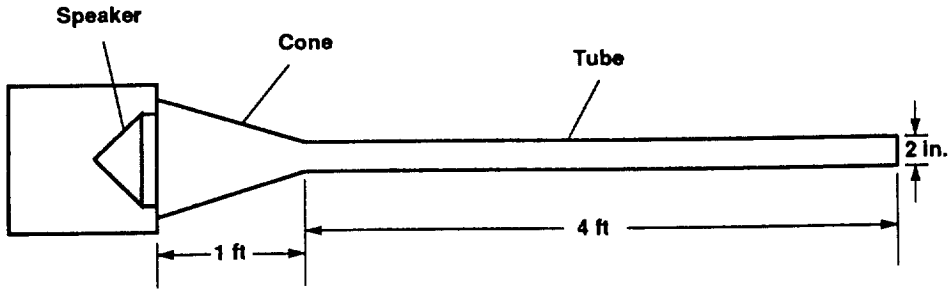


Figure 3. Schematic of acoustic source.

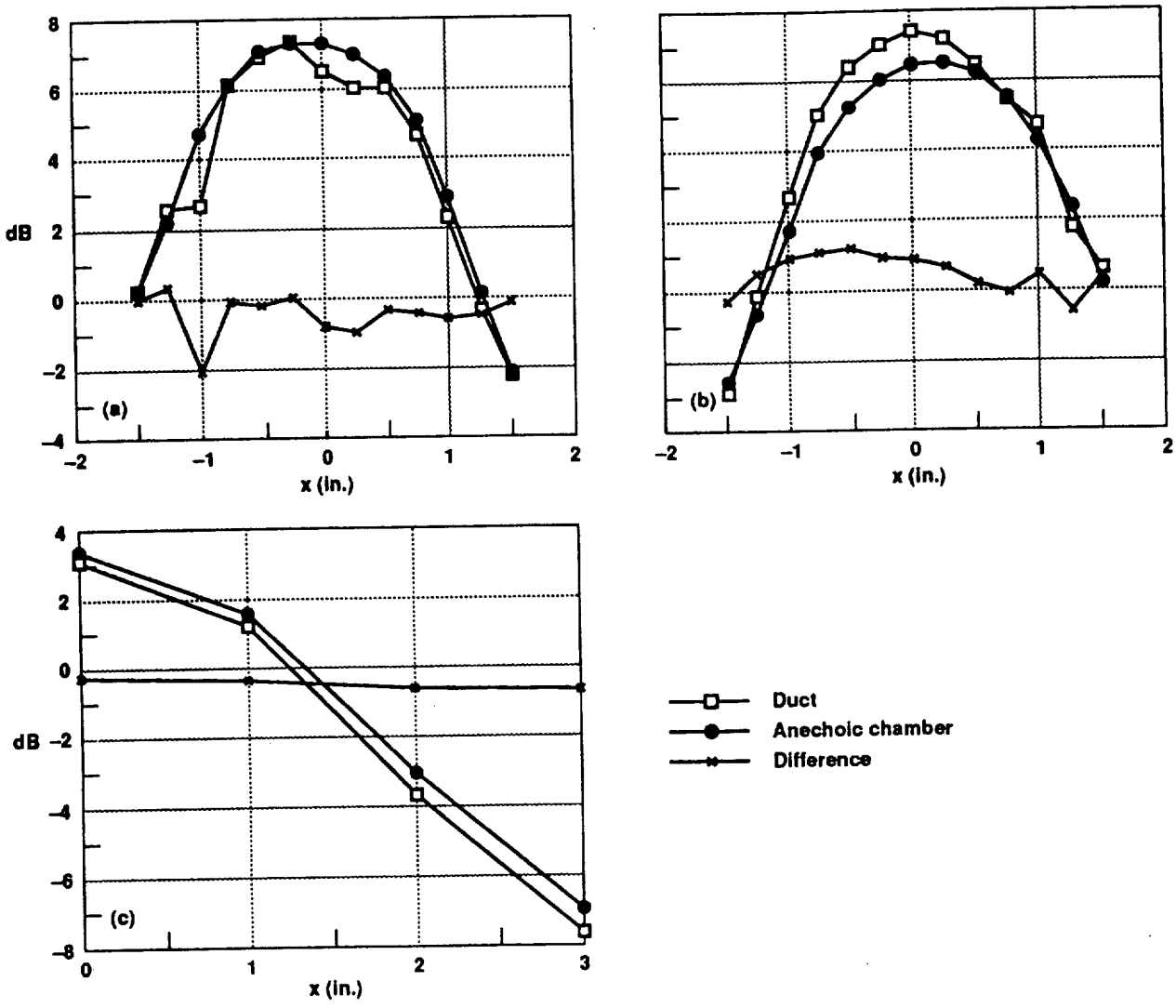


Figure 4. Comparison of acoustic source in the anechoic chamber and in the duct for $ka = 0.6717$, $kl = 22.7994$. (a) $y = 0.5$ in., microphone pointing towards $+x$; (b) $y = 0.5$ in., microphone pointing towards $-x$; (c) $y = 1.0$ in.

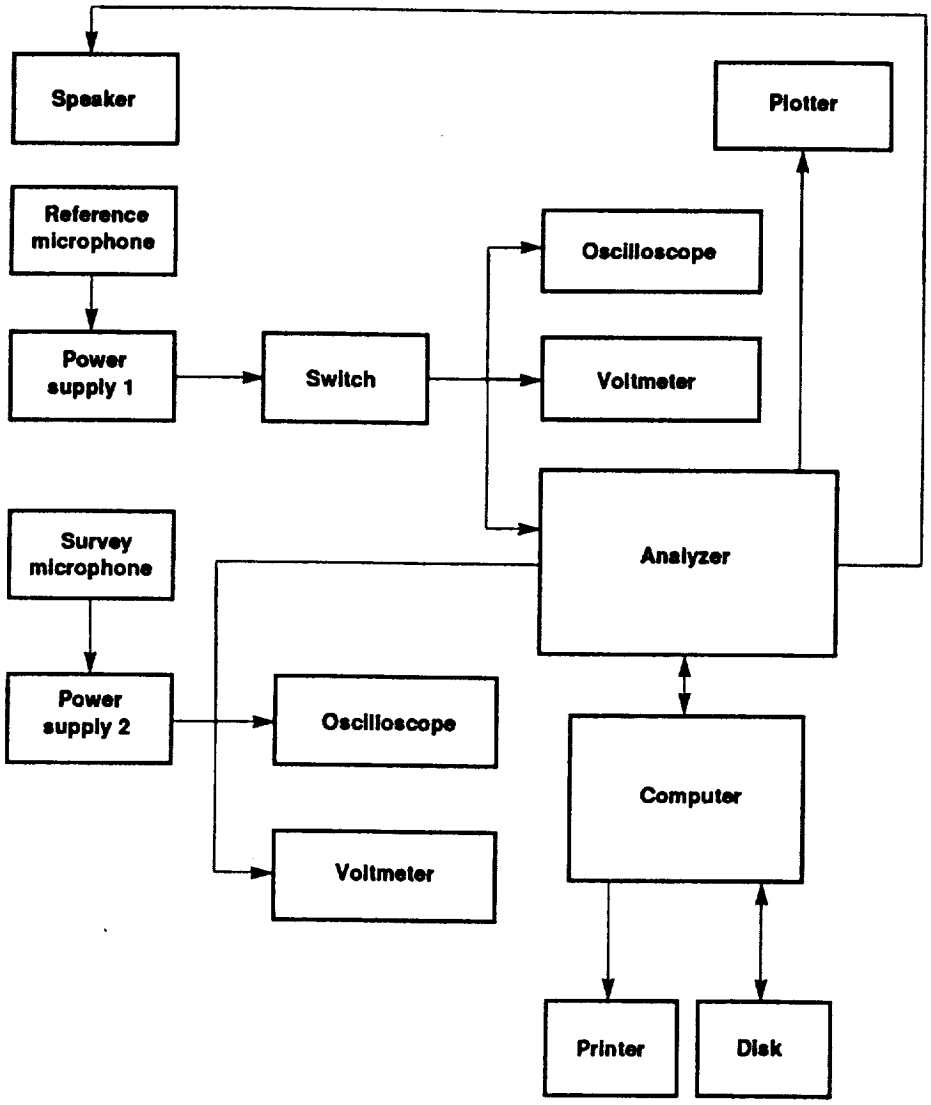


Figure 5. Instrumentation system for measurements in the anechoic chamber and the duct.

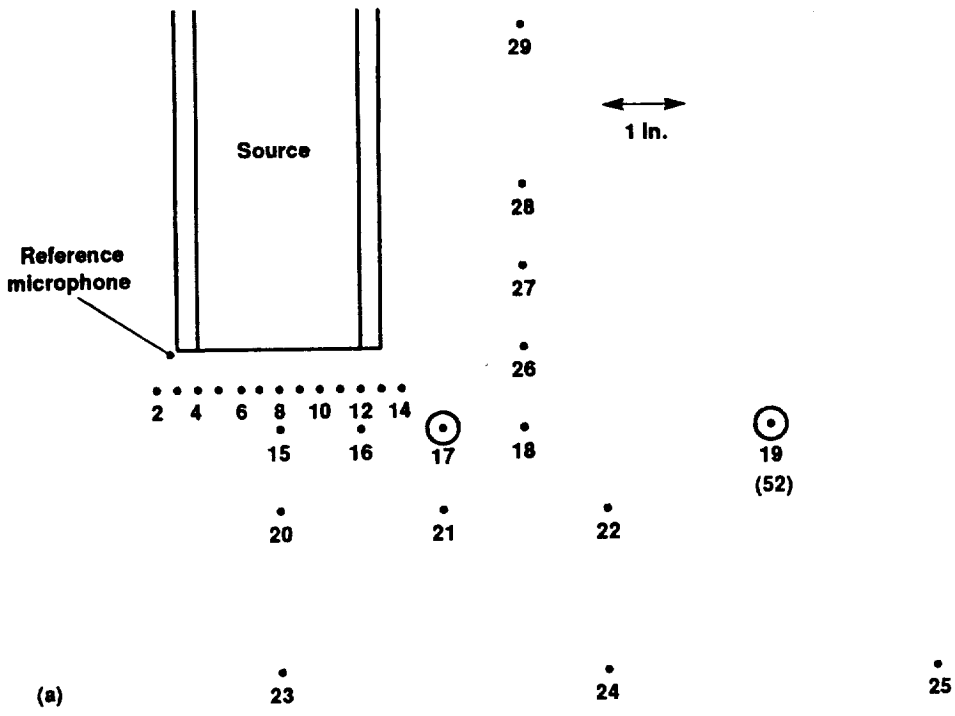


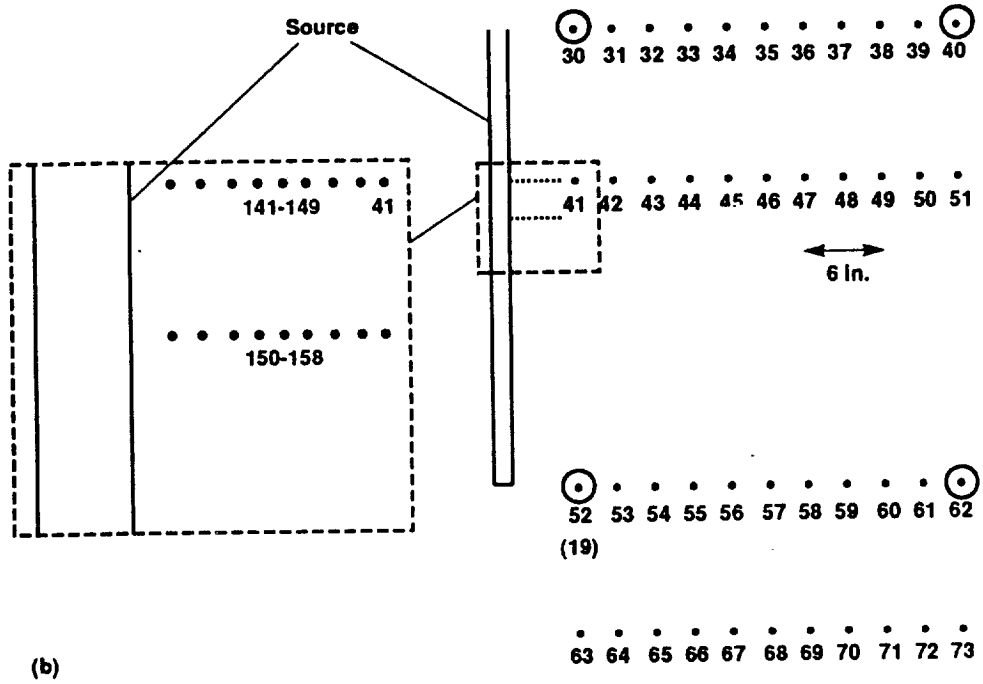


Figure 6. Plan view of microphone locations in anechoic chamber. (a) Close to source; (b) far from source.

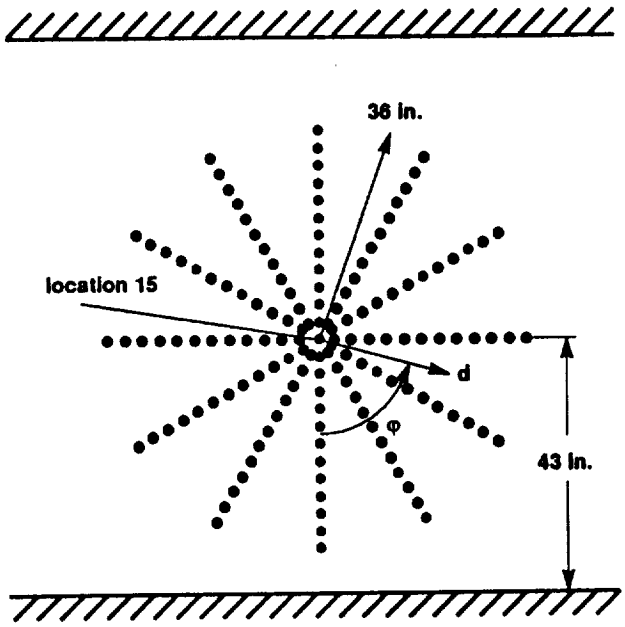


Figure 7. Side view of microphone locations 1 in. in front of the source in the duct.

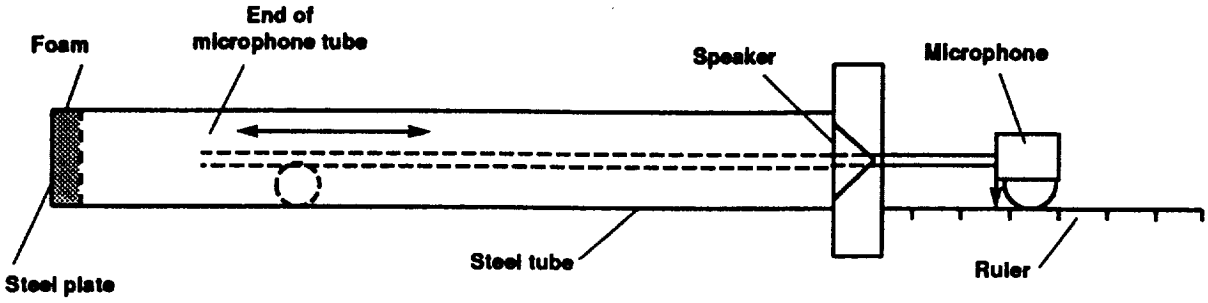


Figure 8. Schematic of standing wave tube used to determine impedance of foam sample.

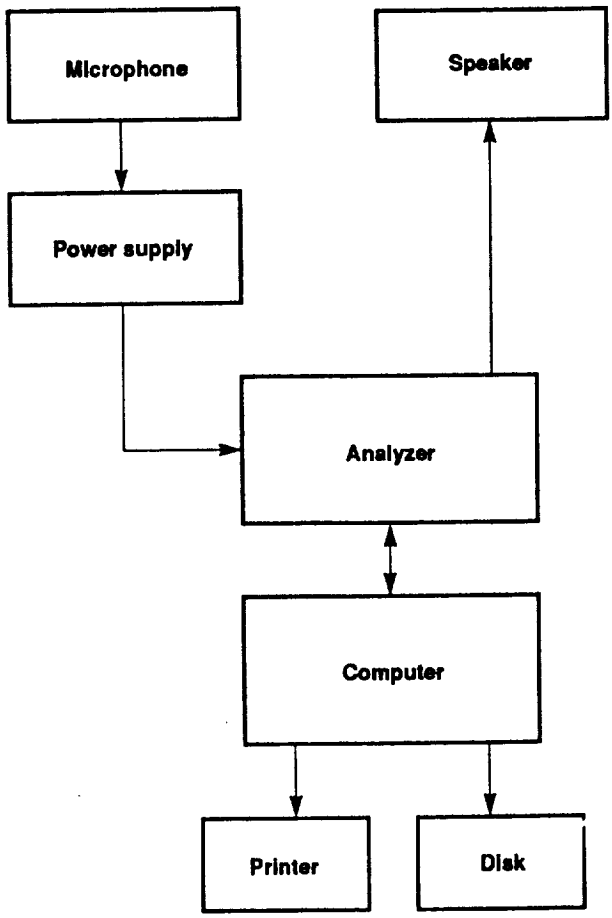


Figure 9. Instrumentation system for measuring impedance in standing wave tube.

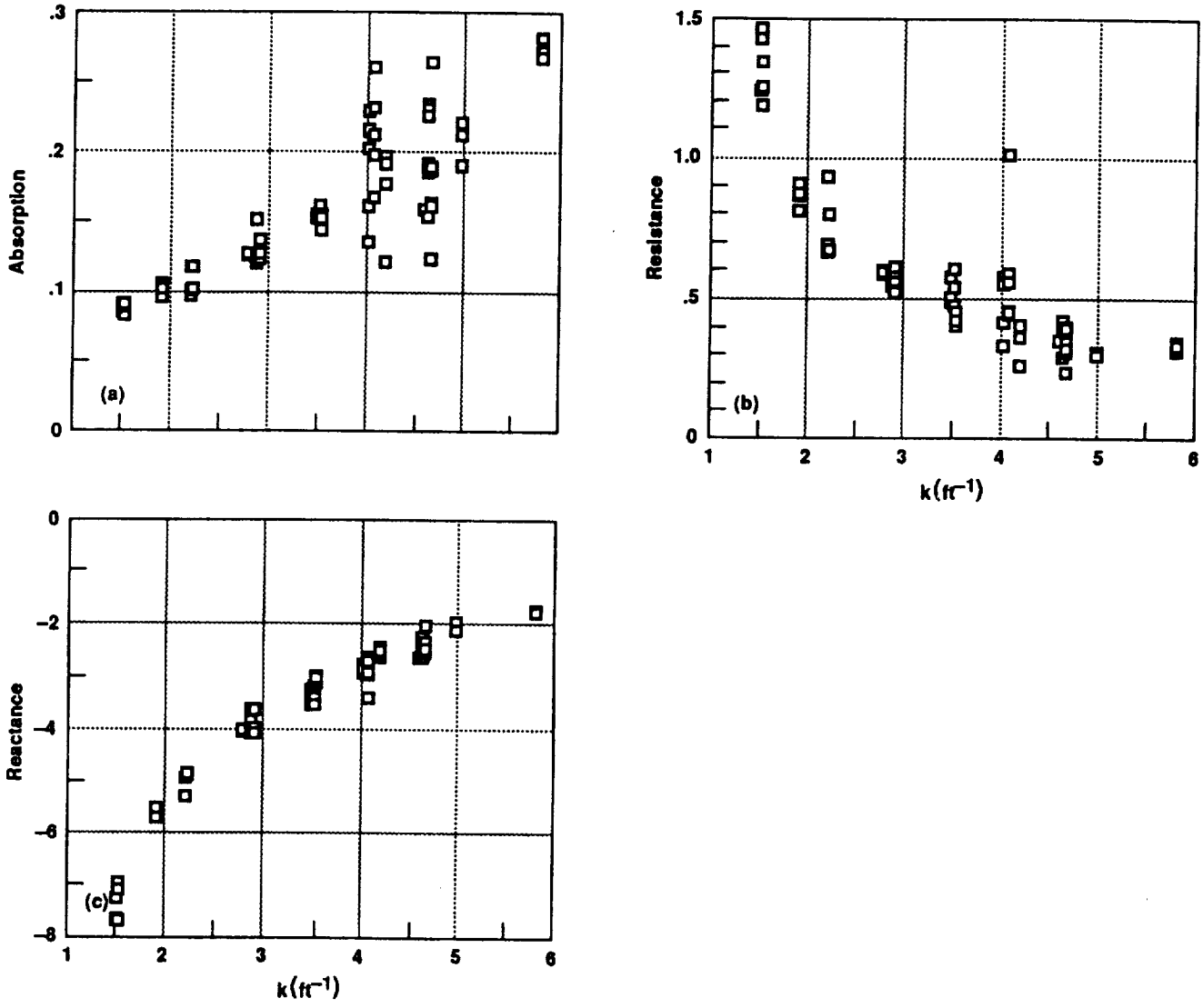


Figure 10. Impedance measurement of 1-in. foam. (a) Absorption at normal incidence; (b) specific acoustic resistance, $\Re(z/\rho_0 c)$, at normal incidence; (c) specific acoustic reactance, $\Im(z/\rho_0 c)$, at normal incidence.

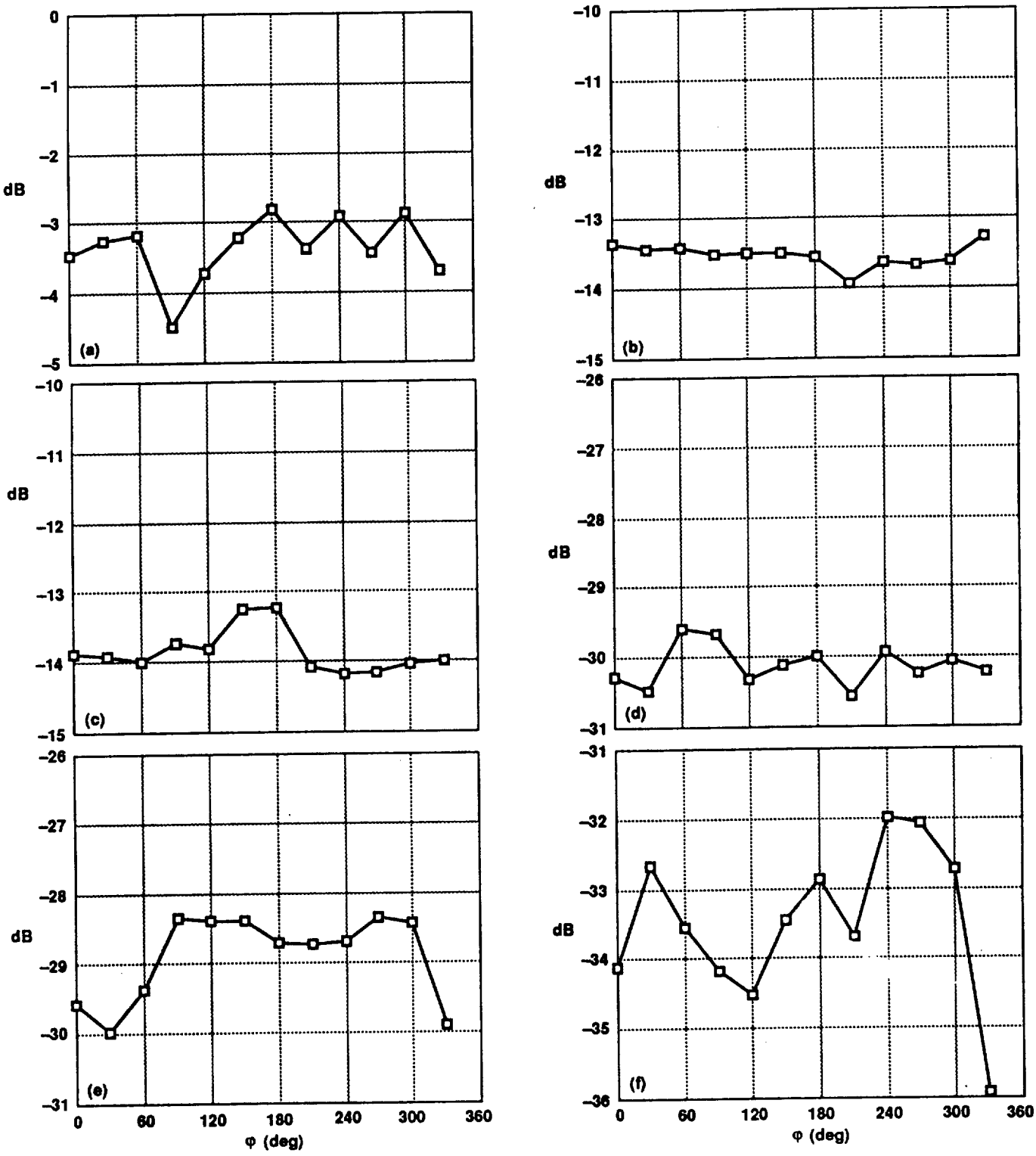


Figure 11. Measurement of source in anechoic chamber for $ka = 0.6717$. (a) Microphone location 17, $d = 2.0$ in., $y = 1.0$ in.; (b) microphone location 19, $d = 6.0$ in., $y = 1.0$ in.; (c) microphone location 52, $d = 6.0$ in., $y = 1.0$ in.; (d) microphone location 62, $d = 36.0$ in., $y = 1.0$ in.; (e) microphone location 30, $d = 6.0$ in., $y = -36.0$ in.; (f) microphone location 40, $d = 36.0$ in., $y = -36.0$ in.

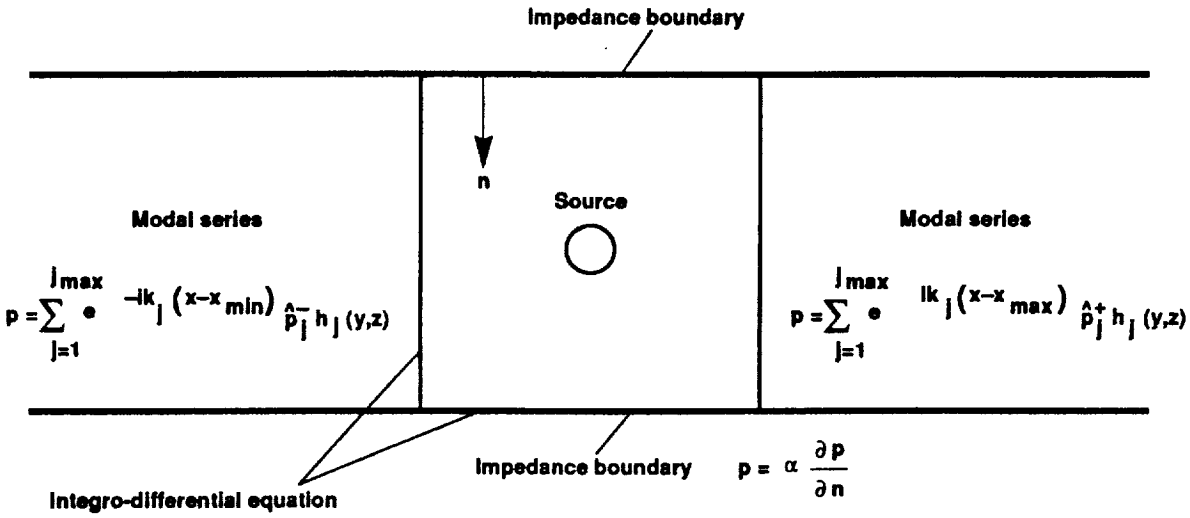


Figure 12. Analytic model of duct (developed in ref. 1).

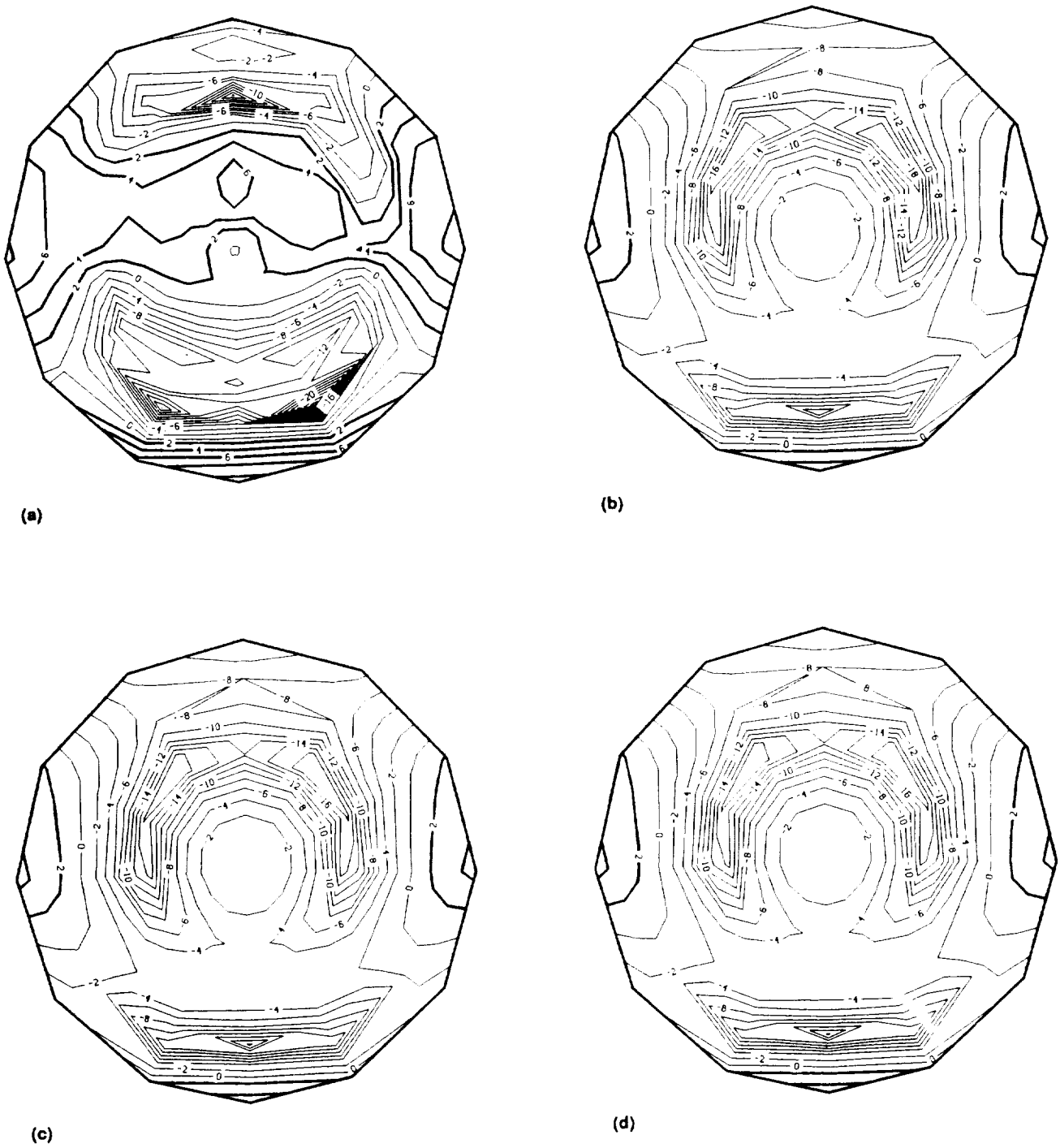


Figure 13. Reverberant field (dB in duct – dB in anechoic chamber) in a plane 1.0 in. in front of source for $kl = 8.5221$. (a) Measurements; (b) calculation $C_\alpha = 0.088$, $z/\rho_0 c = (1.427, -7.663)$; (c) calculation $C_\alpha = 0.089$, $z/\rho_0 c = (1.184, -6.975)$; (d) calculation $C_\alpha = 0.091$, $z/\rho_0 c = (1.253, -7.088)$.

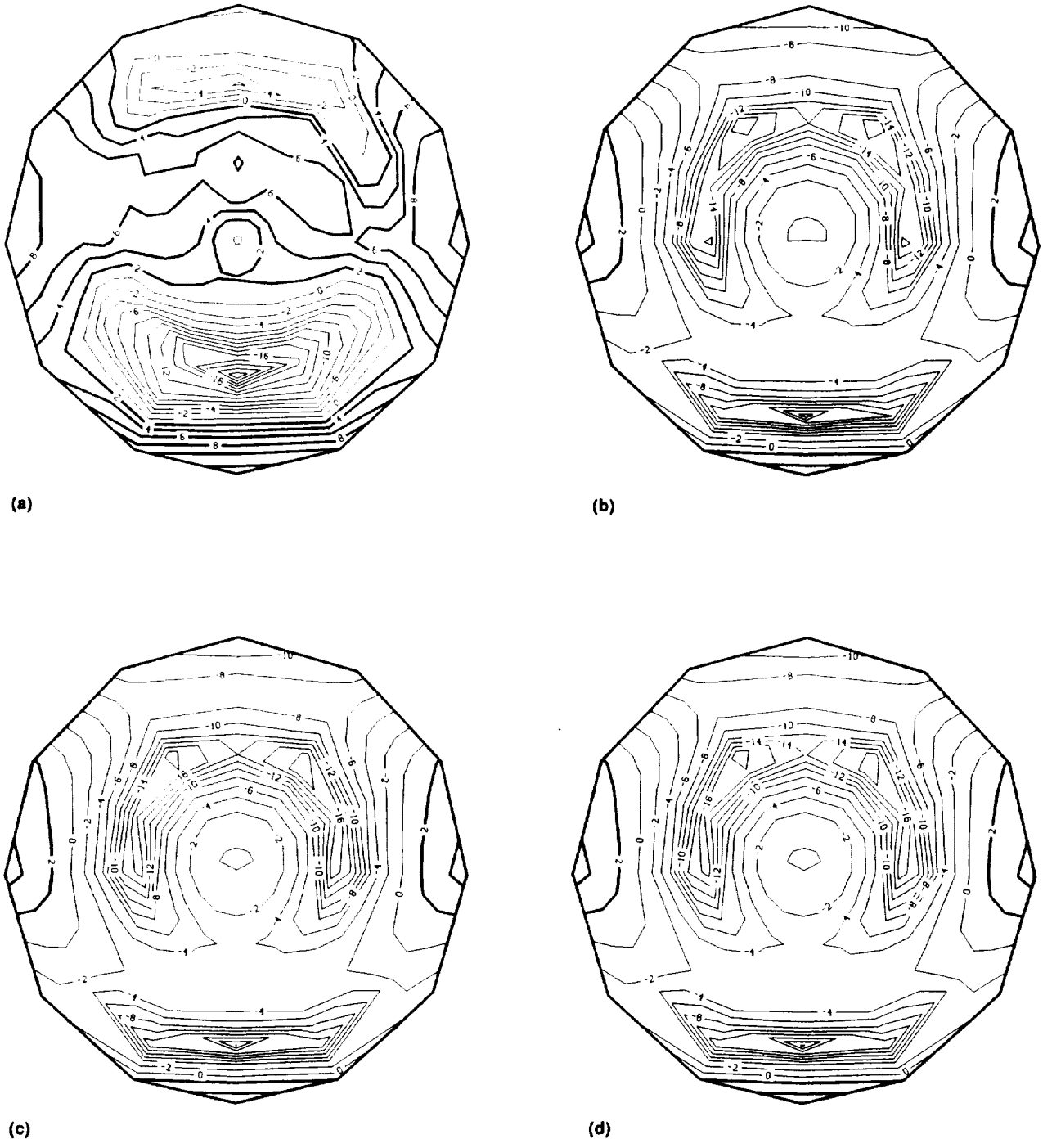


Figure 14. Reverberant field (dB in duct – dB in anechoic chamber) in a plane 1.0 in. in front of source for $kl = 8.6075$. (a) Measurements; (b) calculation $C_\alpha = 0.083$, $z/\rho_0 c = (1.343, -7.692)$; (c) calculation $C_\alpha = 0.086$, $z/\rho_0 c = (1.241, -7.270)$; (d) calculation $C_\alpha = 0.091$, $z/\rho_0 c = (1.465, -7.649)$.

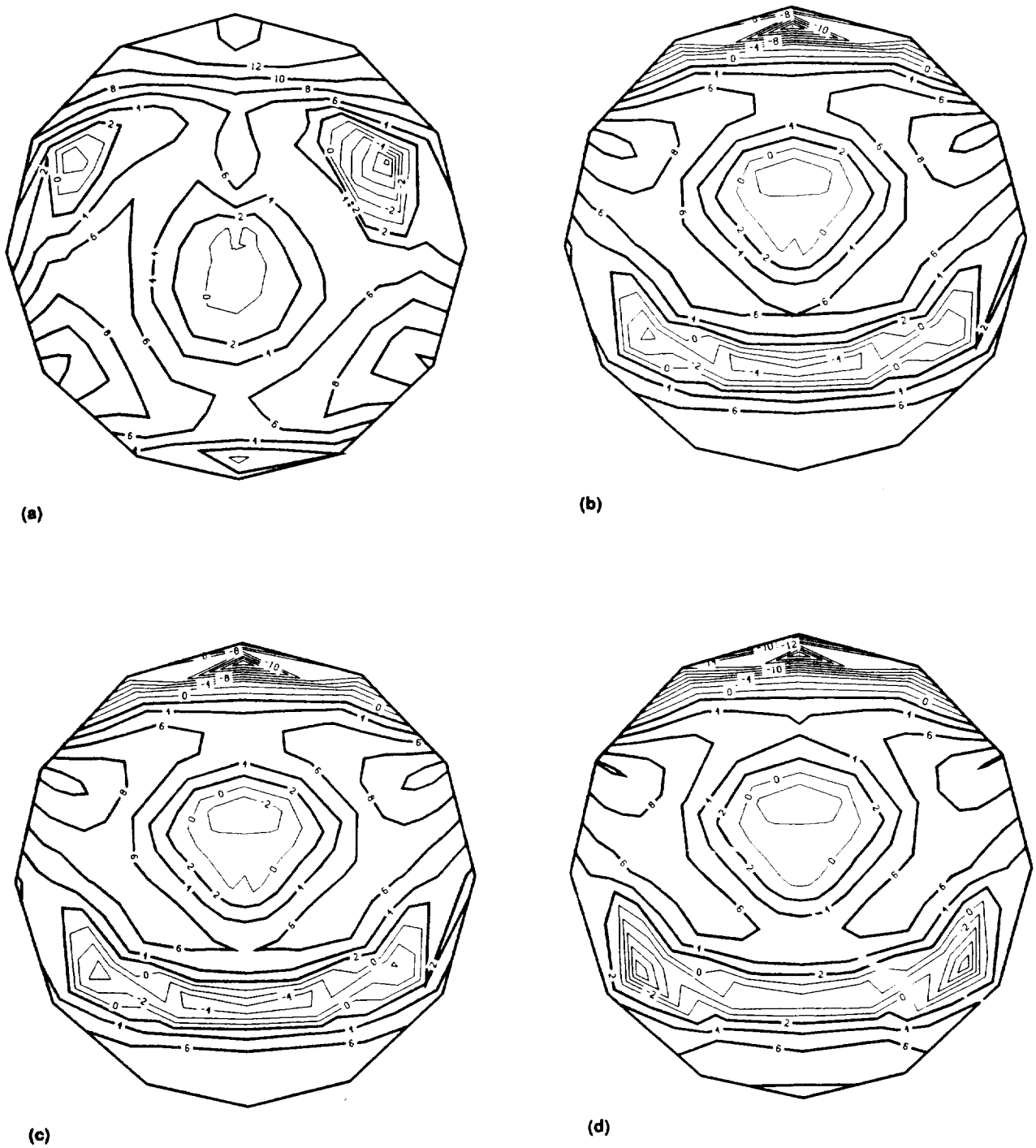


Figure 15. Reverberant field (dB in duct – dB in anechoic chamber) in a plane 1.0 in. in front of source for $kl = 12.4530$. (a) Measurements; (b) calculation $C_\alpha = 0.097$, $z/\rho_0 c = (0.666, -4.961)$; (c) calculation $C_\alpha = 0.101$, $z/\rho_0 c = (0.695, -4.954)$; (d) calculation $C_\alpha = 0.118$, $z/\rho_0 c = (0.936, -5.300)$.

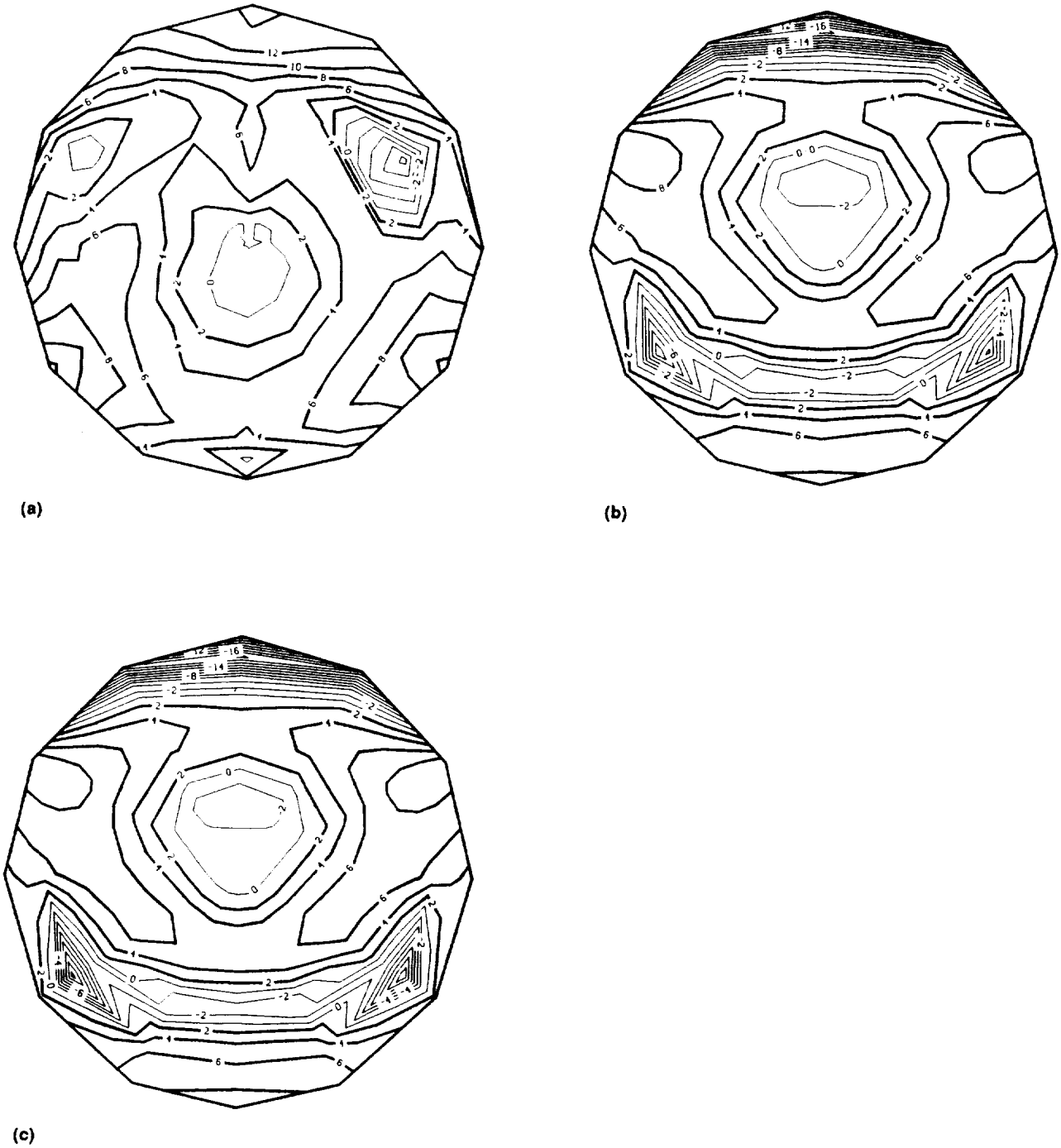


Figure 16. Reverberant field (dB in duct – dB in anechoic chamber) in a plane 1.0 in. in front of source for k = $kl$ = 12.5775. (a) Measurements; (b) calculation $C_\alpha = 0.103$, $z/\rho_0 c = (0.676, -4.840)$; (c) calculation $C_\alpha = 0.118$, $z/\rho_0 c = (0.803, -4.898)$.

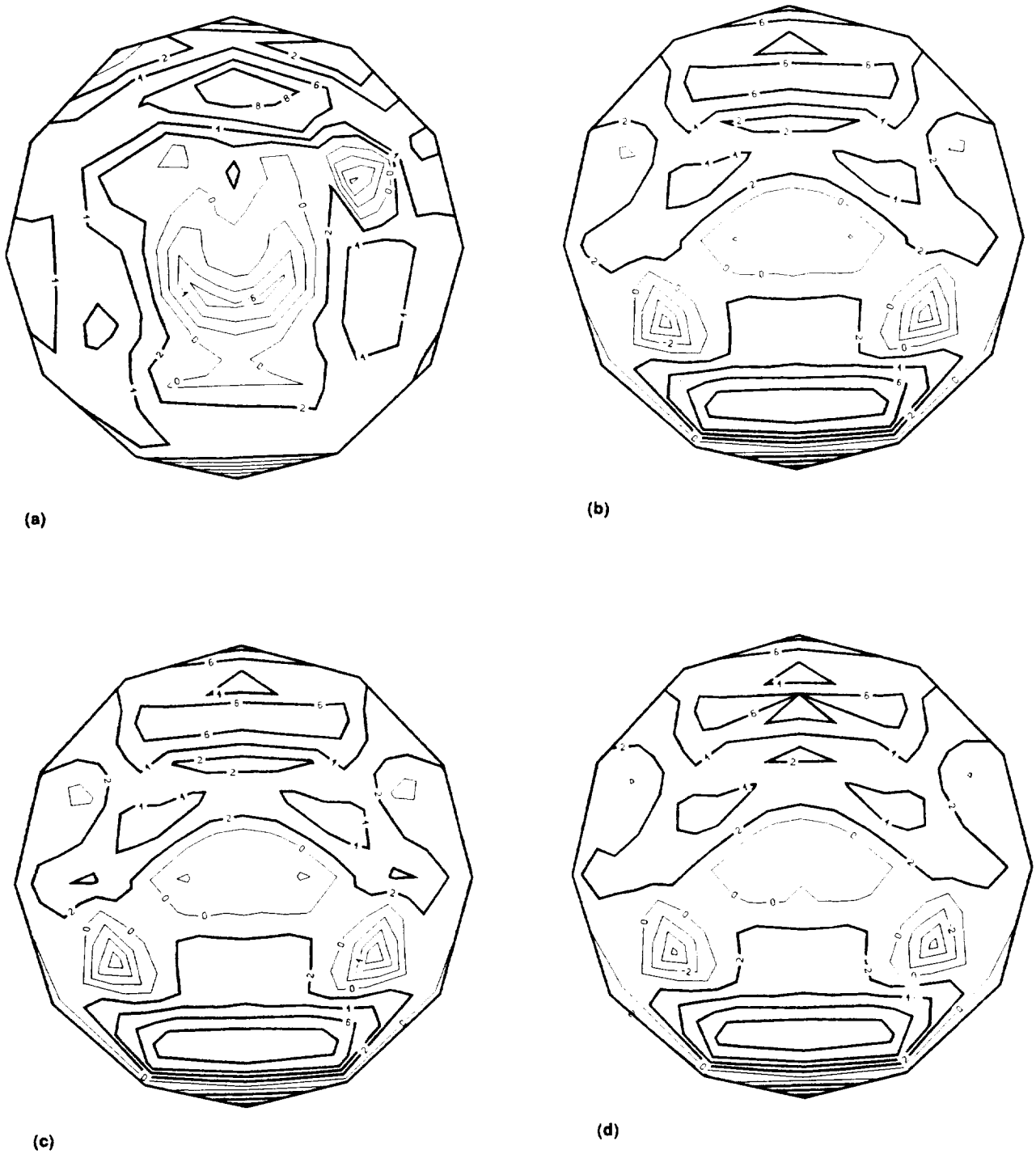


Figure 17. Reverberant field (dB in duct – dB in anechoic chamber) in a plane 1.0 in. in front of source for $kl$ = 16.2267. (a) Measurements; (b) calculation $C_\alpha$= 0.120, $z/\rho_0 c$ = (0.551, –3.998); (c) calculation $C_\alpha$ = 0.122, $z/\rho_0 c$ = (0.590, –4.091); (d) calculation $C_\alpha$ = 0.128, $z/\rho_0 c$ = (0.550, –3.852).

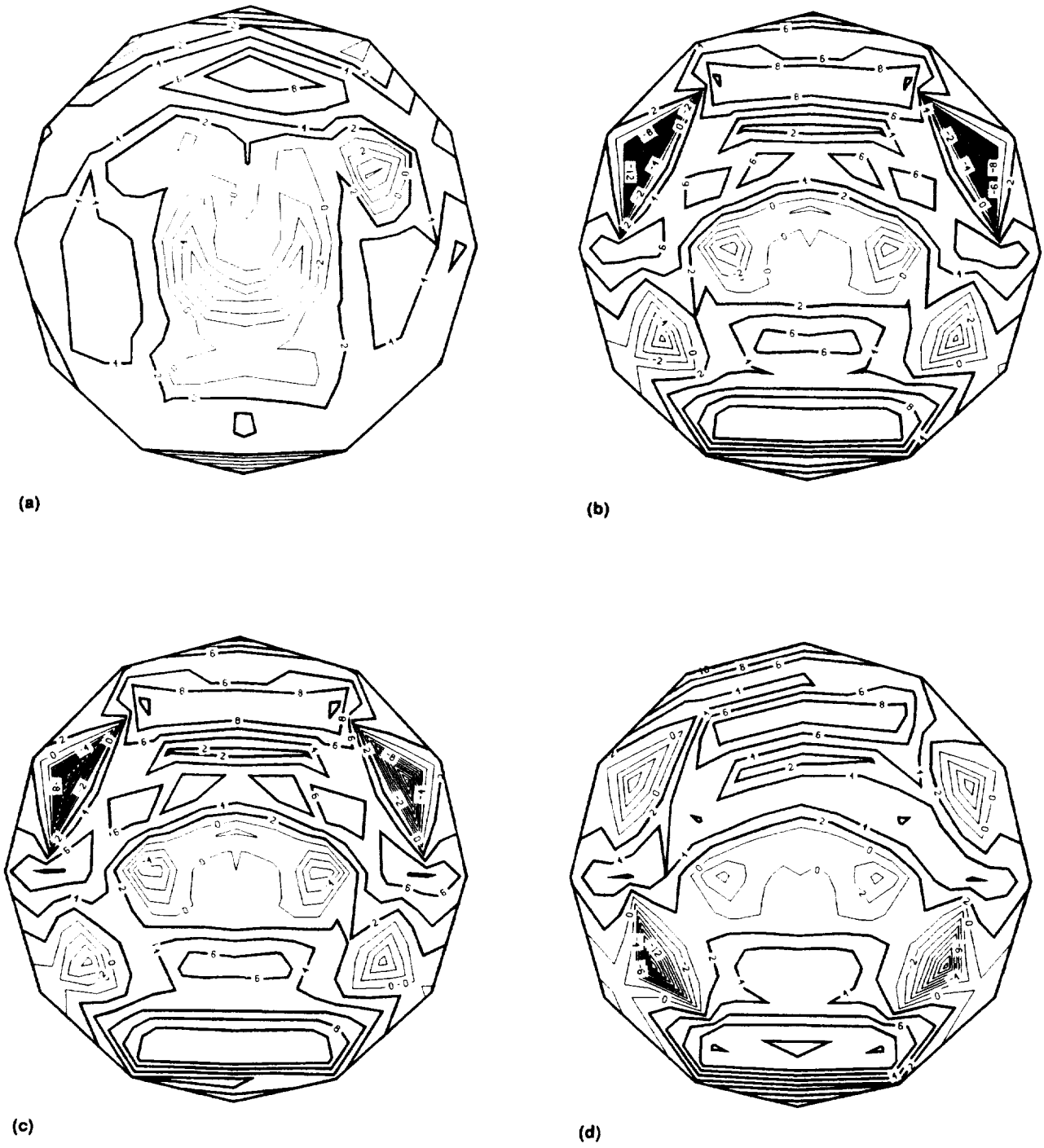


Figure 18. Reverberant field (dB in duct – dB in anechoic chamber) in a plane 1.0 in. in front of source for $kl = 16.8982$. (a) Measurements; (b) calculation $C_\alpha = 0.124$, $z/\rho_0 c = (0.569, -3.993)$; (c) calculation $C_\alpha = 0.128$, $z/\rho_0 c = (0.613, -4.067)$; (d) calculation $C_\alpha = 0.137$, $z/\rho_0 c = (0.526, -3.617)$.

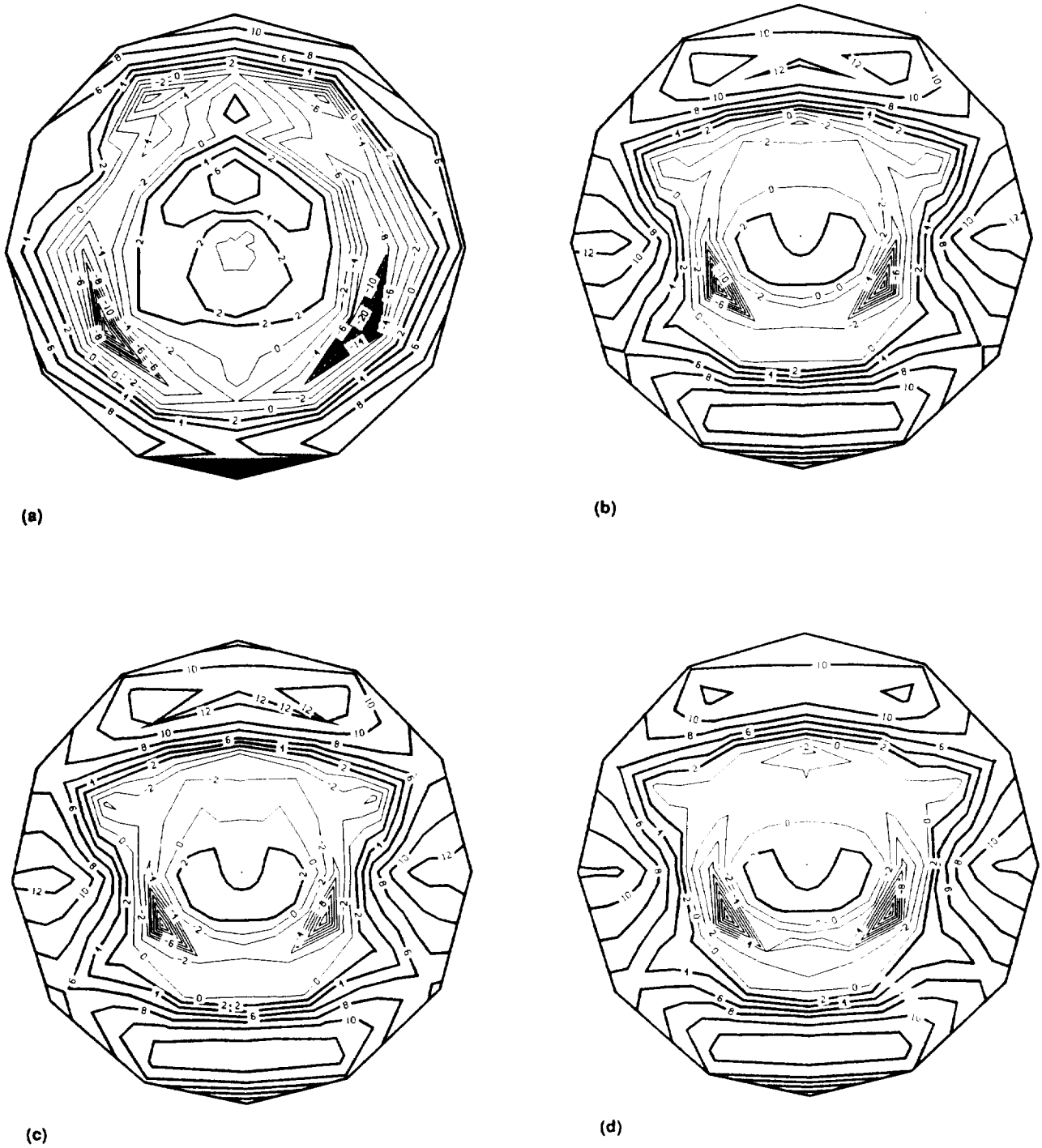


Figure 19. Reverberant field (dB in duct – dB in anechoic chamber) in a plane 1.0 in. in front of source for $kl$ = 19.6764 1/ft. (a) Measurements; (b) calculation $C_\alpha = 0.153$, $z/\rho_0 c = (0.506, -3.311)$; (c) calculation $C_\alpha = 0.154$, $z/\rho_0 c = (0.490, -3.245)$; (d) calculation $C_\alpha = 0.156$, $z/\rho_0 c = (0.579, -3.520)$.

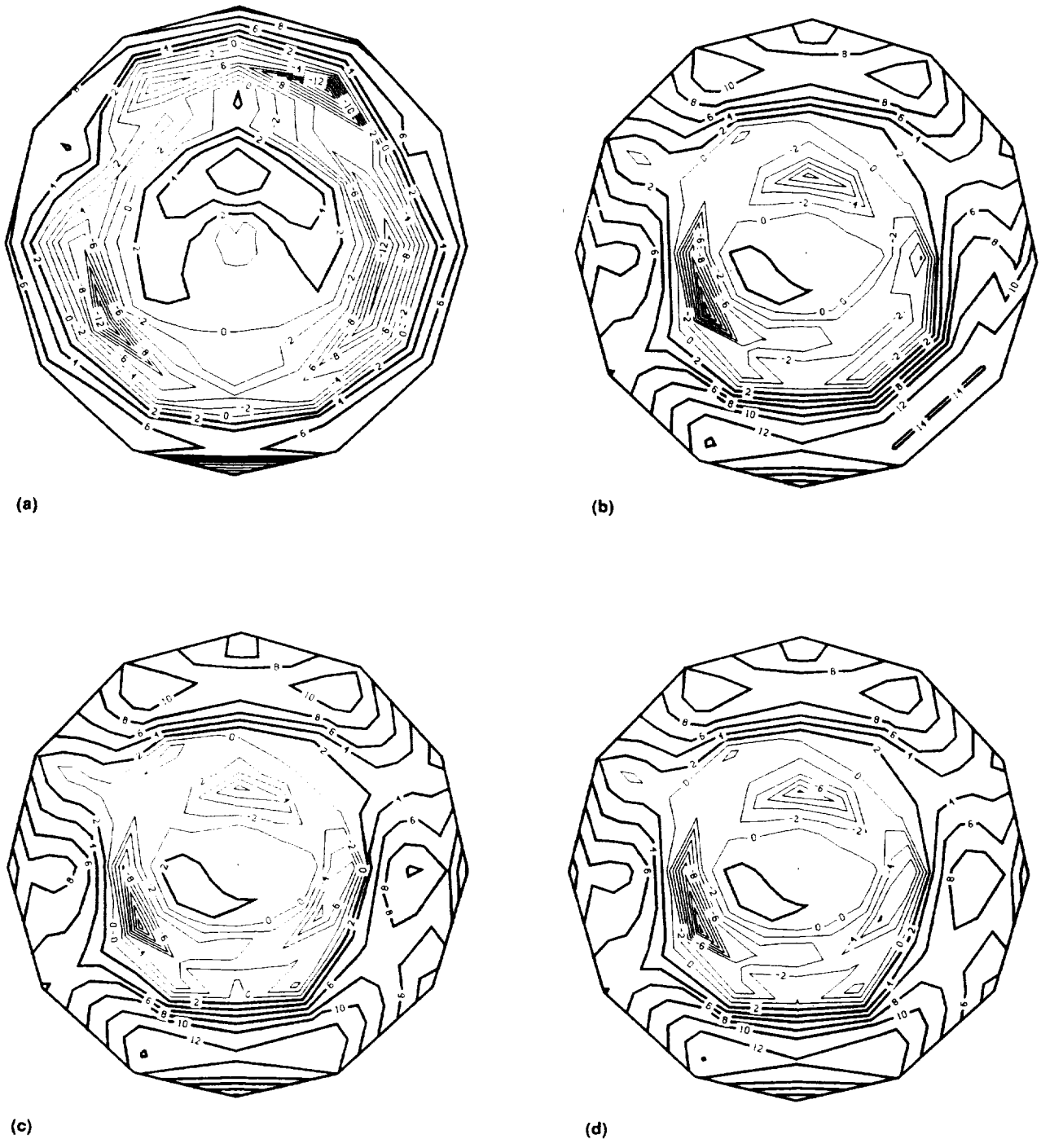


Figure 20. Reverberant field (dB in duct – dB in anechoic chamber) in a plane 1.0 in. in front of source for $kl = 19.8832$. (a) Measurements; (b) calculation $C_\alpha = 0.156$, $z/\rho_0 c = (0.541, -3.393)$; (c) calculation $C_\alpha = 0.156$, $z/\rho_0 c = (0.475, -3.168)$; (d) calculation $C_\alpha = 0.161$, $z/\rho_0 c = (0.606, -3.533)$.

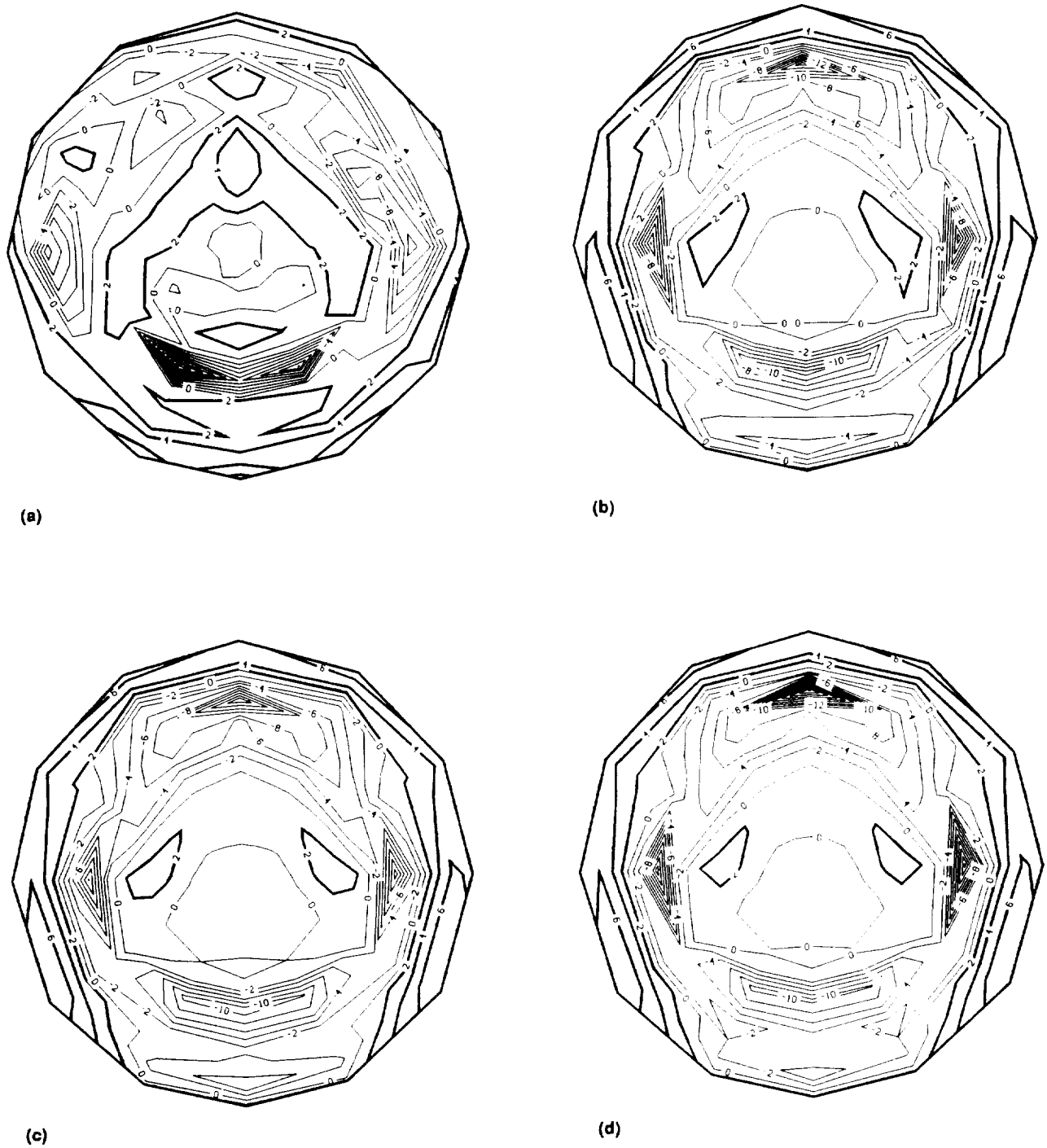


Figure 21. Reverberant field (dB in duct – dB in anechoic chamber) in a plane 1.0 in. in front of source for $kl$ = 22.7994 1/ft. (a) Measurements; (b) calculation $C_\alpha = 0.161$, $z/\rho_0 c = (0.414, -2.875)$; (c) calculation $C_\alpha = 0.202$, $z/\rho_0 c = (0.559, -2.936)$; (d) calculation $C_\alpha = 0.229$, $z/\rho_0 c = (0.579, -2.785)$.

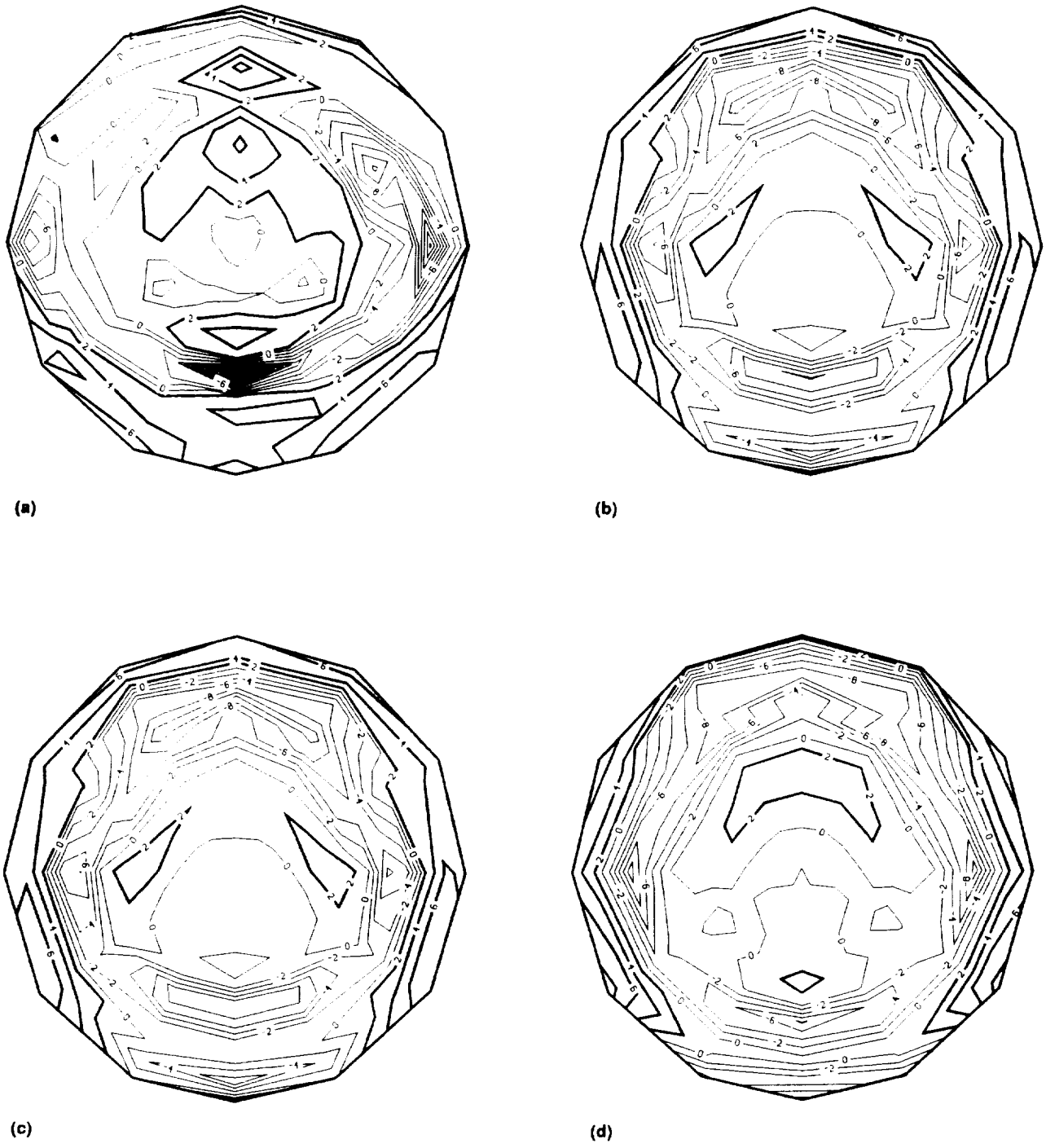


Figure 22. Reverberant field (dB in duct – dB in anechoic chamber) in a plane 1.0 in. in front of source for $kl$ = 23.0274 1/ft. (a) Measurements; (b) calculation $C_\alpha = 0.197$, $z/\rho_0 c = (0.450, -2.649)$; (c)calculation $C_\alpha = 0.198$, $z/\rho_0 c = (0.458, -2.670)$; (d) calculation $C_\alpha = 0.260$, $z/\rho_0 c = (1.012, -3.391)$.

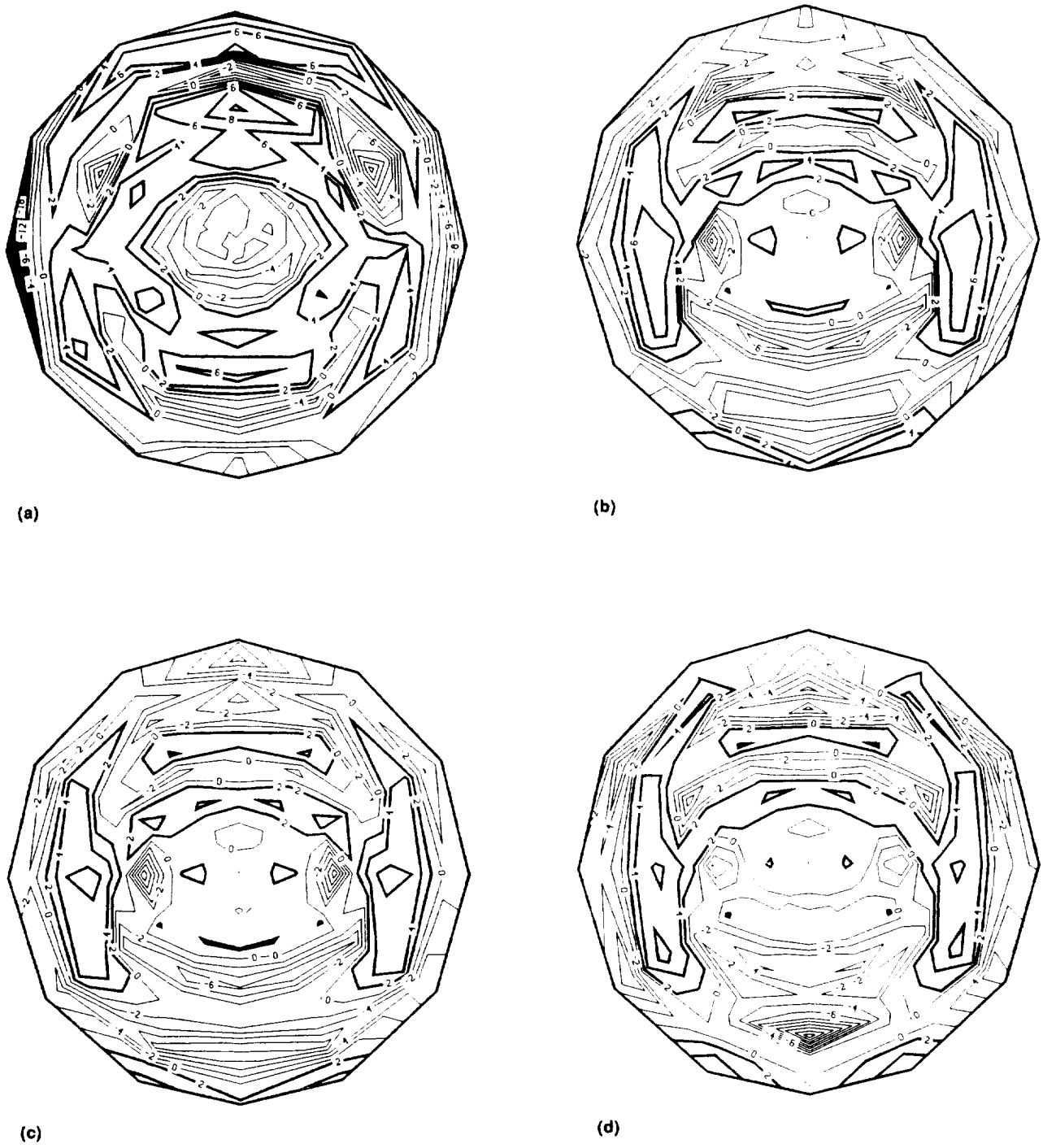


Figure 23. Reverberant field (dB in duct – dB in anechoic chamber) in a plane 1.0 in. in front of source for $kl$ = 26.1957 1/ft. (a) Measurements; (b) calculation $C_\alpha$ = 0.154, $z/\rho_0 c$ = (0.291, –2.422); (c) calculation $C_\alpha$ = 0.191, $z/\rho_0 c$ = (0.394, –2.509); (d) calculation $C_\alpha$ =0.234, $z/\rho_0 c$ = (0.410, –2.238).

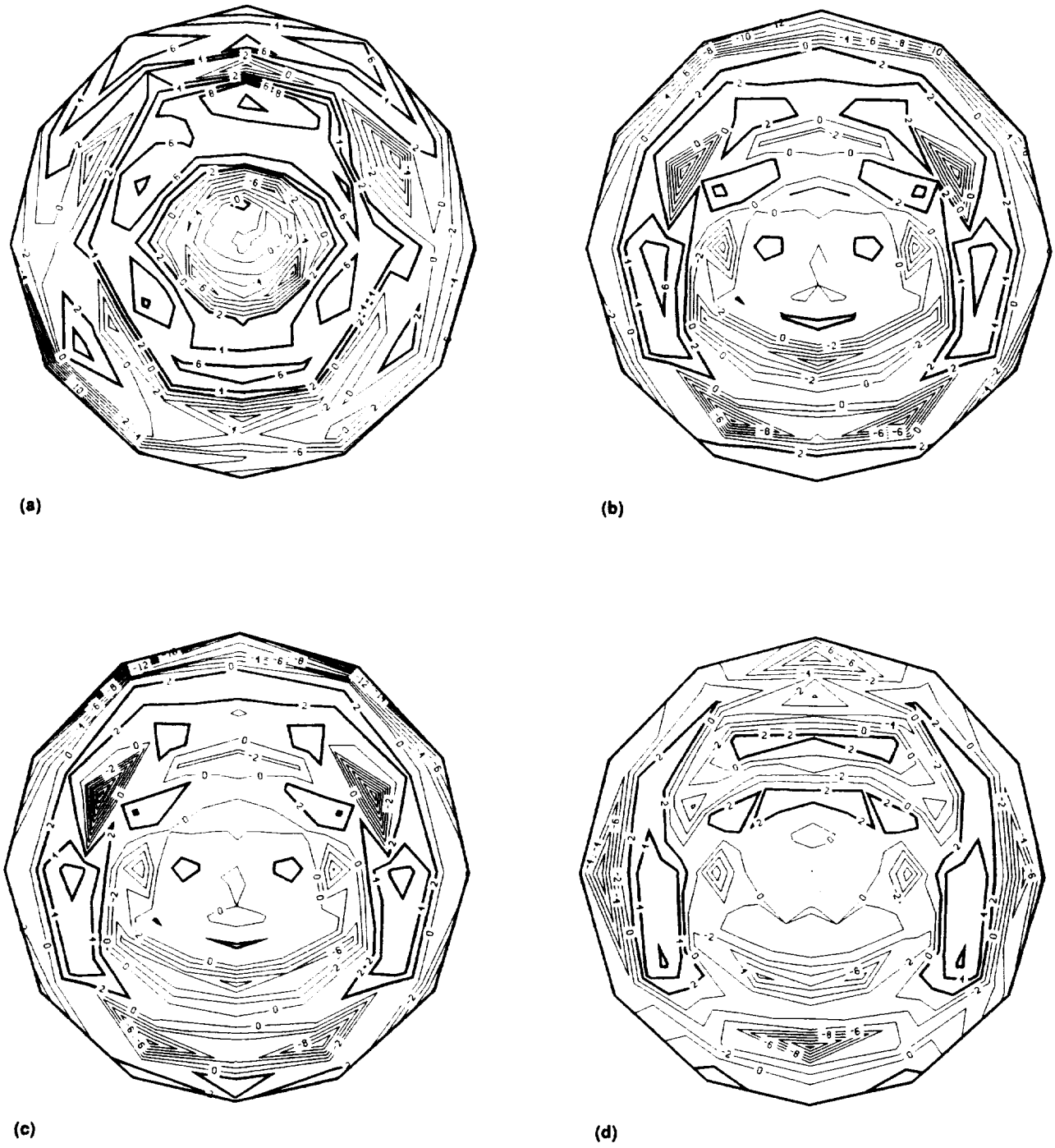


Figure 24. Reverberant field (dB in duct – dB in anechoic chamber) in a plane 1.0 in. in front of source for $kl = 26.4577$. (a) Measurements; (b) calculation $C_\alpha = 0.162$, $z/\rho_0 c = (0.321, -2.490)$; (c) calculation $C_\alpha = 0.187$, $z/\rho_0 c = (0.393, -2.543)$; (d) calculation $C_\alpha = 0.264$, $z/\rho_0 c = (0.395, -2.490)$.

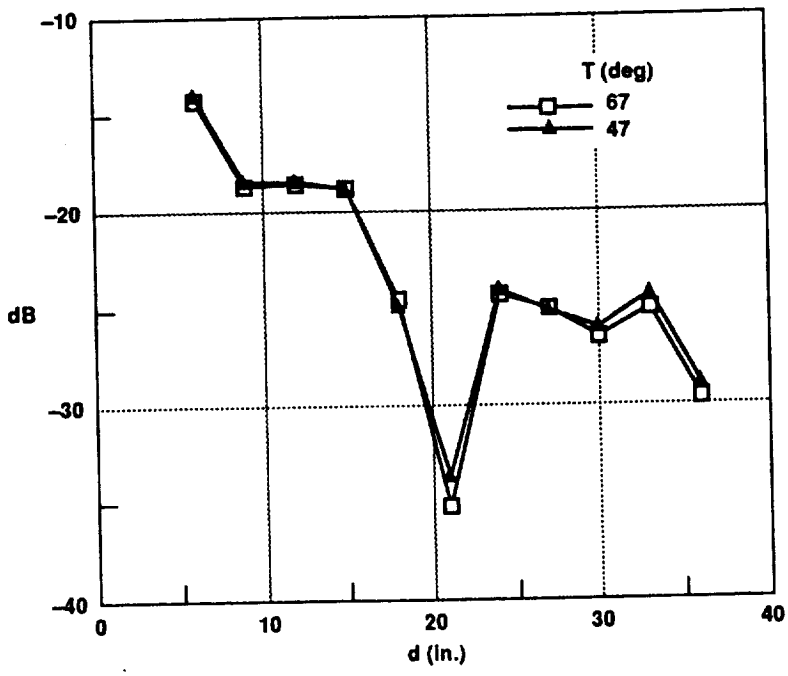


Figure 25. Measurements in duct at two temperatures, $kl = 22.7994$, $\varphi = 0°$.

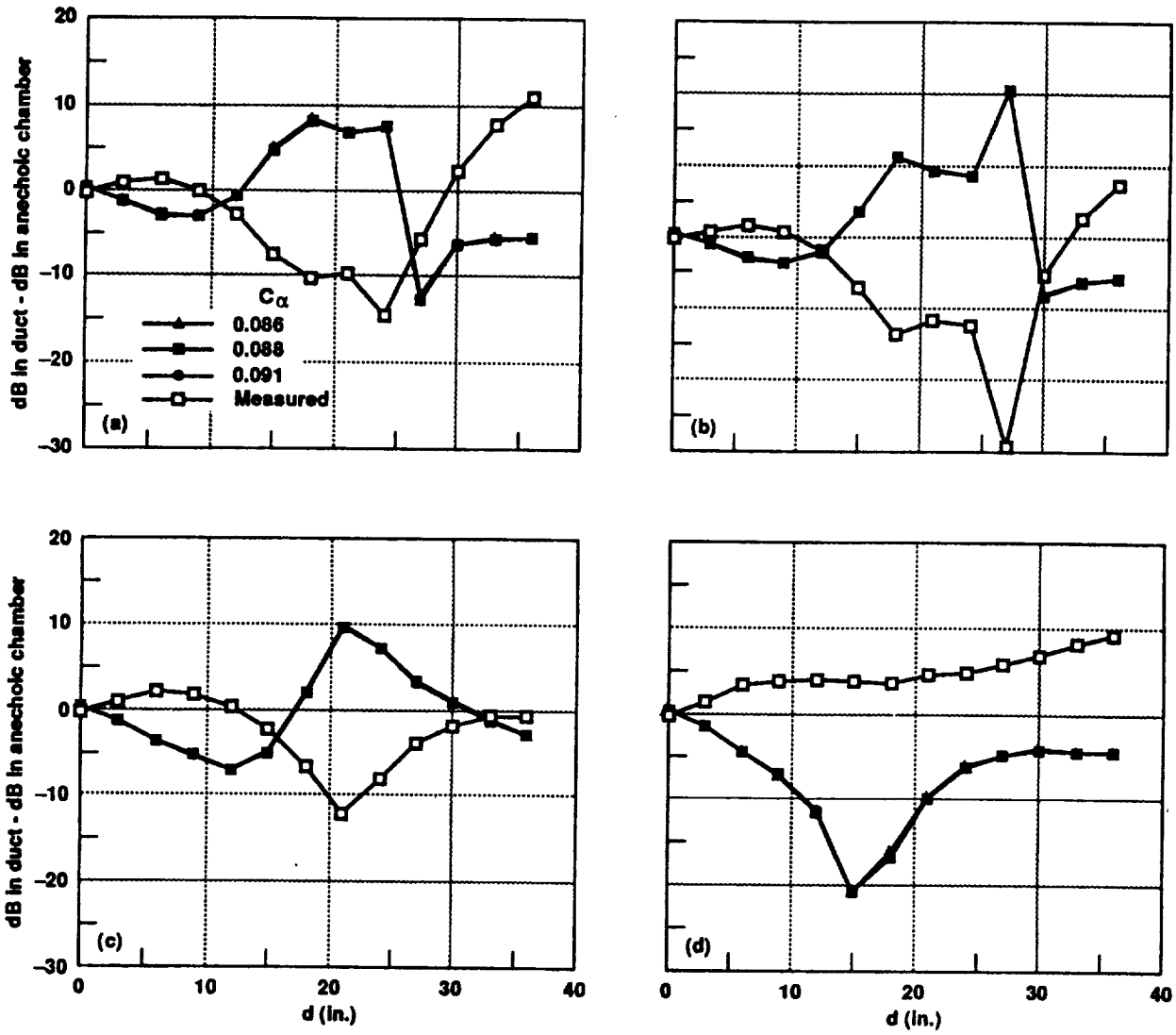


Figure 26. Comparison of measurements and calculations in a plane 1.0 in. in front of the source for $kl = 8.5221$. (a) $\varphi = 0°$; (b) $\varphi = 26°$; (c) $\varphi = 59°$; (d) $\varphi = 89°$.

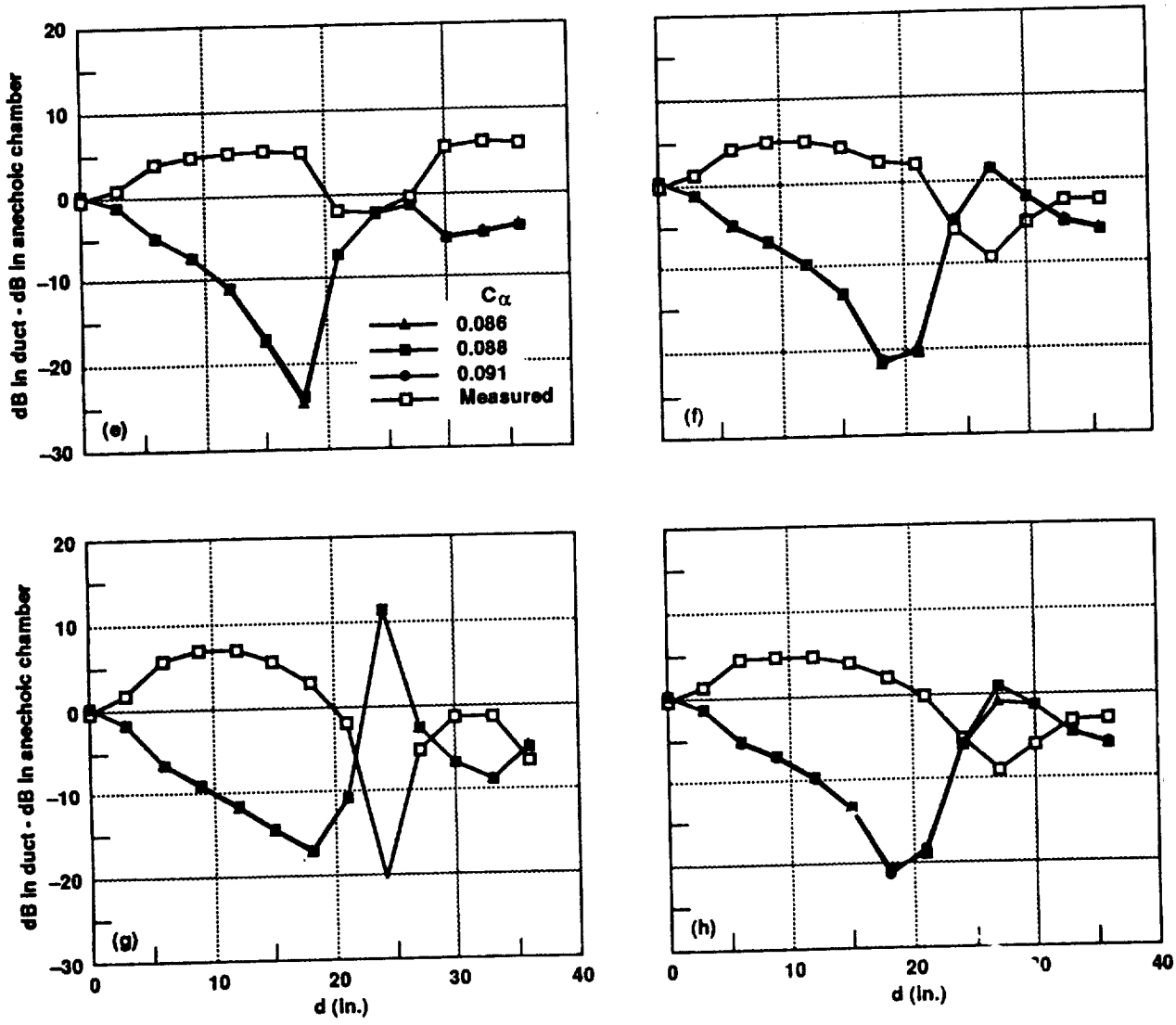


Figure 26. Continued. (e) $\varphi = 118°$; (f) $\varphi = 149°$; (g) $\varphi = 180°$; (h) $\varphi = 210°$.

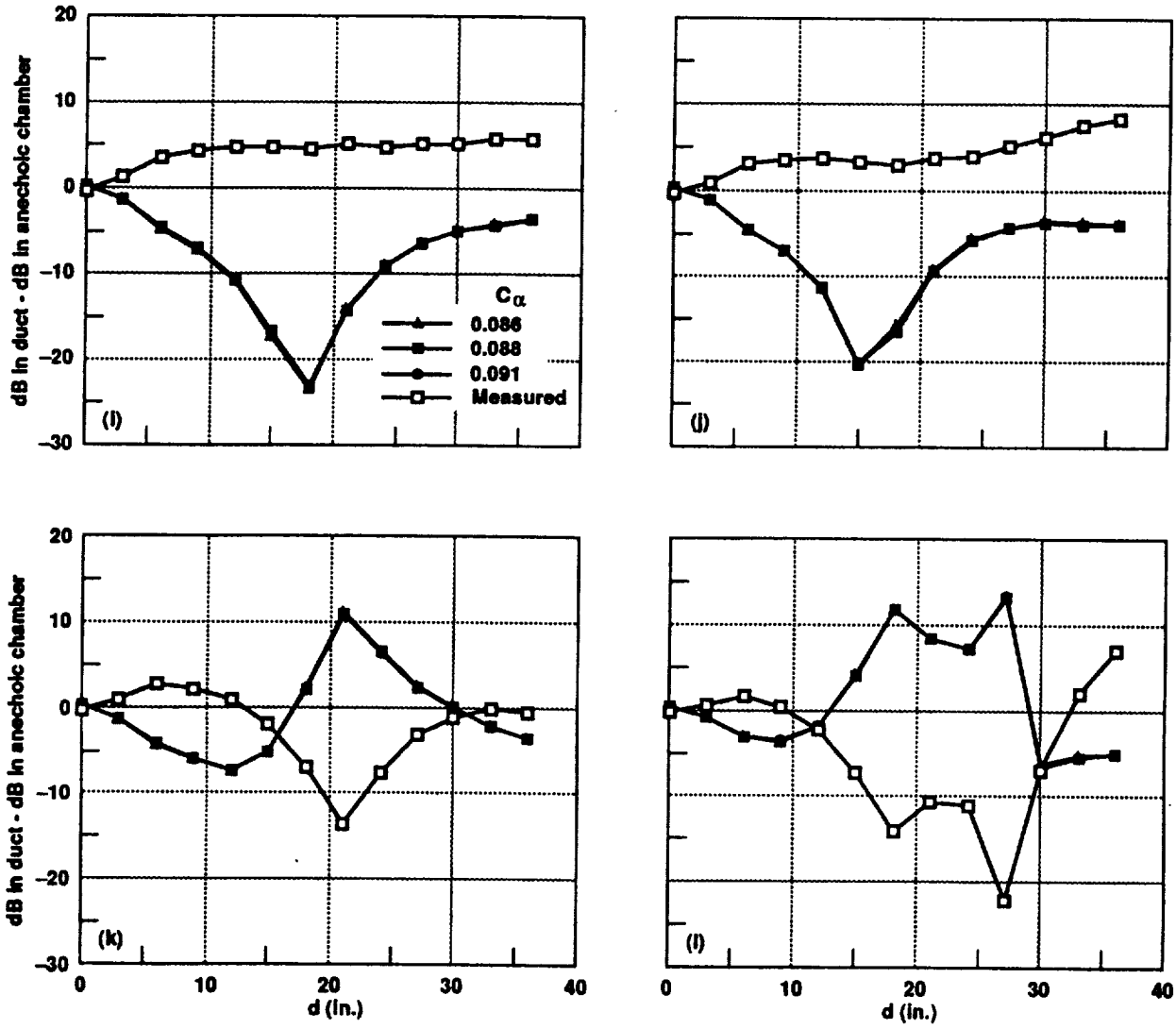


Figure 26. Concluded. (i) $\varphi = 242°$; (j) $\varphi = 271°$; (k) $\varphi = 303°$; ( l) $\varphi = 334°$.

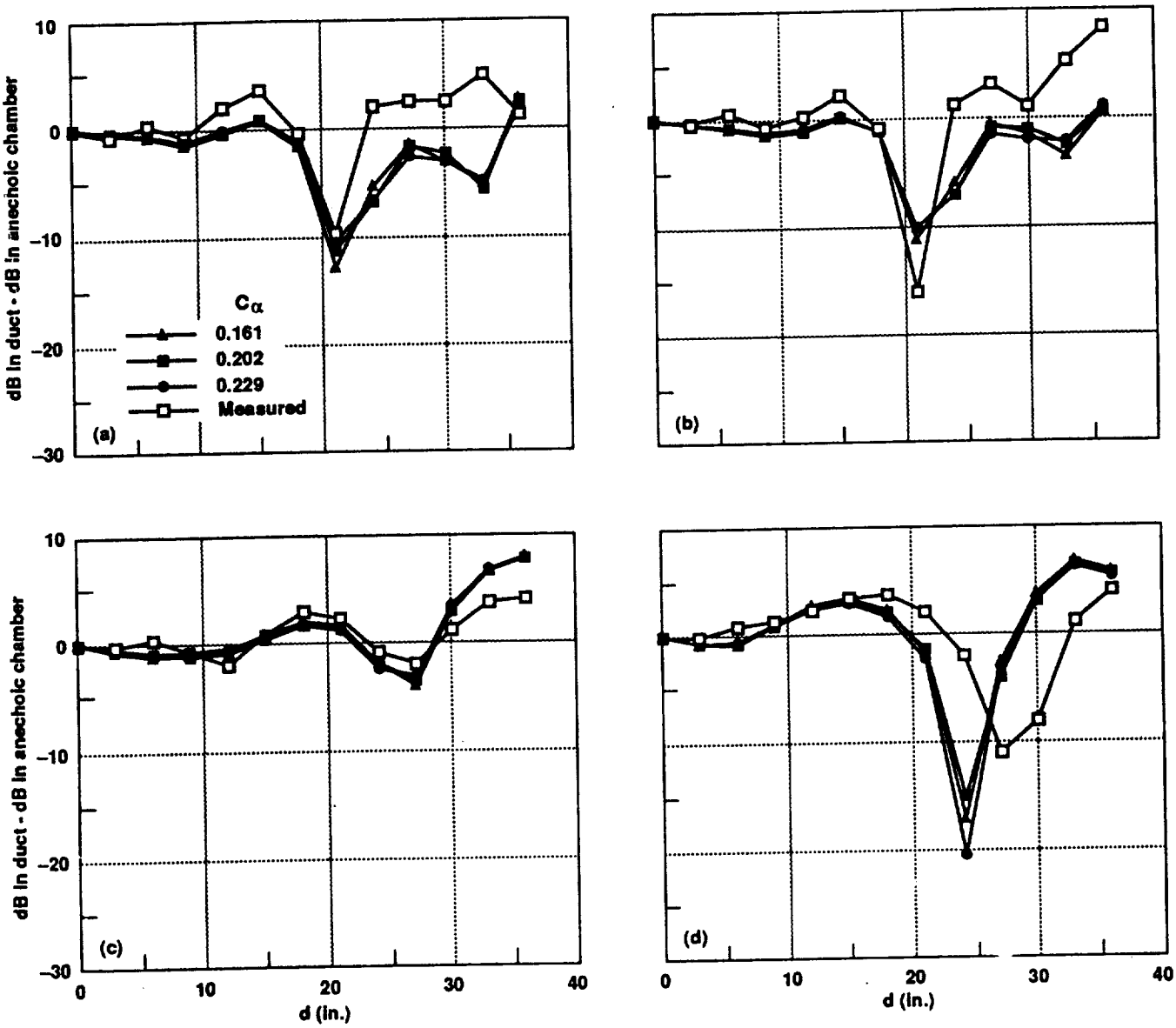


Figure 27. Comparison of measurements and calculations in a plane 1.0 in. in front of the source for $kl = 22.7994$. (a) $\varphi = 0°$; (b) $\varphi = 26°$; (c) $\varphi = 59°$; (d) $\varphi = 89°$.

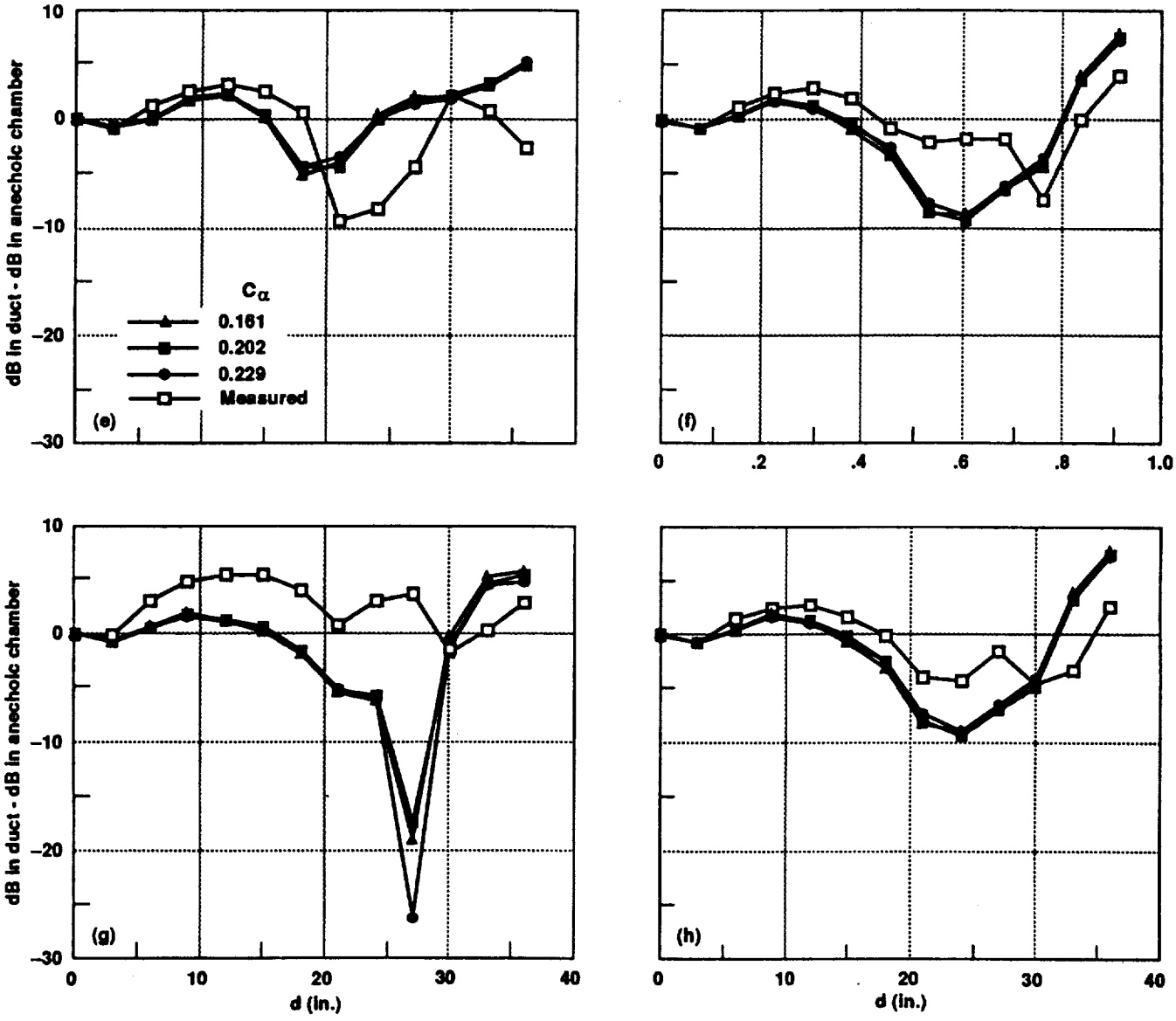


Figure 27. Continued. (e) $\varphi = 118°$; (f) $\varphi = 149°$; (g) $\varphi = 180°$; (h) $\varphi = 210°$.

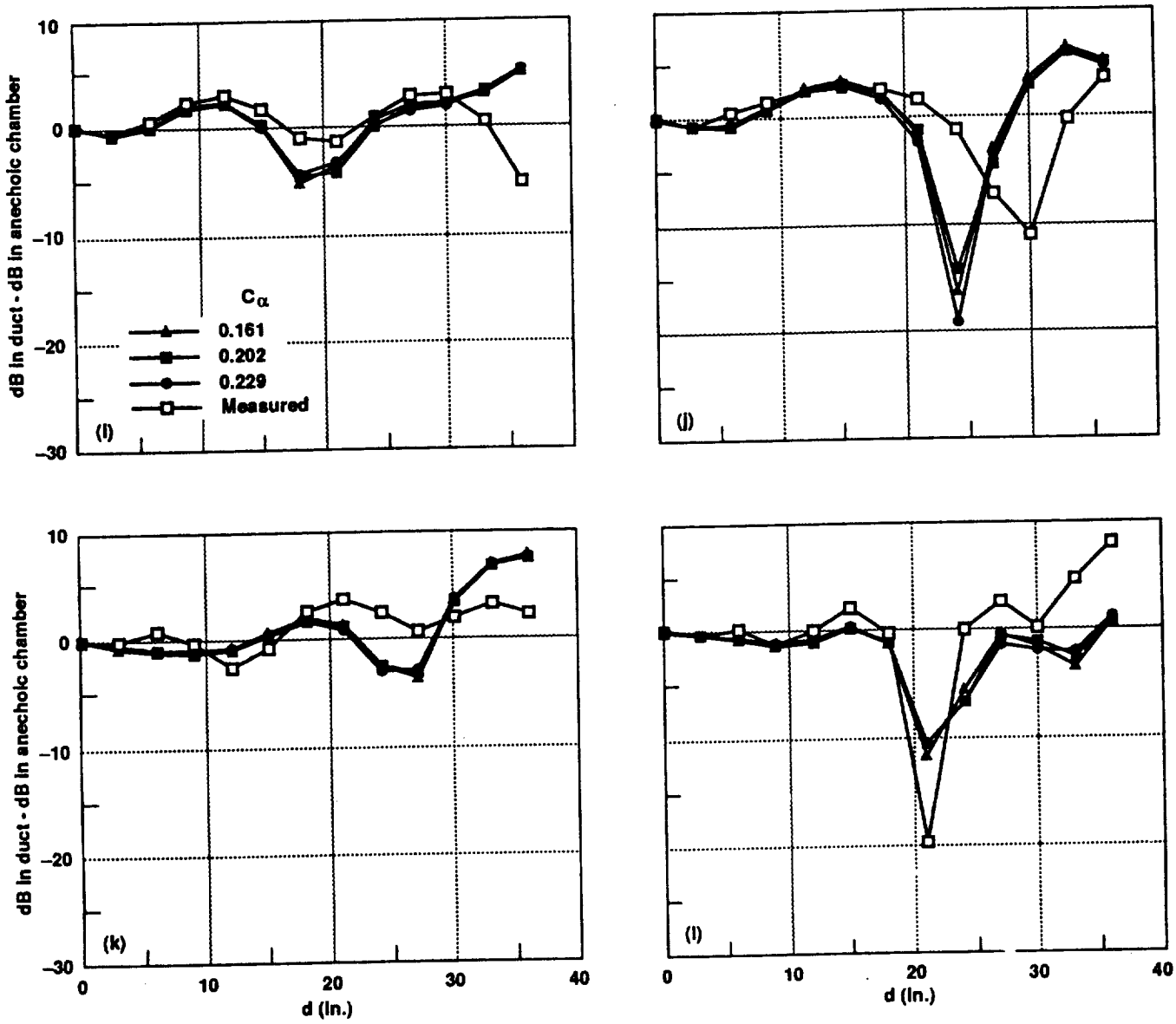


Figure 27. Concluded. (i) $\varphi = 242°$; (j) $\varphi = 271°$; (k) $\varphi = 303°$; ( l) $\varphi = 334°$.

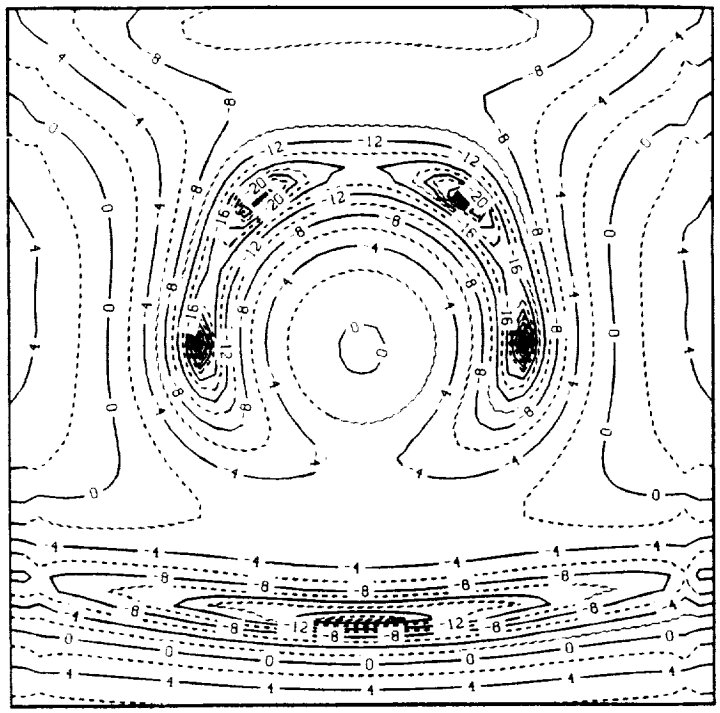

(a)

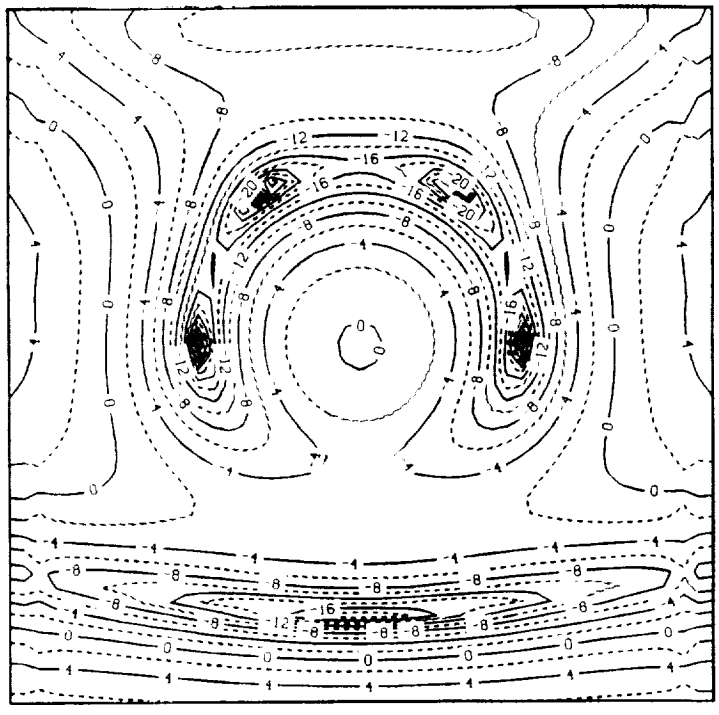

(b)

Figure 28. Calculations of reverberant field (dB in duct – dB in anechoic chamber) in a vertical plane for $kl = 8.5221$ and $C_\alpha = 0.086$. (a) $y = 1.0$ in., plane of microphone locations; (b) $y = 2.0$ in.

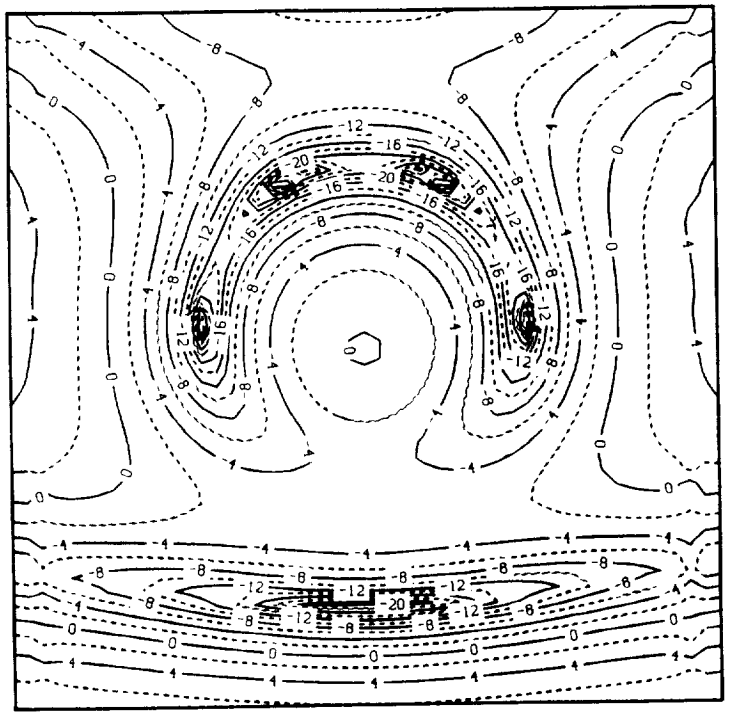


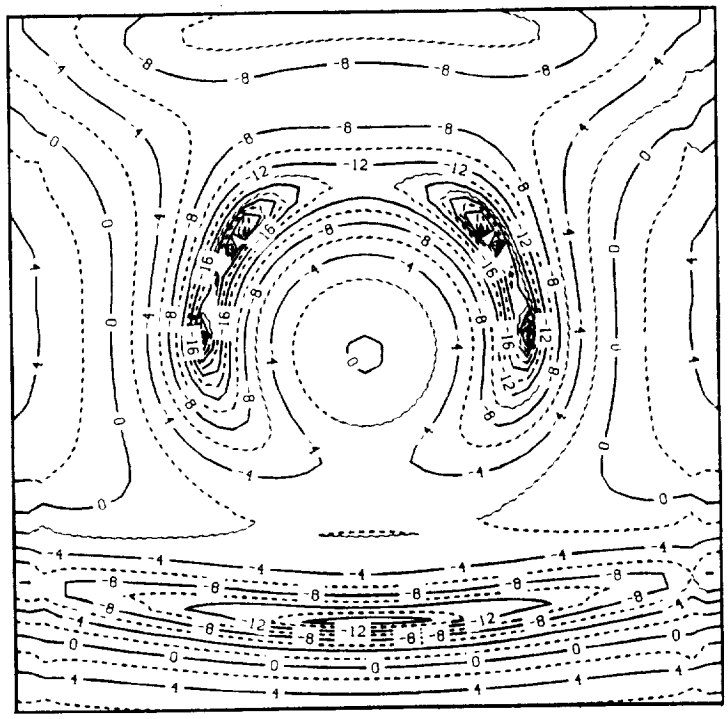


Figure 29. Calculations of reverberant field (dB in duct – dB in anechoic chamber) in a vertical plane 1.0 in. in front of source for $kl = 8.5221$ and $C_\alpha = 0.086$. (a) Source moved down to $z = -1.0$ in.; (b) source moved in to $y = -1.0$ in.

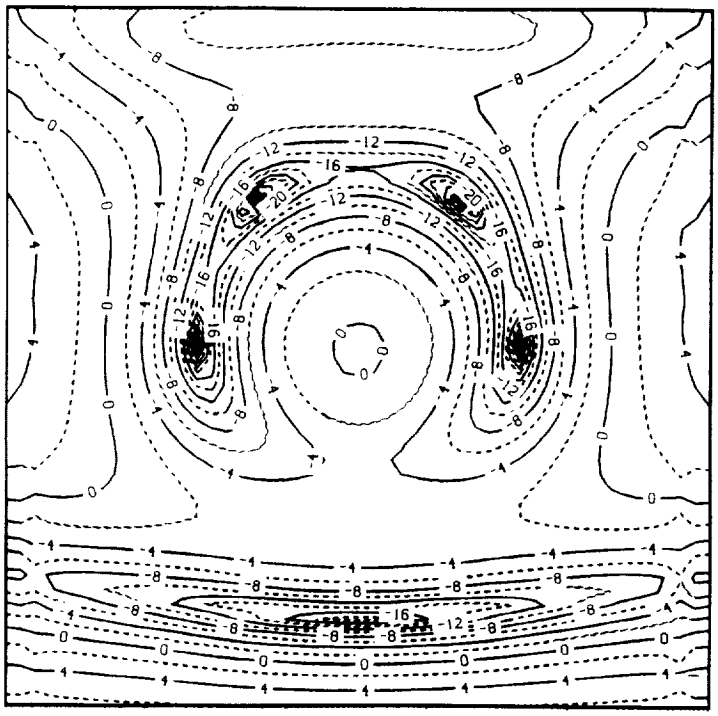

(a)

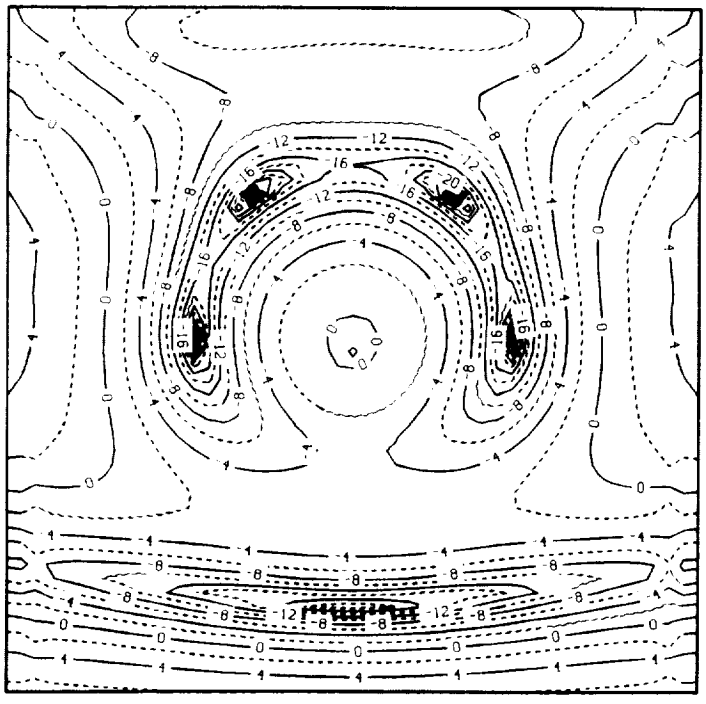

(b)

Figure 30. Calculations of reverberant field (dB in duct – dB in anechoic chamber) in a vertical plane $y = 1.0$ in. for $kl = 8.5221$ and $C_\alpha = 0.086$. (a) Curve fit for source model contains 2 terms and includes locations close to source; (b) curve fit for source model contains 4 terms and includes locations close to source.

NASA
National Aeronautics and Space Administration

# Report Documentation Page

| 1. Report No. | 2. Government Accession No. | 3. Recipient's Catalog No. |
|---|---|---|
| NASA TM-102801 | | |

| 4. Title and Subtitle | 5. Report Date |
|---|---|
| Experimental Validation Study of an Analytical Model of Discrete Frequency Sound Propagation in Closed-Test-Section Wind Tunnels | May 1990 |
| | 6. Performing Organization Code |
| 7. Author(s) | 8. Performing Organization Report No. |
| Marianne Mosher | A-90103 |
| | 10. Work Unit No. 505-61-51 |
| 9. Performing Organization Name and Address | 11. Contract or Grant No. |
| Ames Research Center<br>Moffett Field, CA 94035-1000 | |
| | 13. Type of Report and Period Covered |
| 12. Sponsoring Agency Name and Address | Technical Memorandum |
| National Aeronautics and Space Administration<br>Washington, DC 20546-0001 | 14. Sponsoring Agency Code |

15. Supplementary Notes

Point of Contact: Marianne Mosher, Ames Research Center, MS T042
Moffett Field, CA 94035-1000 (415) 604-4560 or FTS 464-4560

16. Abstract

The principal objective of this study is to assess the adequacy of linear acoustic theory with an impedance wall boundary condition to model the detailed sound field of an acoustic source in a duct. This study compares measurements and calculations of a simple acoustic source in a rectangular concrete duct lined with foam on the walls and anechoic end terminations. Measurement of acoustic pressure for twelve wave numbers provides variation in frequency and absorption characteristics of the duct walls. Close to the source, where the interference of wall reflections is minimal, correlation is very good. Away from the source, correlation degrades, especially for the lower frequencies. Sensitivity studies show little effect on the predicted results for changes in impedance boundary condition values, source location, measurement location, temperature, and source model for variations spanning the expected measurement error.

| 17. Key Words (Suggested by Author(s)) | 18. Distribution Statement |
|---|---|
| Acoustic analysis in duct<br>Experimental validation of analysis<br>Sound propagation in wind tunnels | Unclassified-Unlimited<br><br>Subject Category - 71 |

| 19. Security Classif. (of this report) | 20. Security Classif. (of this page) | 21. No. of Pages | 22. Price |
|---|---|---|---|
| Unclassified | Unclassified | 73 | A02 |



For sale by the National Technical Information Service, Springfield, Virginia 22161